A

TECHNICAL REPORT

Fire Reaction Experiments

*(Denoted herein as **Charring Experiments CE02-CE03**)*

EPFL / CCLab - EMPA / Bauphysik - Craig Tracy - December 18th, 2003

Technical Report 2001.2/2

Charring Experiments 02 & 03 (CE02-CE03)

GFRP Specimens on Small Horizontal Oven

1 Motivation and Summary

Following a successful Exploratory Charring Experiment 01, a full four specimens were used in Charring Experiments 02 and 03 (CE02 and CE03). The goals of the experiments were to measure the temperature profile through the thickness of the specimen over time, to observe the high-temperature behavior, and later, to measure the residual tensile strength of the specimens at room temperature. The specimens were therefore placed in the four exposure windows on the EMPA's small horizontal oven and thermally loaded according to the ISO 834 temperature curve. The first specimens were removed from the oven after 15 minutes, the second at 30 minutes, the third at 45 minutes, and the fourth at 60 minutes. Temperatures where measured by 10 thermocouples on and within each specimen, as well as by 6 thermocouples in the oven. Pictures were taken throughout the duration of the experiments.

2 Origin, Preparation, and Description of Specimens

The specimens under investigation were small samples of Martin Marietta Composites' DuraSpan® 766 bridge deck. The glass-reinforced isophthalic polyester section is produced by the pultrusion process and consists of two face sheets separated by webs (see Figure A-1). The particular samples used in this investigation were cut from specimens used previously in structural experiments at the CCLab in Lausanne and then stored in an outside stockyard for approximately one year. Cutting of the final specimen size was conducted in Lausanne with a hand-held circular saw on September 4th, 2003. Taking from unaffected portions of the structural specimens, the thermal specimens showed no signs of damage. The dimensions of the specimens were 32.5 cm x 41.0 cm, which included two webs connecting the face sheets and

one factory-bonded joint. A commercial transporter was hired to ship the specimens to the EMPA in Dübendorf, where it was stored indoors for approximately 1 month.

To facilitate the placement of thermocouples on the cold faces, the face sheets were cut from the webs by a bandsaw. In order to install the six the thermocouples within the thickness of the face sheets, 40 mm long x 2.5 mm wide slots were cut into the cold faces. Using a computer-piloted router (CNC machine), two slots were cut at each depth of 3.80 mm, 7.6 mm, 11.4 mm, and 15.2 mm from the cold face. The machine used a jet of liquid to cool the cutter head during the approximately three hours of machining required for each specimen, which raised concerns about water absorption in the specimen. Thus, the machining was followed by 4 hours of drying in an oven at 70°C for CE02 specimens and 18 hours for CE03. On average, CE03 specimens lost 11 grams (or equivalently 11 ml.) during this process.

Thermocouples were then placed at the bottom of the slots and on the cold faces of the specimens. Sika Sikadur® 330 two-part epoxy adhesive mixed with powdery grindings of the specimen to fill in the slots over the thermocouples. The adhesive was allowed to cure at least 24 hours. The thermocouples, designated "Artikel-Nr. 24-K-GG" by the supplier, R. Wick AG, were Class II, with an accuracy of ±2.2°C or 0.75% of the measured temperature.

Taking measurements of the as-built dimensions of the specimens and slots, it was found that CE02 specimens were slightly thinner than those of CE03. This is because they were machined from different faces of the deck material (see Figure A-2 for details). Thus, although the slots were cut to an accuracy of ±0.2 mm from the cold face, they varied by as much as 1.2 mm from the hot face. The measured and calculated dimensions are summarized in Table A-1 and Figure A-3.

3 Experiment Proceedings

CE02 began at 9:47am on November 27th. CE03 followed roughly one week later, beginning at 12:45am on December 3rd, 2003. Time began with the firing of the oil burners. The burners were automatically controlled by a computer, which read the oven temperature from the six internal thermocouples and adjusted the intensity of the burners to follow the ISO 834 temperature curve as closely as possible. The notes in Table A-3 and Table A-4 were taken during CE02 and CE03, respectively.

4 Post-Experiment Inspection of Specimens

The hot faces of the specimens showed varying levels of damage depending on the location. While the area towards the center was the most severely damaged on the hot faces, the opposite was true on the cold faces. In the exact footprint of the ceramic insulation bats used to seal the gaps around the perimeter of the specimens, blackened and charred areas were found on the cold faces (see Figure A-19).

The factory-bonded polyurethane (Ashland Chemical Pliogrip® 8000/6660) joint in specimen 02D appeared to have opened during the experiment. It was possible to pry the joint open further during the minutes after its removal from the oven. Handling the specimen after it had cooled for some hours, however, it was found that the joint regained enough strength to resist any prying.

The specimens from CE02 were carefully dissected to investigate the depth of damage. The type and status of each reinforcement layer was noted as successive layers were peeled away from the hot faces. Table A-6 and Table A-7 summarize this investigation. The layers described in Table A-7 may also be seen in the resin burn-off specimen in Figure A-4. A quicker investigation of the CE03 specimens was performed only to discern the first layer in sound condition, i.e. The first layer that could not be peeled away. These results are summarized in Table A-8.

Comparing the lists of reinforcement layers resulting from the dissection of the CE02 specimens, it was found that two specimens (02A & 02D) appeared to have been fabricated according to one fiber architecture schedule, while the other two (02B & 02C) appeared to follow another. The discrepancies consist of the differing location of a +45°/90°/-45° cluster and one missing random mat. To clarify this issue, resin oxidation cycles (also known as burn-off tests) were performed on three similar samples at facilities in Dübendorf and Lausanne. The results were again split between the two architecture schedules. A comparison of these results is shown in Table A-5.

5 Discussion of Results

The progression of damage to the hot face seemed to have proceeded in stages. In the first stage occurring in the first nine minutes, the surface was heated past its decomposition temperature and turned to black as the resin decomposed. The next stage began as the fuel created by this decomposition underwent combustion until roughly two minutes later when the fuel was exhausted. A third stage, also roughly two minutes in duration, followed as decomposition

continued to a deeper level and the scoured fibers near the surface began to turn to a whitish char. A final fourth stage began with the flaming combustion of gases from the decomposition occurring deeper within the laminate. This phase continued for the remainder of the experiment, as the reinforcement layers closer to the surface turned to the whitish char and the resin at deeper levels was decomposed.

The persistence of flaming combustion suggests that no steady-state condition was reached and that the entire thicknesses would have eventually been consumed. The whitish char that remained was only the char from the burnt fibers. The black char from the resin did not remain on outermost reinforcement layers, and appeared only as a kind of powdery fiber coating on the deeper layers. It did not seal the surface or close the gaps between the fibers to prevent the escape of decomposition gasses from the deeper level. Thus, there was no significant fire-resisting effect from the charring of the resin. The burnt-out reinforcement layers, however, probably provided some level of protection by blocking the radiation of the oven and reducing the ablative effects of the exhaust system.

As shown in Figure A-21 and Figure A-22, the groups of thermocouples placed at similar depths measured similar temperature progressions. Some variation can be expected due to the uneven heating of the oven, as was visually noted during the experiments by the staggered progression of damages to the hot faces. In fact, the time at which landmarks such as the first appearance of brown, black and white patches, as well as flames varied from specimen to specimen by as much as several minutes. Additionally, errors in the exact placement of the thermocouples and the accuracy of the thermocouples themselves could be responsible for some variation. Despite these sources of error, the average values showed a direct correlation between thickness of material below and temperature, as shown in Figure A-23. The differences between curves of similar depth ranges show the extreme sensitivity of depth of measurement to temperature. This stands to reason, as the temperature gradient is extremely steep through the thickness of the specimens.

As discussed in the previous section, peeling of the polyurethane joint was evident in one of the eight specimens. It appears that the adhesive has a very low maximum operating temperature, above which it is quite ineffective. Perhaps uneven heating of the materials above and below the joint caused peeling stresses. It would be prudent to expect no strength from bonded joint of this type at elevated temperatures.

During CE02, the epoxy used fill in the slots on specimen 02D began to flow out after approximately nine minutes (Figure A-15). When the sample finally cooled, the epoxy hardened to its proper state. This is most likely the result of mixing the epoxy in improper proportions of the two components. Normally there is little possibility of error when the entire

container of Component A is mixed with the entire container of Component B, as directed by the manufacturer. For these small applications, however, it is not economical to mix five kilograms of epoxy for each task. Thus, the epoxy used in CE02 was mixed by simple visual estimation of proportions. The problems experienced during the testing underlined the importance of exact measurements rather than estimation. Consequently, a digital scale was used to measure the exact quantities of epoxy components for the preparation of CE03 specimens and the problem was resolved.

The method of sealing the gaps around the specimens using ceramic wool had its advantages and disadvantages. Although it did prevent the spread of flames to the cold side of the specimens, it also changed the boundary conditions on that face. While the central portions of the cold faces were cooled by natural convection of air at ambient temperatures, the portions below the insulation were not. As mentioned in the previous sections, this effect resulted in more severe conditions and, thus, more damage around the edges than in the centers of the cold faces (see Figure A-19). One possible solution would be to equalize the boundary condition by covering the entire cold faces of the specimens with the insulation material.

In general, CE02 and CE03 have successfully provided enough data to calibrate the "without water" scenario of the numerical model. In addition, the experiments verify that a large-scale combined structural and thermal test without liquid cooling would be of little use. As shown in Figure A-23, the cold faces reach the glass transition temperature of the material (85°C) in roughly eight minutes. With the entire lower flanges in excess of the glass transition temperature, failure of the deck would soon follow. Thus, the small amount of new data collected would not justify the great time and expense required for such an endeavor. It will be far more useful to concentrate the three large-scale experiments on variations of water flow rate.

Table A-1. CE02 - Measurement of as-built thermocouple slot depths from cold face and calculation of material thickness below slots

Specimen 02A		
Slot (Thermocouple #)	Measured Depth (mm)	Calculated Thickness Underneath (mm)
1	15.2	0.7
2	15.3	0.6
3	11.4	4.5
4	11.7	4.2
5	7.7	8.2
6	7.7	8.2
7	3.9	12
8	4	11.9
9	0	15.9
10	0	15.9

Specimen 02B		
Slot (Thermocouple #)	Measured Depth (mm)	Calculated Thickness Underneath (mm)
1	15.2	0.9
2	15.3	0.8
3	11.4	4.7
4	11.6	4.5
5	7.6	8.5
6	7.7	8.4
7	3.8	12.3
8	4	12.1
9	0	16.1
10	0	16.1

Specimen 02C		
Slot (Thermocouple #)	Measured Depth (mm)	Calculated Thickness Underneath (mm)
1	15.3	0.9
2	15.4	0.8
3	11.5	4.7
4	11.6	4.6
5	7.7	8.5
6	7.8	8.4
7	3.9	12.3
8	4	12.2
9	0	16.2
10	0	16.2

Specimen 02D		
Slot (Thermocouple #)	Measured Depth (mm)	Calculated Thickness Underneath (mm)
1	15.4	0.7
2	15.4	0.7
3	11.5	4.6
4	11.7	4.4
5	7.8	8.3
6	7.7	8.4
7	3.9	12.2
8	4.1	12
9	0	16.1
10	0	16.1

Table A-2. CE03 - Measurement of as-built thermocouple slot depths from cold face and calculation of material thickness below slots

Specimen 03A			
Slot (Thermocouple #)	Measured Depth (mm)	Calculated Thickness Underneath (mm)	
1	15.1	2.3	
2	15.4	2.0	
3	11.5	5.9	
4	11.6	5.8	
5	7.6	9.8	
6	7.7	9.7	
7	3.9	13.5	
8	4.0	13.4	
9	0.0	17.4	
10	0.0	17.4	
Weight Before Drying (gm)	Weight After Drying (gm)	Weight Loss (gm)	% Weight Loss
4776	4768	8	0.17

Specimen 03C			
Slot (Thermocouple #)	Measured Depth (mm)	Calculated Thickness Underneath (mm)	
1	15.2	2.2	
2	15.3	2.1	
3	11.4	6.0	
4	11.5	5.9	
5	7.6	9.8	
6	7.6	9.8	
7	3.8	13.6	
8	3.9	13.5	
9	0.0	17.4	
10	0.0	17.4	
Weight Before Drying (gm)	Weight After Drying (gm)	Weight Loss (gm)	% Weight Loss
4796	4786	11	0.22

Specimen 03B			
Slot (Thermocouple #)	Measured Depth (mm)	Calculated Thickness Underneath (mm)	
1	15.4	1.8	
2	15.4	1.8	
3	11.5	5.7	
4	11.7	5.5	
5	7.8	9.4	
6	7.8	9.4	
7	3.9	13.3	
8	4.1	13.1	
9	0.0	17.2	
10	0.0	17.2	
Weight Before Drying (gm)	Weight After Drying (gm)	Weight Loss (gm)	% Weight Loss
4788	4774	14	0.29

Specimen 03D			
Slot (Thermocouple #)	Measured Depth (mm)	Calculated Thickness Underneath (mm)	
1	15.3	1.9	
2	15.3	1.9	
3	11.5	5.7	
4	11.7	5.5	
5	7.7	9.5	
6	7.7	9.5	
7	3.8	13.4	
8	4.0	13.2	
9	0.0	17.2	
10	0.0	17.2	
Weight Before Drying (gm)	Weight After Drying (gm)	Weight Loss (gm)	% Weight Loss
4789	4778	11	0.23

Table A-3. Notes taken during CE02

Time (min:sec)	Notes
5:00	Hot faces mostly black
5:50	Flames begin to grow in some areas
7:20	Hot face surfaces totally black, flames still only in patches
8:00	Smoke beginning to escape oven
8:30	Flames growing to cover most of hot face surfaces
9:00	Large flames covering all hot face surfaces
9:20	Epoxy adhesive used for thermocouples 1, 4, 5, & 8 of 02D beginning to become soft and flowing out of slots, all other epoxy appears to be remaining rigid
10:00	White patches appearing on hot face surfaces
15:00	First specimen (02C) removed from oven - flames are extinguished by smothering the hot face on piece of ceramic wool, another piece of ceramic wool used to cover empty exposure window of oven
15:30	Woven pattern appearing in white patches
22:30	Slight darkening of epoxy adhesive on cold faces
24:00	Small yellow-brown patches appearing on cold faces
24:30	More smoke escaping around specimens
25:30	Red-hot fiber tips dangling down from hot face
30:00	Second specimen (02D) removed from oven, flames extinguished again by smothering hot face on a piece of ceramic wool, another piece of ceramic wool used to cover empty exposure window in oven, polyurethane glue joint in specimen completed separated
45:00	Third specimen (02B) removed from oven, massive flames engulf specimen and continue despite attempts to smother them with ceramic wool - wet rags are finally successful in extinguishing the flames after approximately 2 minutes of burning outside of the oven
49:00	Random mat cracked across surface, more fiber tips dangling down
60:00	Last specimen (02A) removed from oven, flames quickly extinguished with wet rags, oil burners turned off and experiment concluded, all 4 specimens continue to smolder and emit smoke

Table A-4. Notes taken during CE03

Time (min:sec)	Notes
3:30	Slight browning on hot face of specimens
5:40	Large brownish areas developing on hot faces of specimens - Flames appear on 03B & 03C
6:50	Flames appear on 03B & 03C
8:30	Whole hot face blackened on 03C, flames died down to only corners
9:50	03D seems to be burning slower than the others
12:00	Big flames on 03C, nearly none on 03B
15:00	03A removed from exposure window and placed on piece of ceramic wool with the hot face down, flames extinguished with wet rags
16:40	White patches appearing on 03D
19:00	Fibers hanging down from 03D, grayish patches appearing on blackened hot faces of all specimens, large flames on all specimens
20:00	Large white areas around perimeter of 03B hot face
21:40	Slight bit of smoke escaping around 03B, slight discoloration of epoxy adhesive on 03C
24:00	03D surface veil/random mat totally cleaned of resin char and has small white patches
28:00	03B appears to be much more degraded than 03C
30:00	03B removed from exposure window and placed on piece of ceramic wool with the hot face down, flames extinguished with wet rags
40:30	More smoke escaping on both specimens, epoxy adhesive still rigid over all thermocouples, some liquid bubbling up along a crack in 03D
41:50	03D surface veil/random mat cleared of resin char and white in patches but yet unbroken - 03C much less white and more black, fiber tips hanging down
45:00	03C removed from exposure window and placed on piece of ceramic wool with the hot face down, flames extinguished with wet rags
51:00	03D surface veil/random mat falling down as a large sheet
60:00	03D removed from exposure window and placed on piece of ceramic wool with the hot face down, flames extinguished with wet rags

Table A-5. Glass fiber architecture schedule resulting from dissection of experimental specimens (02A through 02D) and from independent resin burn-off tests ("Burn 1" through "Burn 3")

Reinforcement Schedule A					Reinforcement Schedule B			
#	Burn 1	Burn 2	02B	02C	#	Burn 3	02A	02D
1	surface veil	surface veil	surface veil	surface veil	1	surface veil	surface veil	surface veil
2	random mat	random mat	random mat	random mat	2	random mat	random mat	random mat
3	+45° fabric	+45° fabric	+45° fabric	+45° fabric	3	+45° fabric	+45° fabric	+45° fabric
4	90° fabric	90° fabric	90° fabric	90° fabric	4	90° roving	90° roving	90° roving
5	–45° fabric	–45° fabric	–45° fabric	–45° fabric	5	–45° fabric	–45° fabric	–45° fabric
6	+45° fabric	+45° fabric	+45° fabric	+45° fabric	6	0° roving	0° roving	0° roving
7	90° fabric	90° fabric	90° fabric	90° fabric	7	random mat	random mat	random mat
8	–45° fabric	–45° fabric	–45° fabric	–45° fabric	8	+45° fabric	+45° fabric	+45° fabric
9	random mat	random mat	random mat	random mat	9	90° roving	90° roving	90° roving
10	0° roving	0° roving	0° roving	0° roving	10	–45° fabric	–45° fabric	–45° fabric
11	+45° fabric	+45° fabric	+45° fabric		11	0° roving	0° roving	0° roving
12	90° fabric	90° fabric	90° fabric		12	+45° fabric	+45° fabric	
13	–45° fabric	–45° fabric	–45° fabric		13	90° roving	90° roving	
14	random mat	random mat	random mat		14	–45° fabric	–45° fabric	
15	0° roving	0° roving	0° roving		15	random mat	random mat	
16	+45° fabric	+45° fabric	+45° fabric		16	+45° fabric	+45° fabric	
17	90° fabric	90° fabric	90° fabric		17	90° roving	90° roving	
18	–45° fabric	–45° fabric	–45° fabric		18	–45° fabric	–45° fabric	
19	random mat	random mat	random mat		19	0° roving	0° roving	
20	+45° fabric	+45° fabric	+45° fabric		20	random mat	random mat	
21	90° fabric	90° fabric	90° fabric		21	+45° fabric	+45° fabric	
22	–45° fabric	–45° fabric	–45° fabric		22	90° roving	90° roving	
23	random mat	random mat	random mat		23	–45° fabric	–45° fabric	
24	0° roving	0° roving	0° roving		24	random mat	random mat	
25	+45° fabric	+45° fabric	+45° fabric		25	+45° fabric	+45° fabric	
26	90° roving	90° roving	90° roving		26	90° roving	90° roving	
27	–45° fabric	–45° fabric	–45° fabric		27	–45° fabric	–45° fabric	
28	random mat	random mat	random mat		28	0° roving	0° roving	
29	0° roving	0° roving	0° roving		29	+45° fabric	+45° fabric	
30	+45° fabric	+45° fabric	+45° fabric		30	90° roving	90° roving	
31	90° roving	90° roving	90° roving		31	–45° fabric	–45° fabric	
32	–45° fabric	–45° fabric	–45° fabric		32	random mat	random mat	
33	random mat	random mat	random mat		33	surface veil	surface veil	
34	surface veil	surface veil	surface veil					

Table A-6. Dissection of reinforcement layers from hot face towards cold face

	#	Reinforcement Schedule B	Status – Specimen 02D – 30 min.	Status – Specimen 02A – 60 min.
▲ Outer Deck Face (Hot Face)	1	surface veil	~30% whitish grey, ~70% blackened, unbroken	fibers white, brittle and broken
	2	random mat	"	"
	3	+45° fabric	blackened, brittle, unbroken	"
	4	90° fabric	blackened, slightly brittle	fibers blackened and brittle
	5	–45° fabric	"	"
	6	0° roving	blackened, still pliable	fibers blackened and slightly brittle
	7	random mat	black/brown, pliable	fibers blackened, still pliable
	8	+45° fabric	brown/yellow, pliable	"
	9	90° fabric	"	"
	10	–45° fabric	"	"
	11	0° roving	resin remaining in lower ½ of layer	"
	12	+45° fabric	composite appears in sound condition	"
	13	90° fabric	"	"
	14	–45° fabric	"	"
	15	random mat	"	"
	16	+45° fabric	"	"
	17	90° fabric	"	"
	18	–45° fabric	"	"
	19	0° roving	"	"
	20	random mat	"	"
	21	+45° fabric	"	"
	22	90° roving	"	"
	23	–45° fabric	"	"
	24	random mat	"	"
	25	+45° fabric	"	"
	26	90° roving	"	"
	27	–45° fabric	"	"
	28	0° roving	"	"
	29	+45° fabric	"	"
	30	90° roving	"	"
	31	–45° fabric	"	"
	32	random mat	"	"
▼ Inner Deck Face (Cold Face)	33	surface veil	"	"

Table A-7. Dissection of reinforcement layers from hot face towards cold face

	#	Reinforcement Schedule A	Status – Specimen 02C – 15 min.	Status – Specimen 02B – 45 min.
▲ Outer Deck Face (Hot Face)	1	surface veil	resin ash remaining	fibers white and brittle
	2	random mat	"	"
	3	+45° fabric	fibers blackened, slightly brittle	fibers blackened and brittle
	4	90° fabric	"	"
	5	–45° fabric	fibers blackened, still pliable	"
	6	+45° fabric	"	"
	7	90° fabric	"	"
	8	–45° fabric	"	"
	9	random mat	"	fibers blackened and slightly brittle
	10	0° roving	resin remaining in lower ½ of layer	fibers blackened, still pliable "
	11	+45° fabric	composite appears in sound condition	"
	12	90° fabric	"	"
	13	–45° fabric	"	"
	14	random mat	"	"
	15	0° roving	"	"
	16	+45° fabric	"	"
	17	90° fabric	"	"
	18	–45° fabric	"	"
	19	random mat	"	"
	20	+45° fabric	"	"
	21	90° fabric	"	"
	22	–45° fabric	"	"
	23	random mat	"	"
	24	0° roving	"	"
	25	+45° fabric	"	"
	26	90° roving	"	"
	27	–45° fabric	"	"
	28	random mat	"	"
	29	0° roving	"	"
	30	+45° fabric	"	"
	31	90° roving	"	"
	32	–45° fabric	"	"
	33	random mat	"	"
▼ Inner Deck Face (Cold Face)	34	surface veil	"	"

Table A-8. Dissection of reinforcement layers from hot face towards cold face

	#	Reinforcement	03A	03B	03C	03D
▲ Outer Deck Face (Hot Face)	1	surface veil	Damaged	Damaged	Damaged	Damaged
	2	random mat	"	"	"	"
	3	+45° fabric	"	"	"	"
	4	90° fabric	"	"	"	"
	5	–45° fabric	"	"	"	"
	6	0° roving	"	"	"	"
	7	random mat	Sound	"	"	"
	8	+45° fabric	"	"	"	"
	9	90° fabric	"	"	"	"
	10	–45° fabric	"	"	"	"
	11	0° roving	"	"	"	"
	12	+45° fabric	"	"	"	"
	13	90° fabric	"	"	"	"
	14	–45° fabric	"	"	"	"
	15	random mat	"	"	"	"
	16	+45° fabric	"	"	"	"
	17	90° fabric	"	"	"	"
	18	–45° fabric	"	"	"	"
	19	0° roving	"	Sound	"	"
	20	random mat	"	"	"	"
	21	+45° fabric	"	"	"	"
	22	90° roving	"	"	"	"
	23	–45° fabric	"	"	"	"
	24	random mat	"	"	"	"
	25	+45° fabric	"	"	"	"
	26	90° roving	"	"	"	"
	27	–45° fabric	"	"	"	"
	28	0° roving	"	"	"	"
	29	+45° fabric	"	"	"	"
	30	90° roving	"	"	"	"
	31	–45° fabric	"	"	"	"
	32	random mat	"	"	"	"
▼ Inner Deck Face (Cold Face)	33	surface veil	"	"	"	"

Figure A-1. Martin Marietta Composites' DuraSpan® 766 deck system

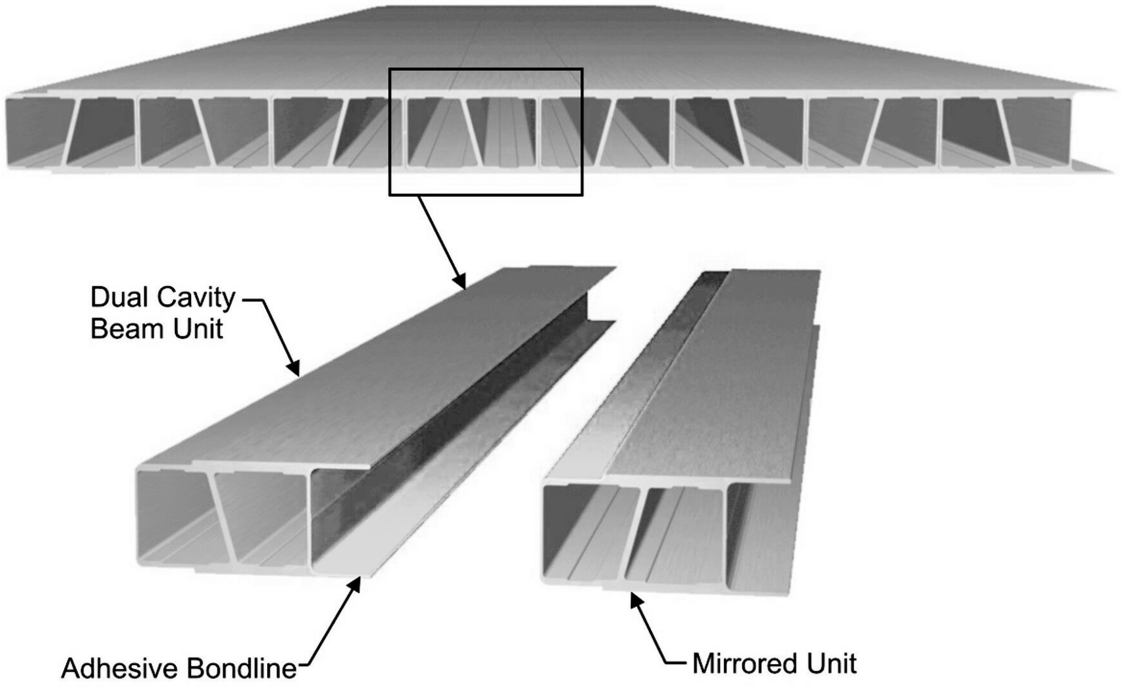

Figure A-2. Origin of specimens

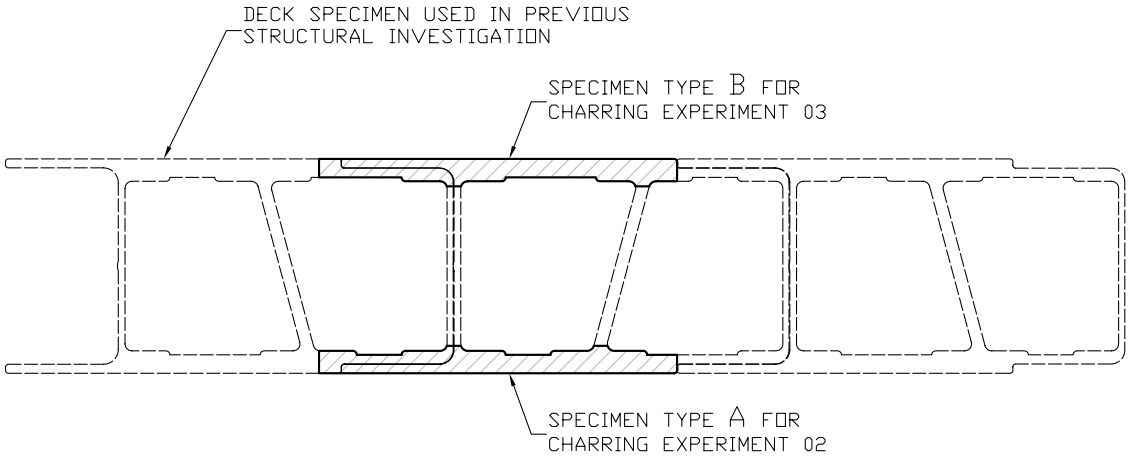

Figure A-3. Typical specimen after machining of thermocouple slots

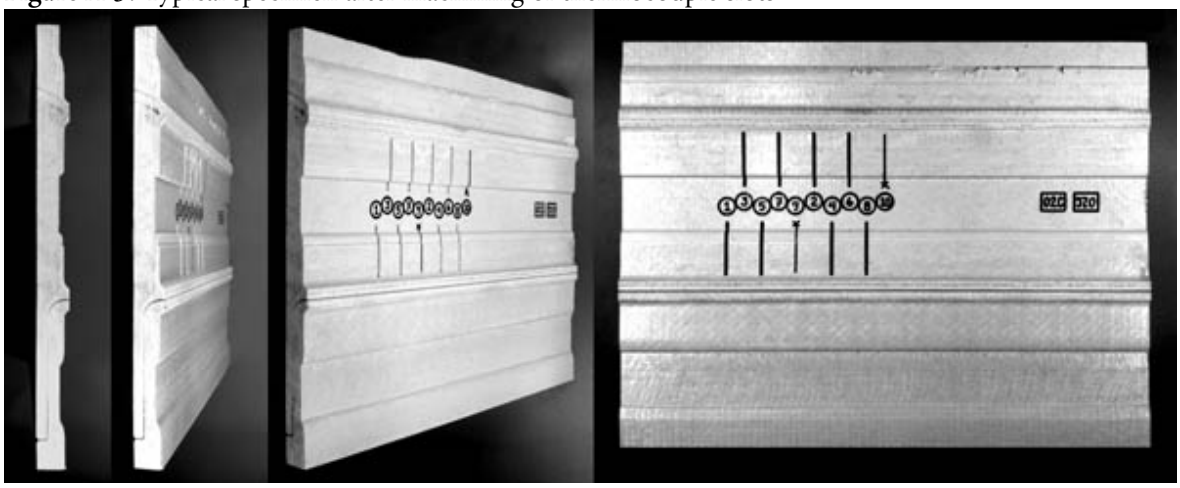

Figure A-4. DuraSpan 766 reinforcement layers (numbers correspond to Table A-5 - Schedule B)

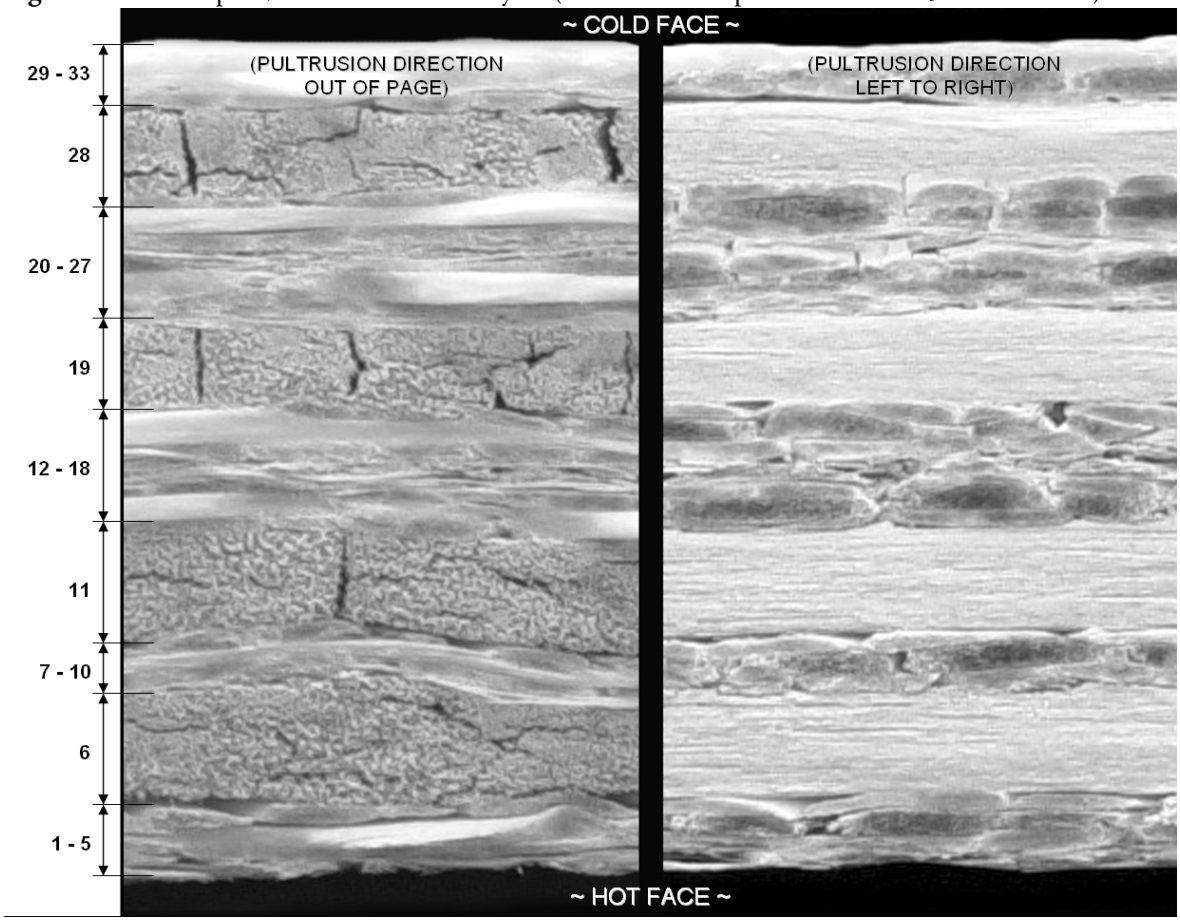

Figure A-5. CNC routing of slots for placement of thermocouples throughout depth

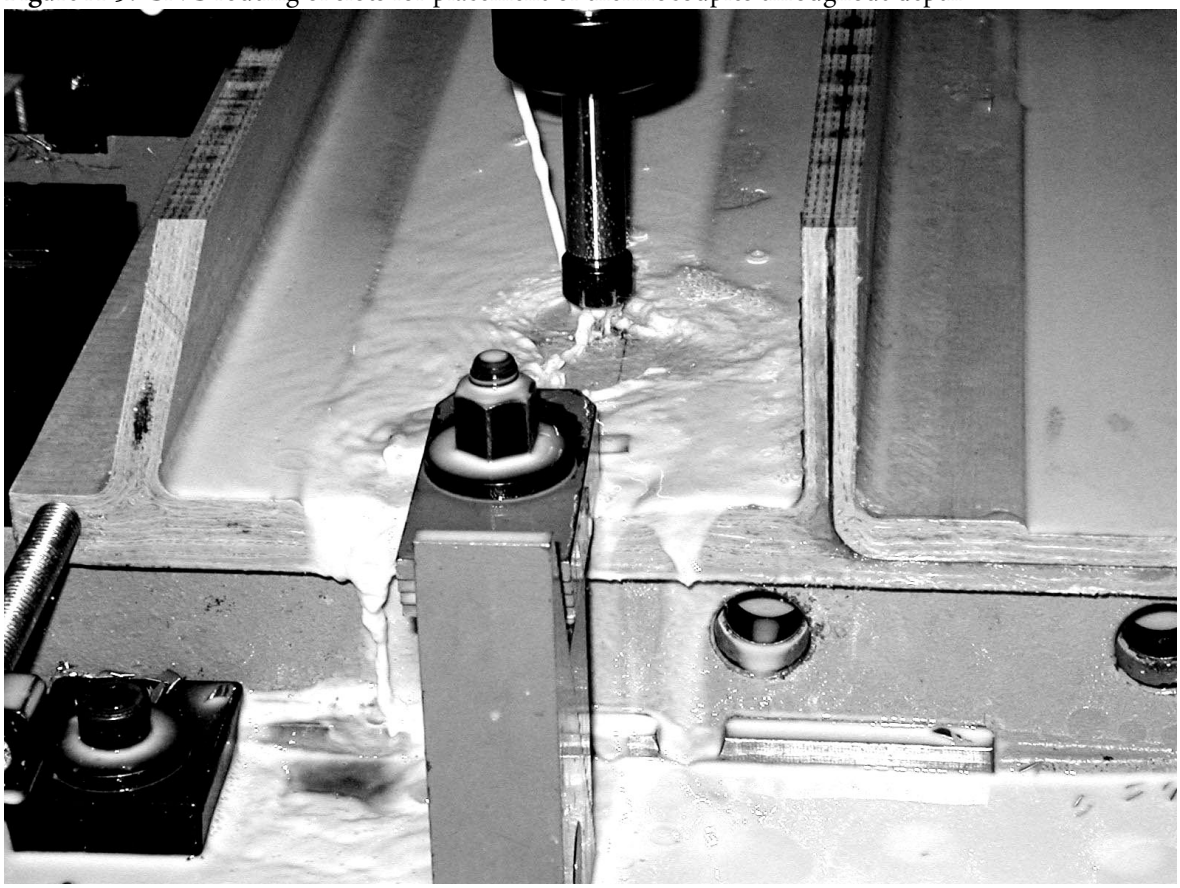

Figure A-6. Close-up photo of thermocouple slots

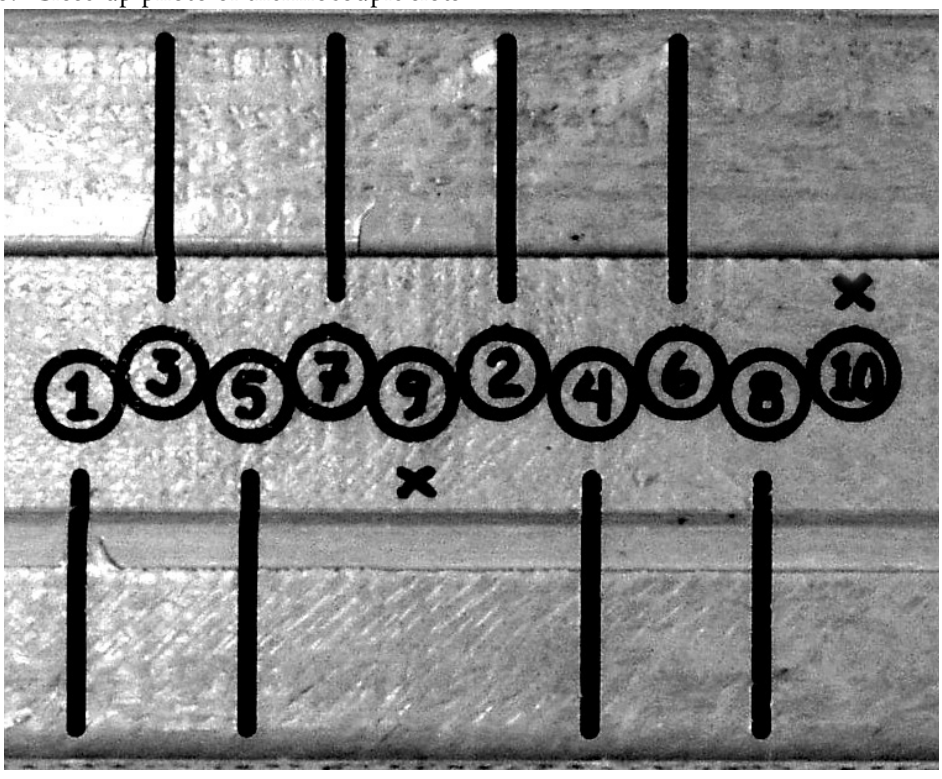

Figure A-7. Layout of thermocouples (all dimensions in millimeters)

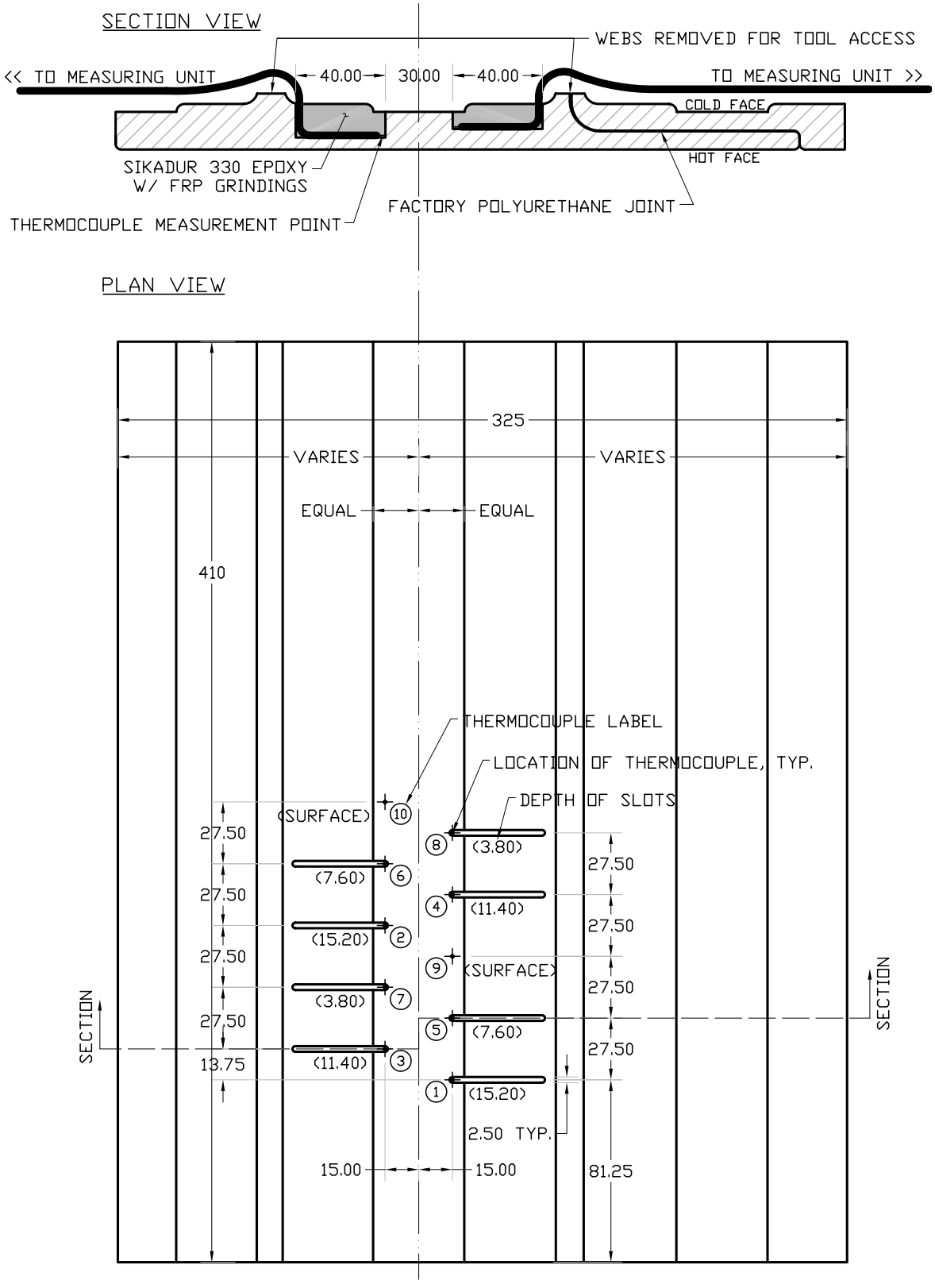

Figure A-8. CE02 - EMPA small horizontal oven with custom-built concrete cap

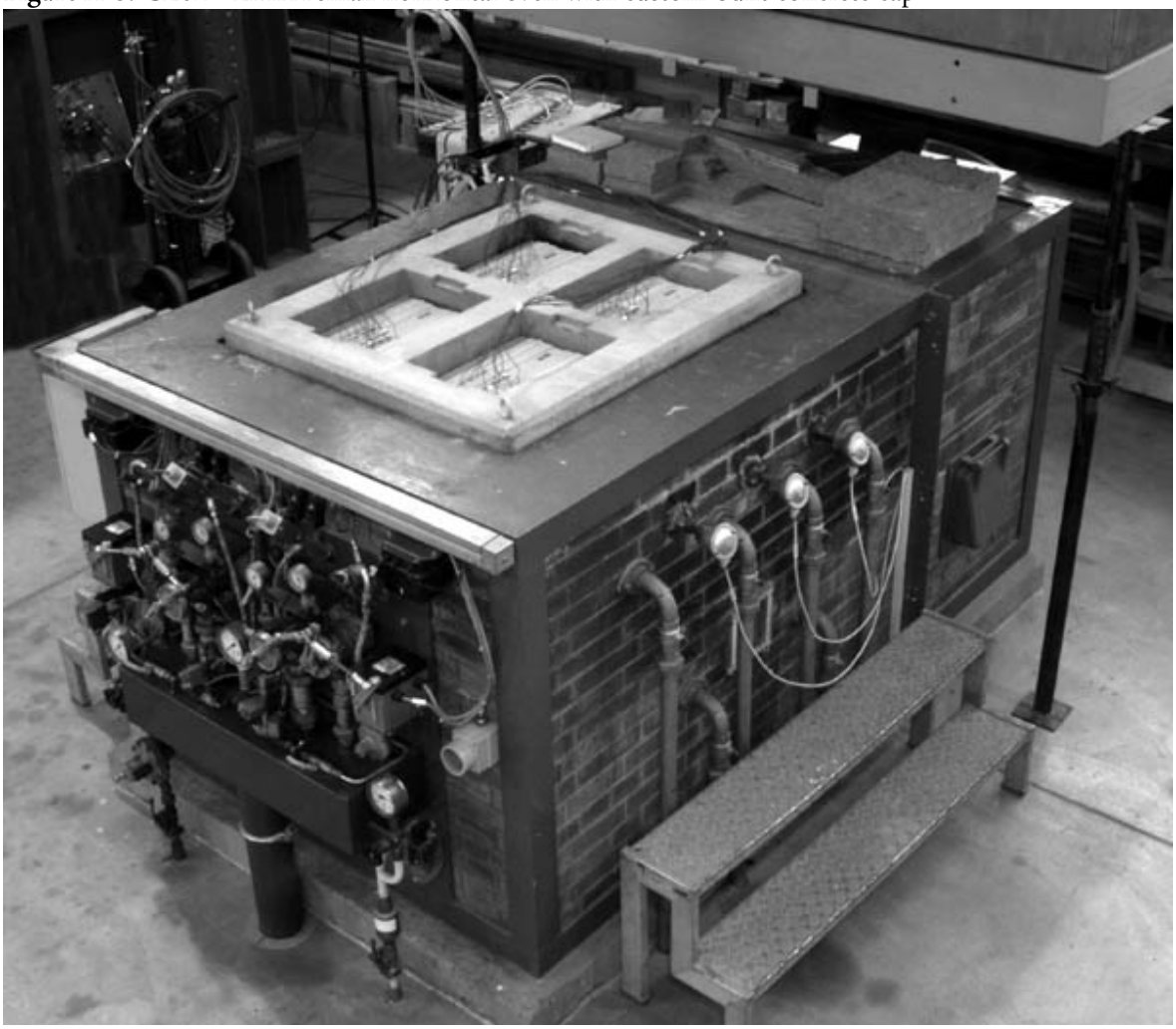

Figure A-9. CE02 - Ceramic wool insulation used to prevent the escape and spread of flames

Figure A-10. CE02 - 8 Minutes - Specimen hot face showing dark spots with no flaming combustion

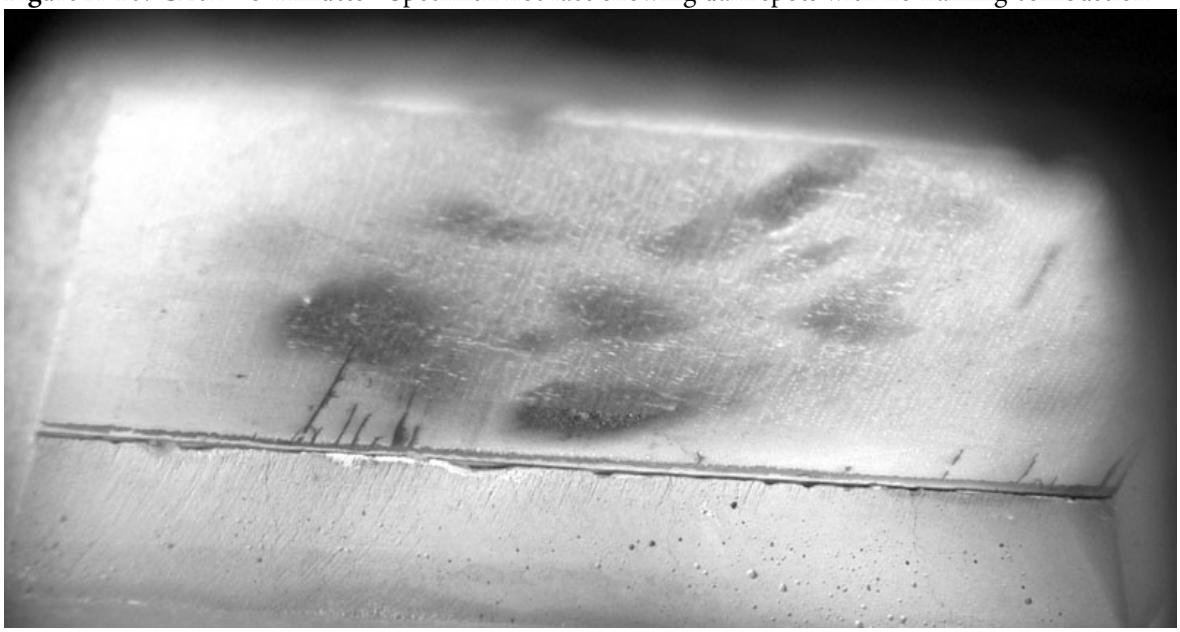

Figure A-11. CE02 - 12 Minutes - Flaming combustion engulfing hot face of specimen

Figure A-12. CE02 - 34 Minutes - Black char from resin mostly cleared out from hot face, white glass fiber char from random mat clearly visible

Figure A-13. CE03 - 52 Minutes - Surface veil/random mat cleared of resin char, fibers whitened, some fiber tips hanging down and glowing red

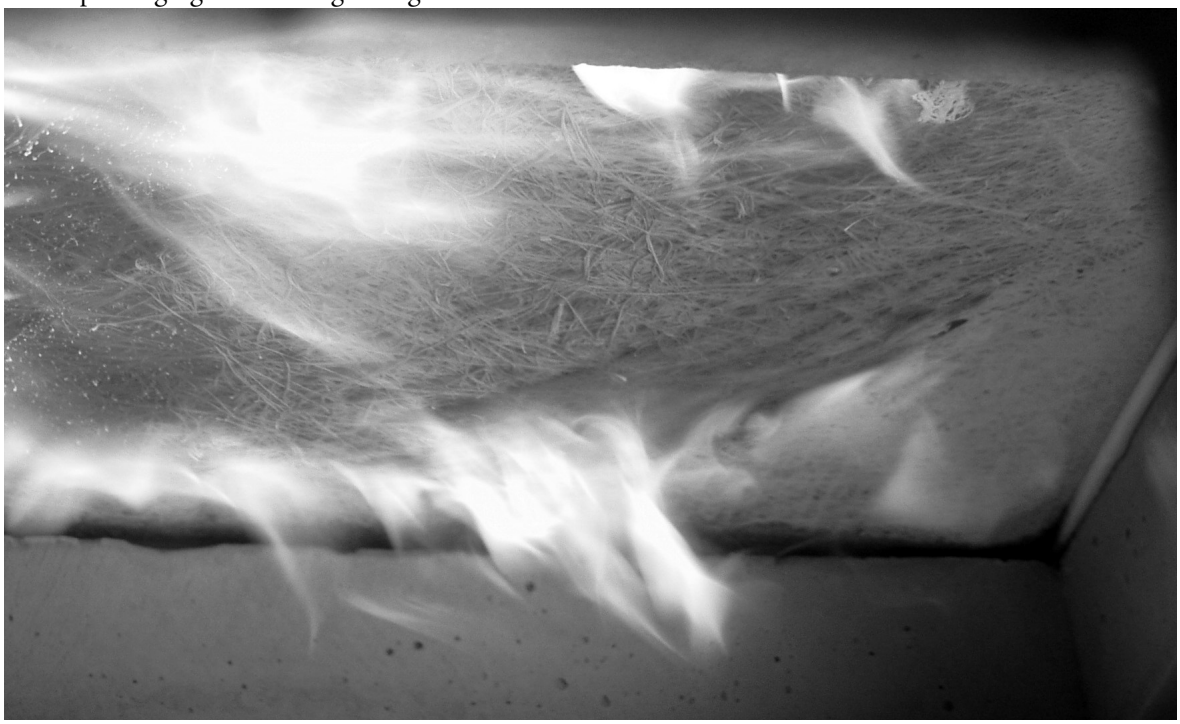

Figure A-14. CE02 - 59 Minutes - White char from surface veil/random mat fibers beginning to crack (flames still present, though not visible due to long exposure time of photograph)

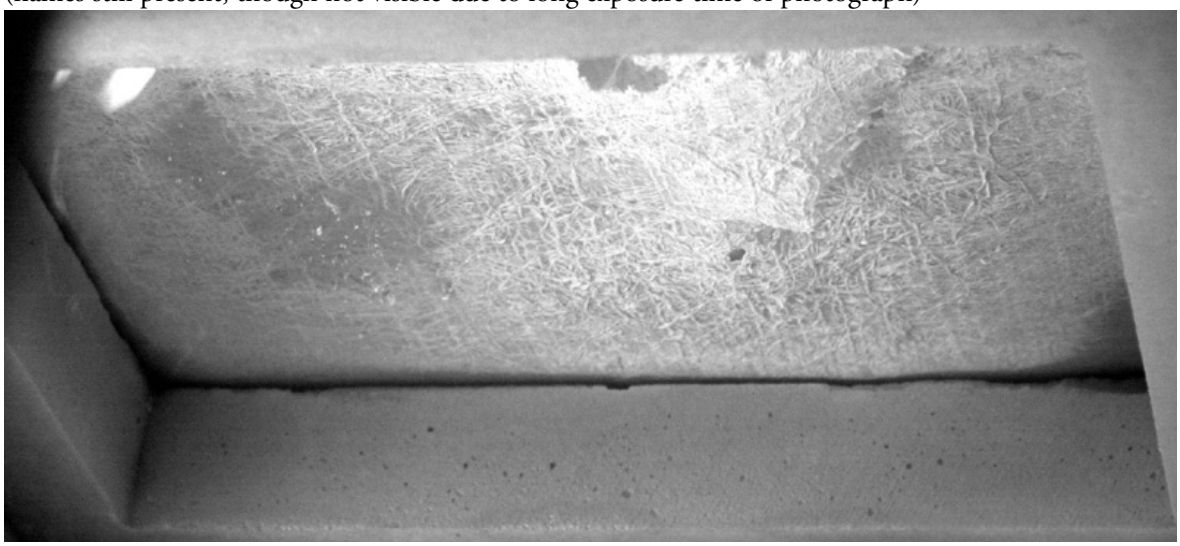

Figure A-15. CE02 - Epoxy used to fill in slots over thermocouples 1, 4, 5, and 8 of specimen 02D softening and flow out of slots

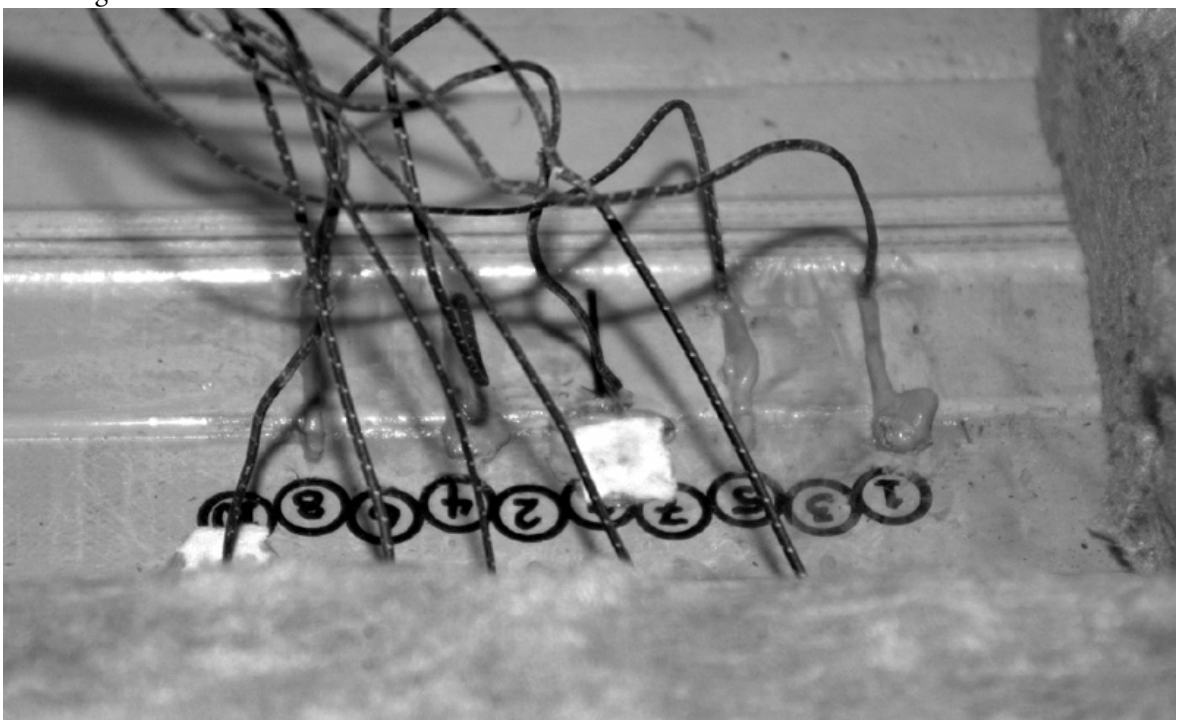

Figure A-16. CE03 - Styrene slowly bubbling up through cold face of specimen 03D

Figure A-17. CE02 - Removal of specimen 02D from oven exposure window after 30 minutes

Figure A-18. CE03 - Removal of specimen 03C from oven exposure window after 45 minutes

Figure A-19. CE03 - Cold faces of specimens after conclusion of experiment

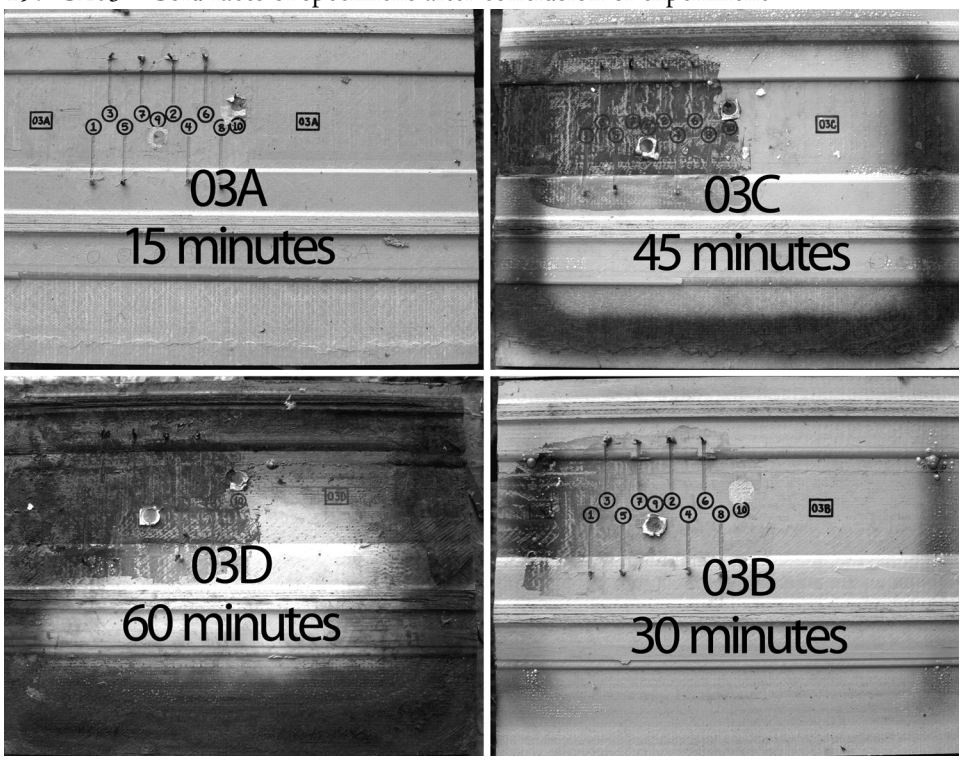

Figure A-20. CE03 - Hot faces of specimens after conclusion of experiment

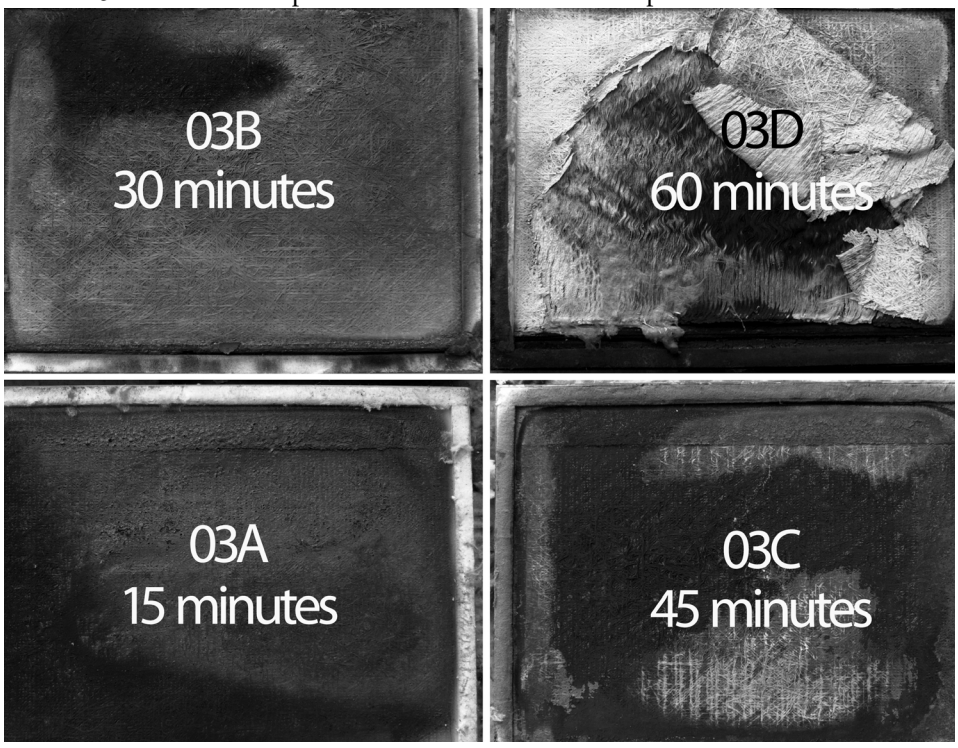

Figure A-21. CE02 - Temperature vs. time (labels refer to the thickness of material between the thermocouple and the hot face, dashed lines represent average values)

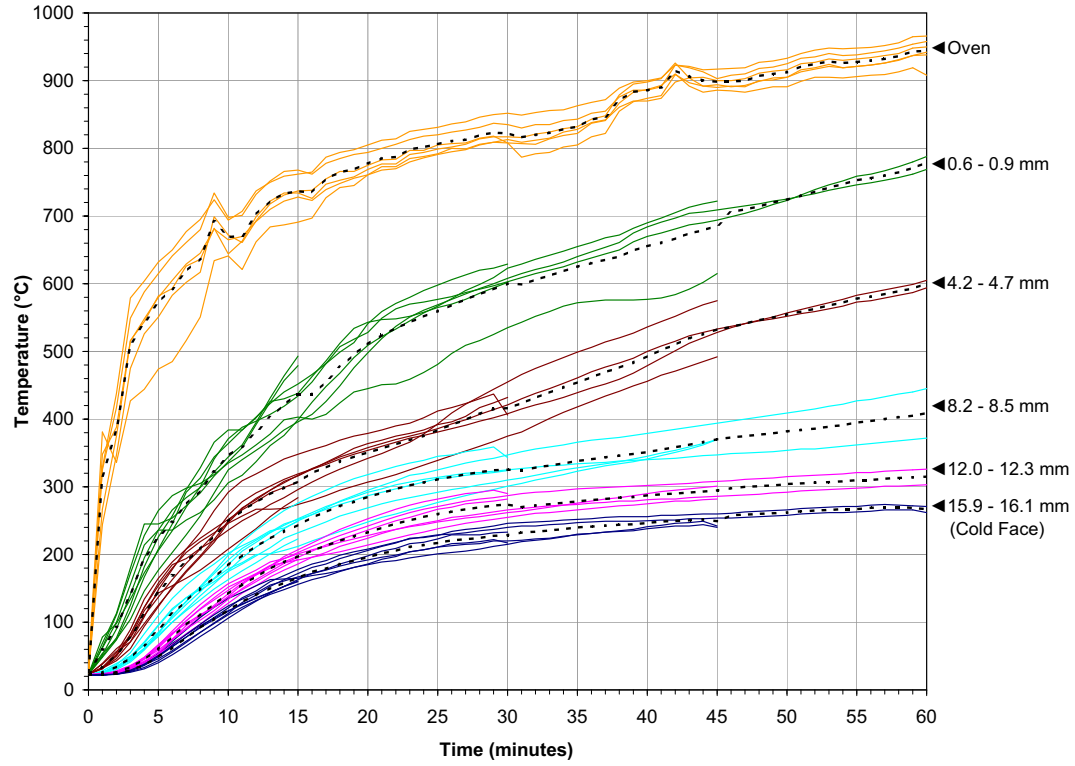

Figure A-22. CE03 - Temperature vs. time (labels refer to the thickness of material between the thermocouple and the hot face, dashed lines represent average values)

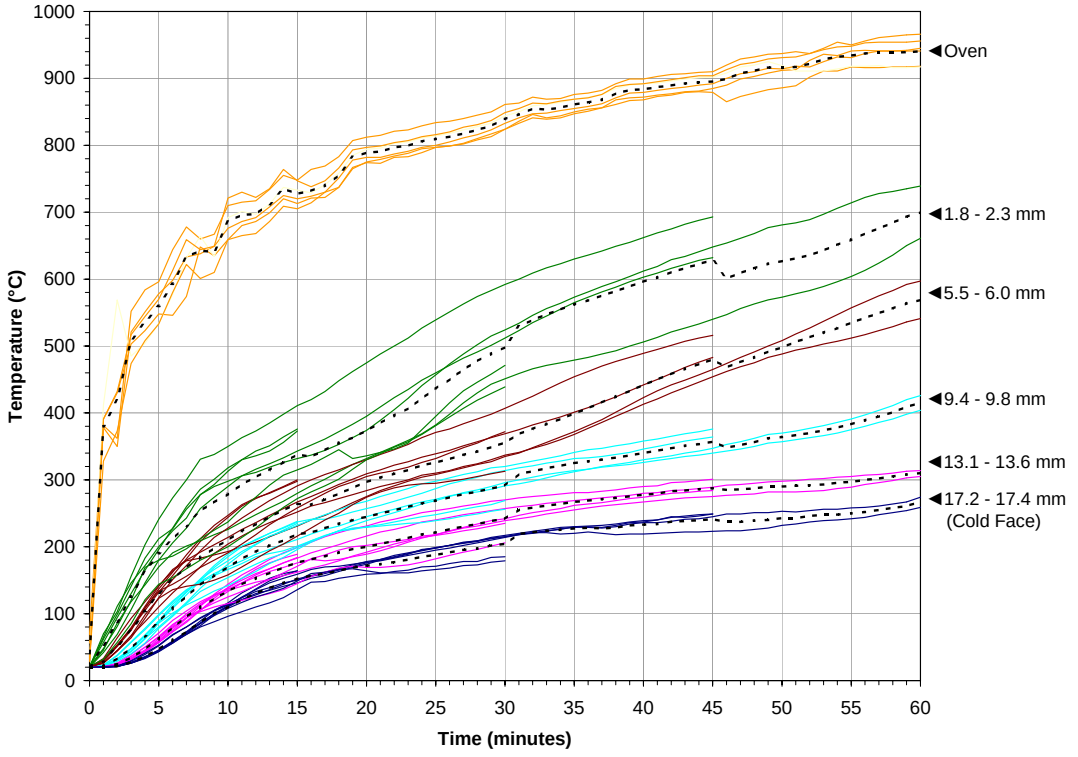

Figure A-23. Comparison of thermocouple readings from CE02 and CE03 (labels refer to experiment number and thickness of material below thermocouple)

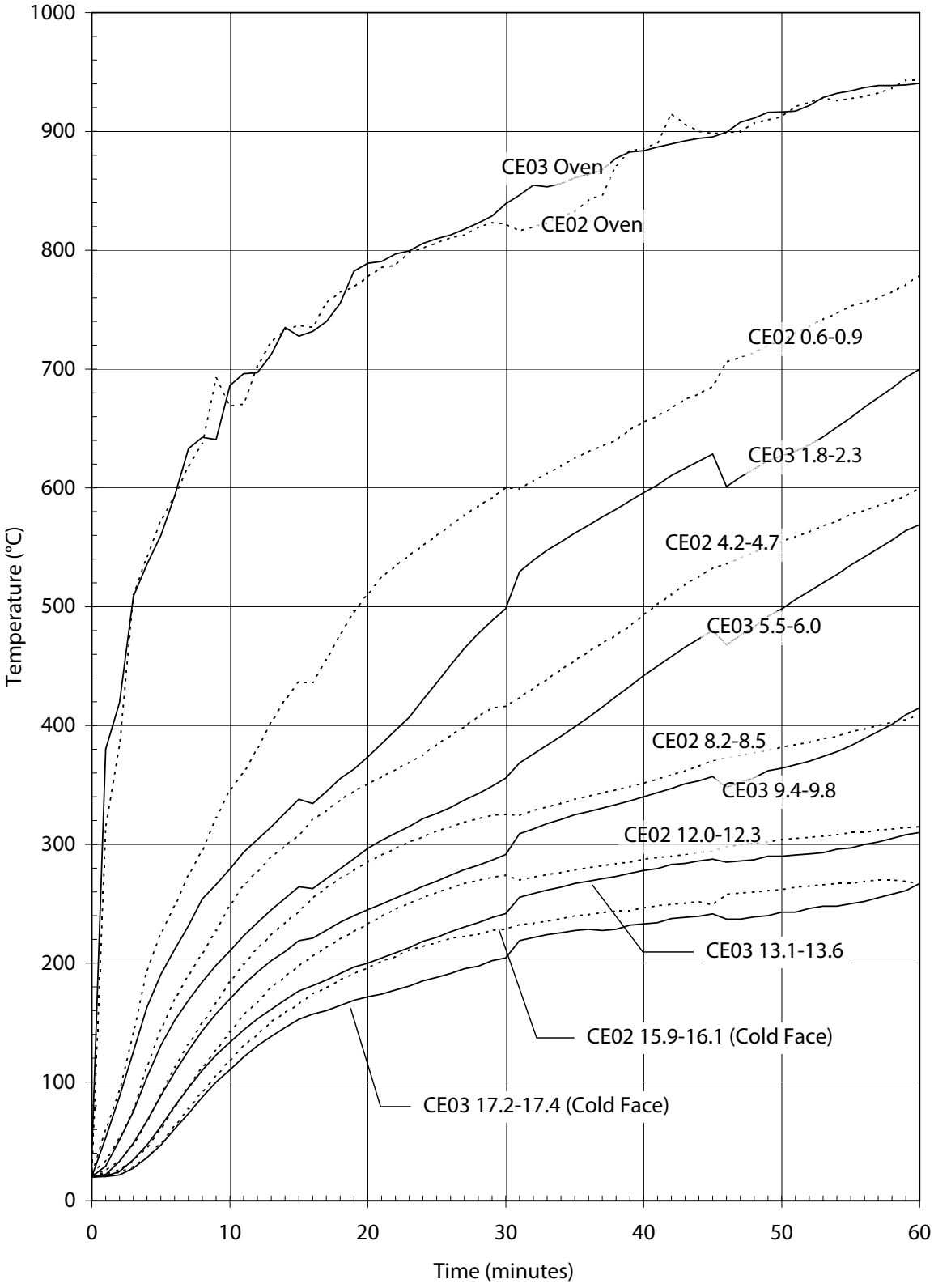

B

TECHNICAL REPORT

Liquid Cooling Experiments

*(Denoted herein as **Liquid Cooling Experiments LC01-LC03**)*

EPFL / CCLab - EMPA / Bauphysik - Craig Tracy - May 17th, 2004

Technical Report 2001.2/3

Liquid Cooling Experiments (LC01-LC03)

Liquid-Cooled GFRP Specimens on Small Horizontal Oven

1 Motivation and Summary

Small-Scale Liquid Cooling Experiments 01-03 (LC01-LC03) continue the investigation into the behavior of a glass fiber-reinforced polymer (GFRP) section exposed to high temperatures. Following the investigations where the cold face was cooled by natural convection of ambient air in Charring Experiments 01-03 (CE01-CE03), the LC experiments have been conducted to observe the thermal behavior of the same material when cooled instead by flowing water. All variables were kept as constant as possible in the three LC experiments except the water flow rate, which varied from 0.16 m^3/hr to 4.00 m^3/hr. The temperature profiles measured in both the CE and LC experiments will be used to calibrate the heat transfer of the numerical model. In addition, the small-scale experiments were helpful in discovering and resolving the issues that would be encountered in the large-scale experiments. These issues include the design of reliable water delivery and data acquisition systems and the verification of techniques for achieving water-tightness of the specimens. With the threat of hundreds of liters of water suddenly pouring into the 1000°C large oven facility during the large-scale experiments, the LC experiments provided a lower risk method to verify the safety of the procedures for both the people and the equipment.

2 Description of Specimens

2.1 Origin and Description of Basic Elements

The specimens under investigation were sections of Martin Marietta Composites' DuraSpan® 766 bridge deck. The glass-reinforced isophthalic polyester section is produced by the pultrusion process and resembles 19.5 cm tall trapezoidal tubes stacked in alternating directions.[1] The particular samples used in this investigation were cut from specimens used previously in structural experiments at the CCLab in Lausanne and then stored in an outside stockyard for approximately one year. Cutting of the final specimen size was conducted in Lausanne with a hand-held circular saw in December 2003. Taking from unaffected portions of the structural specimens, the thermal specimens showed no signs of damage.

The dimensions of the specimens were chosen to be 0.32 m x 1.13 m so that two full deck cells would be included and that the specimens would fit snugly on the test oven. Due to the tongue-and-groove connection method of the deck elements, the tongues of a second deck element were bonded to the specimen to create a rectangular shape. Sika Sikadur® 330 two-part epoxy adhesive was used for this bond.

To create a watertight vessel, Pultruded GRFP channel sections were bonded to over the ends of the specimens using the same epoxy adhesive. Just outside of the flanges of these channels, 2.5 cm holes were bored through the top flanges at one end of each cell. A rectangular section of 100 cm² was then cut away from the web separating the two cells at the opposite end. This permitted the water to enter through an orifice at one end, pass through the length of one cell (Cell A), cross over to the other cell (Cell B), and return the length of the specimen to the outlet orifice.

2.2 Instrumentation

In order to measure the temperature gradient between the oven interior and the flowing water, thermocouples were placed throughout the thickness of the lower face sheet. This was accomplished by routing slots from the interior face (cold face), which necessitated the cutting of access holes in the top flange. As the thermal performance of the top flange was not under

1. For clarity in terminology, the top and bottom of the deck will be referred to as the "upper face sheet" and "lower face sheet", while the inner and outer sides of the lower face sheet will be referred to as the "cold face" and "hot face".

study, the cutting of the holes had little effect on the experimental performance. When the machining was completed and the thermocouples were installed, the holes were sealed by bonding thin FRP plates to the interior face of the upper face sheet.

In an attempt to maintain the thermal continuity in the vicinity of the temperature readings, the slots that were cut to receive the thermocouples were refilled using a mixture of the previously mentioned epoxy adhesive and a powder made by grinding down other samples of the deck material.

The thermocouples, designated "Artikel-Nr. 24-K-GG" by the supplier, R. Wick AG, were Class II, with an accuracy of ±2.2°C or 0.75% of the measured temperature. The thermocouple wires exited the slots and passed along the walls of the cell interior until passing through one of the holes drilled through the sides of the specimens. But because the electrical insulation of the thermocouple wire was a fire-resistant fabric rather than a watertight plastic, a heat-shrink plastic insulation was placed over the portions of the wires that were within the specimens. This ensured that electricity could only pass between the two individual leads of the thermocouple wires where intended, i.e. at the soldered tips.

To verify the water tightness, water was circulated through the specimens the day before the thermal experiment. Small leaks were sometimes found at the holes where the thermocouple wires passed through the side walls, at the bonded joints, and at the plumbing connections. These leaks were all repaired with a rapid curing epoxy adhesive (Araldit® 5 Min. Rapid Epoxy - Ciba Spezialitätenchemie AG).

3 Experimental Set-up

Water was supplied by either the standard or the high-pressure fire plumbing of the test laboratory, depending on the required flow rate. The water passed through a calibrated and certified digital flow rate meter (accurate to 0.001 m^3/hr) before entering the specimens. Special pipe elbows that suspended thermocouples amidst the flowing water were placed just above the inlet and outlet couplings. An analog graphic recorder plotted water inlet and outlet temperatures versus time. An analog manometer was also installed just above the outlet coupling to observe the water pressure within the specimen for the high-flow experiment. After passing through the specimen, water passed through approximately 25 m of 2.5 cm rubber hose to a drain. A second outlet coupling was installed for the high-flow experiment to reduce the internal pressure. For the low-flow experiment, the end of the outlet hose was elevated 0.5 m above the specimen to maintain a positive pressure within. Summarizing, the path of the water was therefore: inlet hose » flow-rate control valve » flow-rate meter » inlet

thermocouple » interior of specimen Cell A » interior of specimen Cell B » manometer » outlet thermocouple » outlet hose.

4 Experimental Proceedings

4.1 Selection of Water Flow Rates

The first experiment, LC01, was conducted at very modest flow rate of 0.800 m^3/hr (0.220 l/s). The second experiment, LC03, was conducted at a very low flow rate of 0.160 m^3/hr (0.044 l/s), which is one-fifth the flow rate of LC01. The third experiment, LC02, was conducted at a rather high flow rate of 4.000 m^3/hr (1.111 l/s), which is five times the flow rate of LC01.

4.2 Duration of Experiments

In each of the experiments, two criteria were set to determine the end of the experiment: that water cannot leak into the oven and that the water cannot approach boiling. To enforce the first criterion, the limit was set that none of the four thermocouples 4-5 mm below the cold face of the lower flange could approach the decomposition temperature of the resin (250°C) and were thus limited to 200°C. This ensured that a minimum of 4-5 mm of material would remain in good condition to contain the water. The second criterion was enforced by limiting the temperature of the water at the outlet to 70°C.

Fortunately, neither of these criteria was needed for any of the experiments. Taking caution in the first experiment, LCO1 was stopped after 90 minutes, though neither of the limits had been exceeded. Gaining confidence from the post-experimental evaluation of the LC01 specimen, LC03 and LC02 were both run for a full 120 minutes, exceeding the code-required endurance time for load-bearing components in Swiss multiple-story buildings.

4.3 Temperature Loading

The experiments began with the circulation of water at the desired flow rate for approximately 10 minutes. This time permitted the water and the specimen temperatures to stabilize before the fire loading. Time began with the firing of the oil burners. The burners were automatically controlled by a computer, which read the oven temperature from the six internal thermocouples

and adjusted the intensity of the burners to follow the ISO 834 temperature curve. Oven and specimen temperatures were automatically logged every 60 seconds by a central digital unit, while water temperature was continuously recorded by a graphical unit. Notes and photos were taken through the observation window of the oven.

5 Post-Experimental Inspection of Specimens

The hot faces of the three specimens differed significantly from those of the Charring Experiments. While the hot faces of the CE specimens consisted of white glass char and black resin char, the LC specimens appeared far more damaged. The glass reinforcement appeared to have first melted and then drooped down directly into the burner flames. From there, it was completely oxidized into a sort of lightweight, brittle, foam-like char and eventually fell away. For the LC03 specimen (which had the lowest flow rate), the lower flange was reduced to roughly one-half of its original thickness. Large quantities of charred glass reinforcement were found at the bottom of the oven. For the LC01 specimen (which had the medium flow rate), more flange thickness was retained and less material was found at the bottom of the oven. For the LC02 specimen (which had the highest flow rate), it appeared that only the first of the four unidirectional roving layers was oxidized in this manner and nearly no material was found at the bottom of the oven.

6 Discussion of Results

6.1 Comparison to Charring Experiments

6.1.1 Damage to Hot Faces

As was stated in the previous section, the hot faces of the LC specimens appeared to be more severely damaged than the CE specimens. This is due to two important factors: the exposure time and geometrical shape of the specimens. The most harshly tested CE specimens were exposed to one hour of the ISO temperature curve, while LC specimens continued for another 30 to 60 minutes. Because this temperature curve follows a logarithmic function, doubling the exposure time has the effect of more than doubling the heat flux applied. The geometric differences were also an important factor because of the drooping effect in the reinforcement layers. In the Charring Experiments, the specimens were small rectangles that were supported

on all edges. This meant that the layers of reinforcement were less likely to droop down after the resin was removed and the glass was melted. The LC specimens, in contrast, were only supported on the short ends and were approximately 3.5X as long. This configuration made the reinforcement layers more susceptible to the drooping behavior. As each layer sagged and fell down, the radiation shielding that it provided was lost and the damage was allowed to penetrate further. Thus, the geometry and the exposure time make it difficult to make any useful conclusions about the effectiveness of the liquid cooling system by the comparison of the CE and LC hot faces.

6.1.2 Temperature Profile

As seen in Figure B-18, the LC specimens remained substantially cooler than the CE specimens. This effect is most prominent towards the cold faces, the greatest differences registering at the cold faces themselves. The effect was also more pronounced as the exposure time increased. While the curves all appeared similar during the first 10 minutes, the cold faces differed by ~200°C at 60 minutes. Comparing the steep slope of the CE02-Surface curve to the relatively flat LC-Surface curves, it is likely that this disparity would have further increased with additional exposure time.

It is also interesting to compare the temperatures recorded by the thermocouples placed approximately 4 mm below the cold face. The thermocouples of LC02 and LC03 were still below the glass transition temperature of the resin after 60 minutes, while those of the CE exceeded this limit in less than eight minutes. This suggests that liquid cooling could allow approximately 20% of the hot face material to provide structural resistance after one hour of fire loading.

6.2 Heat Transfer to Water

Using the recorded input and output temperatures of the flowing water, the amount of energy removed from the specimens by liquid cooling can be roughly calculated. Taking a linear approximation of the change in temperature, *T,* versus time, *t,* curves in Figure 13, one obtains the following functions:

$$\text{LC01:} \quad T = 0.5 + 0.0675 \cdot t \tag{B-1}$$

$$\text{LC02:} \quad T = \textit{no change measured}^{2} \tag{B-2}$$

2. Due to the high flow rate in LC02, the change in water temperature was too small to be measured by the equipment used.

$$\text{LC03:} \quad T = 0.5 + 0.2542 \cdot t \tag{B-3}$$

The change in temperature is related to energy absorbed through the equation:

$$H = m \cdot C_P \cdot \Delta T \tag{B-4}$$

Where H is the energy required to change a mass, m, of material with specific heat capacity, C_P, by ΔT degrees. Because ΔT varies with time, an average change in temperature, ΔT_{AVG}, will be substituted. Thus, the equation becomes:

$$H = m \cdot C_P \cdot \Delta T_{AVG} \tag{B-5}$$

The value of ΔT_{AVG} is found by integrating the change in temperature with respect to time and then dividing by the total time:

$$\Delta T_{AVG} = \left(\frac{1}{t_1} \right) \int_0^{t_1} t\,dt \tag{B-6}$$

Evaluating this equation for t_1 = 120 minutes and substituting into Equation 5, one obtains:

$$H_{LC01} = 15.3\ MJ \tag{B-7}$$

$$H_{LC03} = 10.6\ MJ \tag{B-8}$$

Further, if it is assumed that for LC02, $0 < \Delta T_{AVG} \leq 2°C$ (roughly the accuracy of the measurement), one can estimate:

$$0 < H_{LC02} \leq 33.6\ MJ \tag{B-9}$$

As expected, the amount of heat transferred to the water increased as the flow rate increased. This is explained by two factors. The first is that the convection heat transfer coefficient increases with increasing fluid velocity. The second is that the water remained cooler as the flow rate increased, which maintained a larger temperature gradient between the materials and thus a higher rate of heat transfer. This verifies that, within the range of water flow rates used, increasing the flow rate increases the cooling effect.

6.3 Internal Pressure

The act of forcing water to flow through a tortuous path within the specimen and then through the exit pipes and hoses caused friction. Increasing the velocity of the flowing water by increasing the flow rate increases the friction. The energy loss due to friction manifests itself as increased water pressure. Therefore, the higher the flow rate, the higher the internal pressure will be. This was observed in LC03 and LC02, where the internal pressure increased by

roughly 0.6 bars as the flow rate increased from 0.16 m³/hr to 4.00 m³/hr. The pressure increase would have been even higher if a second exit hose were not added to the high flow experiment.

As seen in Figure B-12, the high pressure in LC02 caused water to leak up through pinhole-sized imperfections in the thin plates. The decrease in negative gas pressure in the oven also suggests that some water was leaking into the oven. Though invisible to the eye, small amounts of water leaking into the oven would turn to vapor immediately and their increased volume would have the effect of lowering the negative oven pressure. This possibly occurred as the material below the thermocouple slots was removed and a passage for the water was created.

7 Conclusions

The following conclusions can be drawn from the three LC experiments:

- Temperatures within the lower flanges of the specimens remained significantly lower in the liquid cooling experiments than in the Charring Experiments.
- The cooling effect improved with increased flow rates. More sensitive temperature readings were necessary to quantify this effect at the highest flow rate.
- Internal pressures also increased with increasing flow rates. If future experiments retain the two-cell flow pattern and 2.5 cm ∅ outlet orifices, flow rates should be limited to 2 m³/hr per flow path to reduce the risk of leaking.
- At best, no more than 20% of the structural capacity of the bottom flange should be expected after one hour of fire loading.

Table B-1. Notes taken during LC01 - December 18, 2003

Time (hh:mm:ss)	Observations
0:02:50	No discoloration yet - small pieces of masking tape burning
0:05:40	First appearance of flames
0:07:00	Joint opening, flames dying out, random mat scoured clean of resin char
0:08:15	Flames starting to reappear
0:15:00	First white patches appearing on hot face, still flames
0:17:30	Small patches peeling away at far end of hot face (end farther from oil burner), white patches appearing at near end of hot face
0:23:00	Hot face completely white
0:33:00	Big section of random mat hanging down and blocking view of hot face
0:59:00	Lots of strips of glass char hanging down, some already fallen
1:16:00	Very small flames in limited areas

Table B-2. Notes taken during LC03 - January 15, 2004

Time (hh:mm:ss)	Observations
0:04:00	Starting to see delamination of bonded joint
0:04:40	First appearance of flames
0:05:19	Hot face blackened and flaming in front corner (closest to oil burner) where bonded joint is peeling apart
0:06:50	Flames died down, random mat totally blackened
0:10:10	Flames now covering entire hot face
0:17:10	Whitening in front portion, whole section below bonded joint hanging down
0:21:30	Water flow rate has dropped down to 0.11 m3/hr - had to open valve to build back flow rate - someone will constantly monitor the flow rate from now on and make adjustments accordingly, manometer reading 0.0 bars
0:30:50	Large white flap hanging down below bonded joint
0:36:15	Flaps hanging down and glowing red on both ends of specimen
0:39:10	According to fiber architecture schedule, specimen has lost surface veil, random mat, +45°, 90°, and -45° reinforcement layers
0:50:20	O° roving white and cracking

Time (hh:mm:ss)	Observations
1:02:00	First pieces of 0° roving hanging down
1:08:00	Larger section of 0° roving has fallen down
1:10:00	Another large section of 0° roving hanging down
1:24:00	Still another large section of 0° roving hanging down
1:52:00	No noticeable changes to hot face in past 30 minutes, very flew flames

Table B-3. Notes taken during LC02 - January 16, 2004

Time (hh:mm:ss)	Observations
0:00:30	Manometer reading 0.6 bars
0:03:30	Flames starting in front corner (closest to oil burner)
0:10:30	Hot face totally black, flames have spread from front to back end
0:14:20	Whitening in front corner and peeling away
0:25:00	White area extending along bonded joint
0:28:00	Bonded joint area hanging on at one edge
0:35:00	White flap turning to foam and bubbling up
0:41:00	Flap from main section of specimen hanging down, whitened, bubbling up, appears to consist of surface veil, random mat, and first +45° reinforcement layer
1:02:00	A segment of 0° roving hanging down near bonded area
1:11:00	Small flames in small patches
1:27:00	Even fewer flames, pressure in oven has dropped several times from -10 to -2 Pa, which might mean that water is leaking into the oven

Figure B-1. Construction of specimens

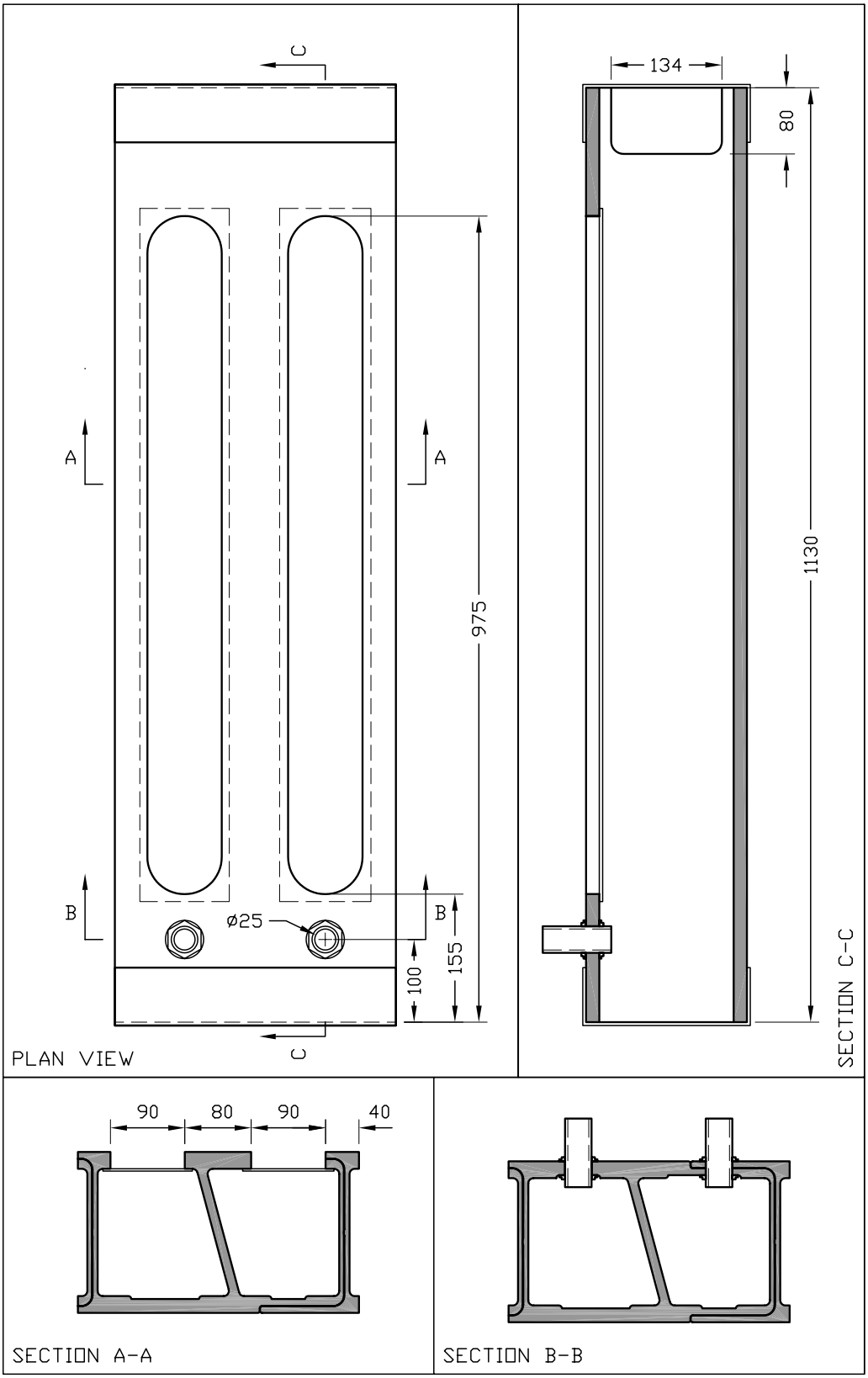

Figure B-2. Layout of thermocouples

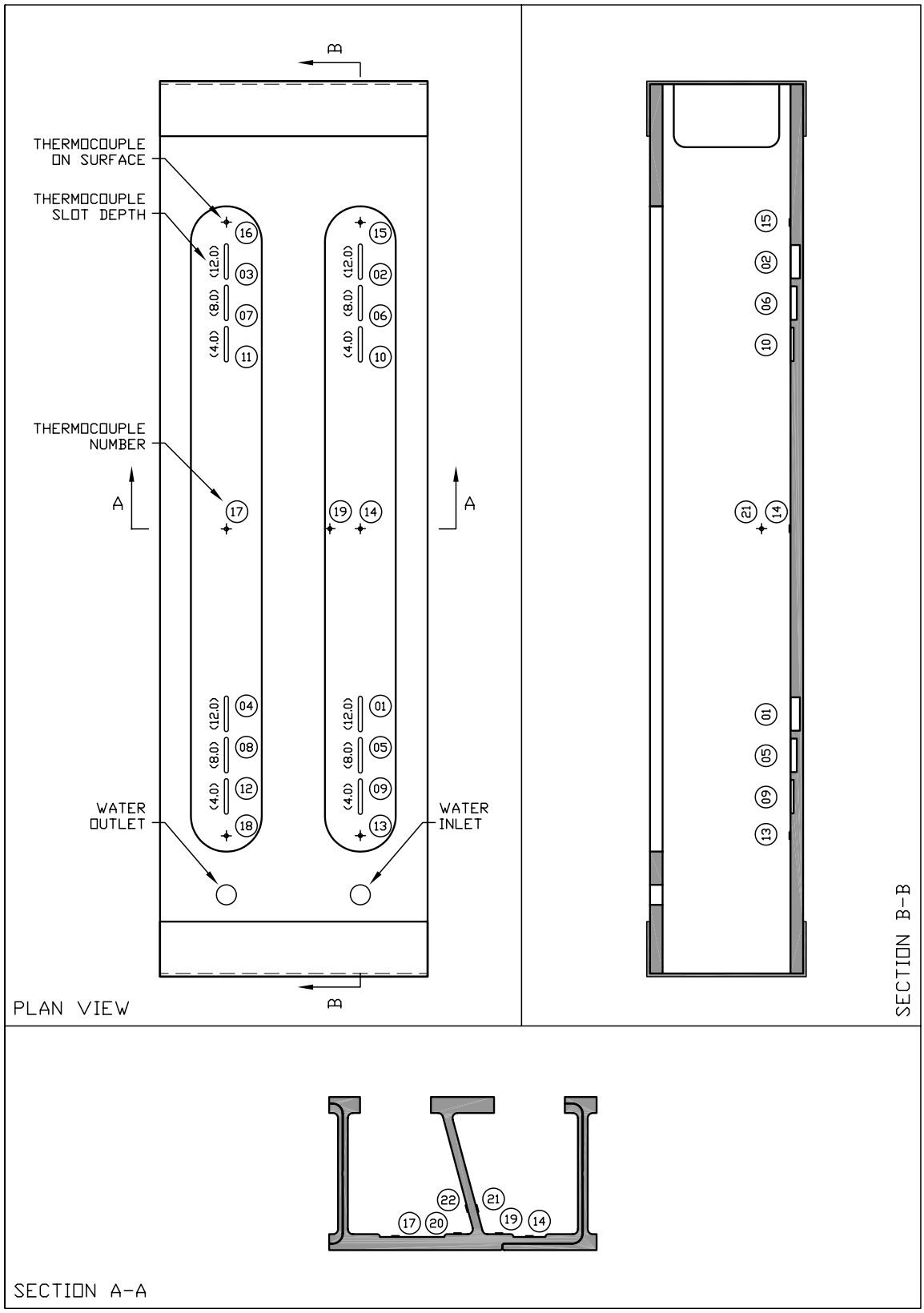

Table B-4. Measurement of as-built thermocouple slot depth and flange thickness (all dimensions in mm)

LC01 - Cell A	A	B	C	D	AVG	THICKNESS UNDER
Total Thickness	18.11	18.29	17.83	18.14	**18.1**	
Slot 1	11.03	11.03	-	-	11.0	**7.1**
Slot 2	5.15	5.18	-	-	5.2	**12.9**
Slot 3	4.75	4.78	-	-	4.8	**13.3**
Slot 4	10.21	10.16	-	-	10.2	**7.9**

LC01 - Cell B	A	B	C	D	AVG	THICKNESS UNDER
Total Thickness	17.50	17.44	17.45	17.41	**17.5**	
Slot 5	9.92	9.69	-	-	9.8	**7.7**
Slot 6	5.12	5.16	-	-	5.1	**12.4**
Slot 7	10.07	9.91	-	-	10.0	**7.5**
Slot 8	8.05	7.77	-	-	7.9	**9.6**

LC02 - Cell A	A	B	C	D	AVG	THICKNESS UNDER
Total Thickness	17.76	17.89	17.33	17.24	**17.7**	
Slot 1	11.87	11.82	-	-	11.8	**5.9**
Slot 2	11.56	11.56	-	-	11.6	**6.1**
Slot 5	7.69	7.68	-	-	7.7	**10.0**
Slot 6	7.62	7.63	-	-	7.6	**10.1**
Slot 9	4.27	4.24	-	-	4.3	**13.4**
Slot 10	3.84	3.88	-	-	3.9	**13.8**

LC02 - Cell B	A	B	C	D	AVG	THICKNESS UNDER
Total Thickness	17.05	17.13	17.05	16.95	**17.1**	
Slot 3	11.84	11.85	-	-	11.8	**5.3**
Slot 4	11.82	11.78	-	-	11.8	**5.3**
Slot 7	7.85	7.80	-	-	7.8	**9.3**
Slot 8	7.74	7.95	-	-	7.8	**9.3**
Slot 11	3.92	3.90	-	-	3.9	**13.2**
Slot 12	4.13	4.11	-	-	4.1	**13.0**

LC03 - Cell A	A	B	C	D	AVG	THICKNESS UNDER
Total Thickness	17.83	17.60	18.28	18.15	**17.9**	
Slot 1	11.64	11.77	-	-	11.7	**6.2**
Slot 2	11.59	11.59	-	-	11.6	**6.3**
Slot 5	7.38	7.39	-	-	7.4	**10.5**
Slot 6	7.63	7.64	-	-	7.6	**10.3**
Slot 9	3.61	3.60	-	-	3.6	**14.3**
Slot 10	4.13	4.12	-	-	4.1	**13.8**

LC03 - Cell B	A	B	C	D	AVG	THICKNESS UNDER
Total Thickness	17.40	17.38	17.31	17.40	**17.4**	
Slot 3	11.71	11.73	-	-	11.7	**5.7**
Slot 4	12.03	12.05	-	-	12.0	**5.4**
Slot 7	7.92	7.88	-	-	7.9	**9.5**
Slot 8	7.68	7.73	-	-	7.7	**9.7**
Slot 11	4.36	4.33	-	-	4.3	**13.1**
Slot 12	3.89	3.93	-	-	3.9	**13.5**

Figure B-3. LC01 Specimen prepared for installation of thermocouples

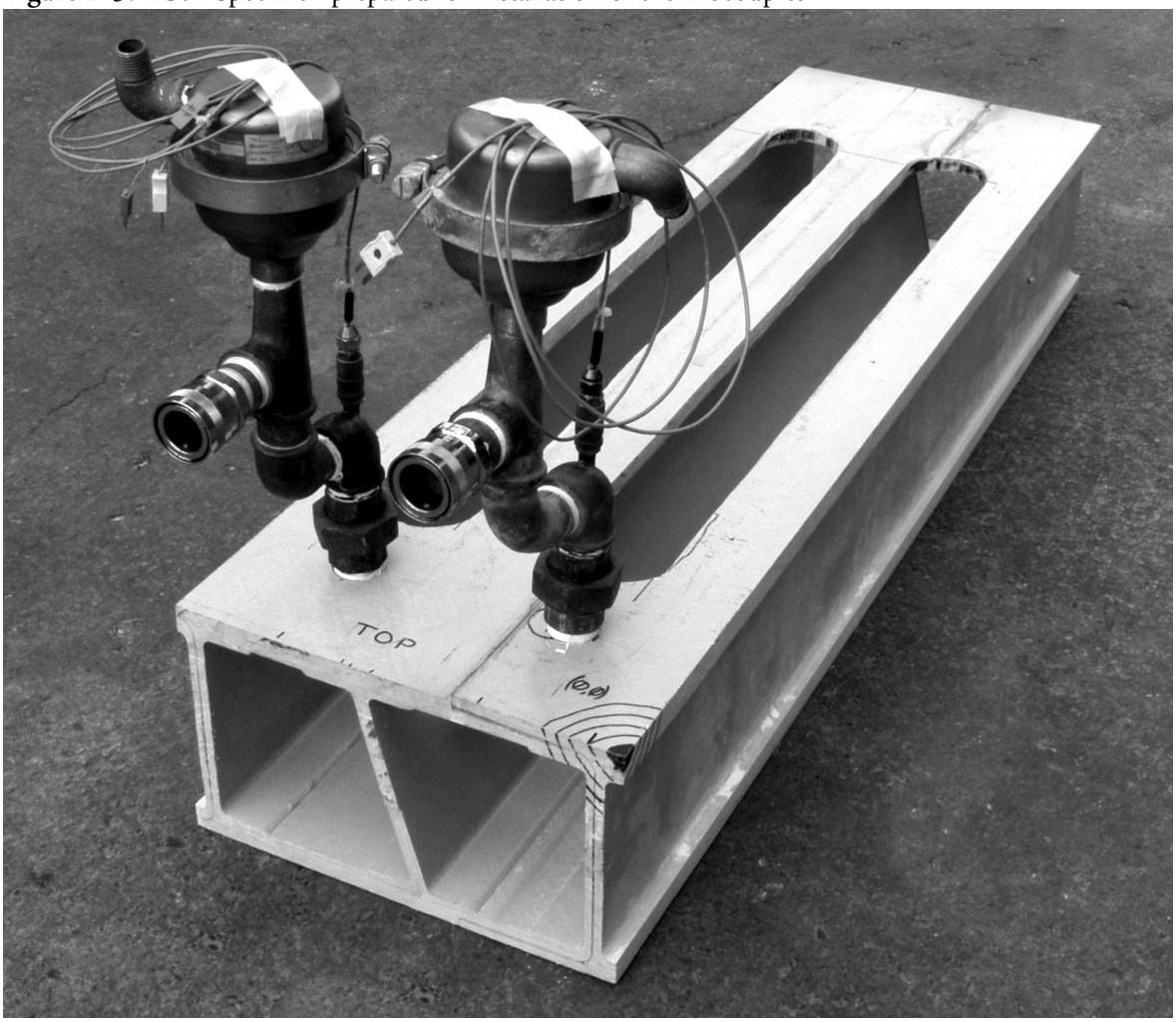

Figure B-4. Installation of thermocouples on Specimen LC03

Figure B-5. Detail of specimen LC02 showing end-closure channels and water connections

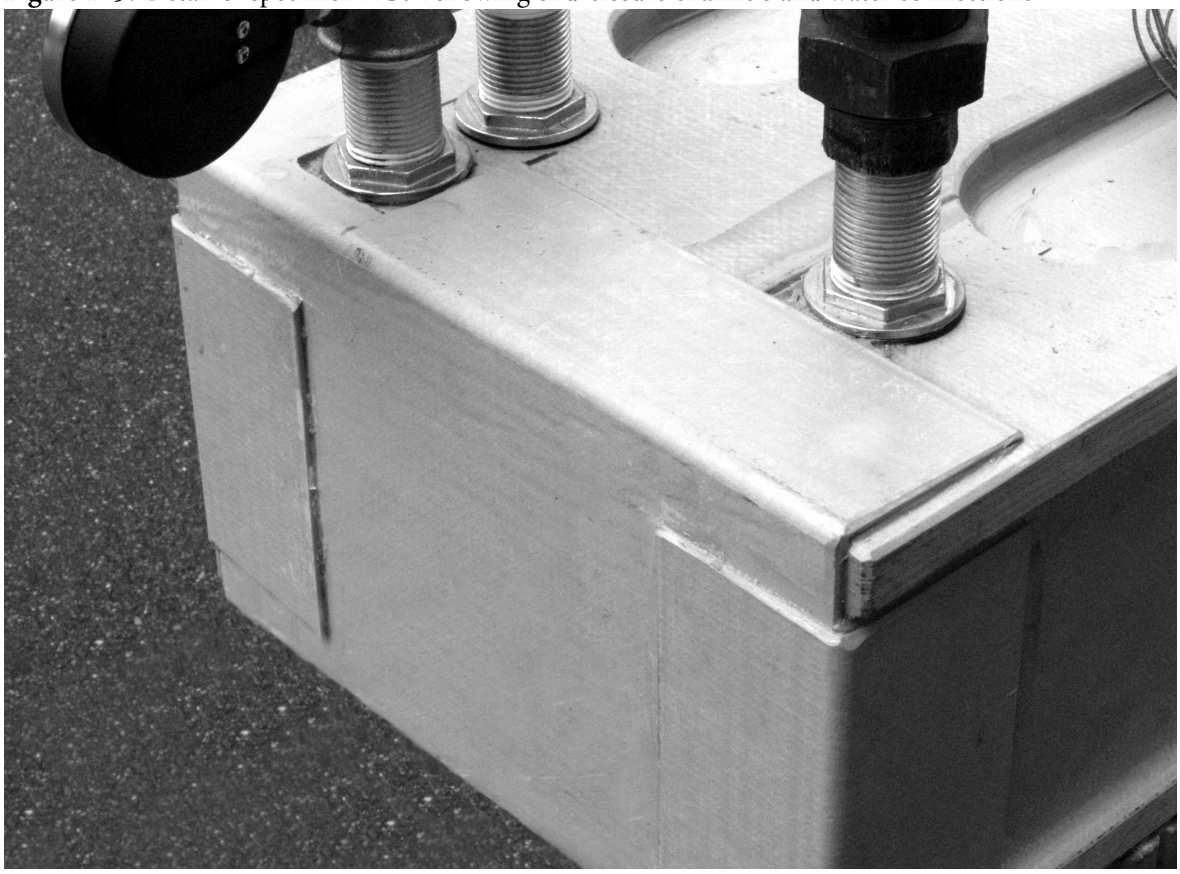

Figure B-6. Experimental set-up for LC03 with inlet hose on left and outlet hose on right

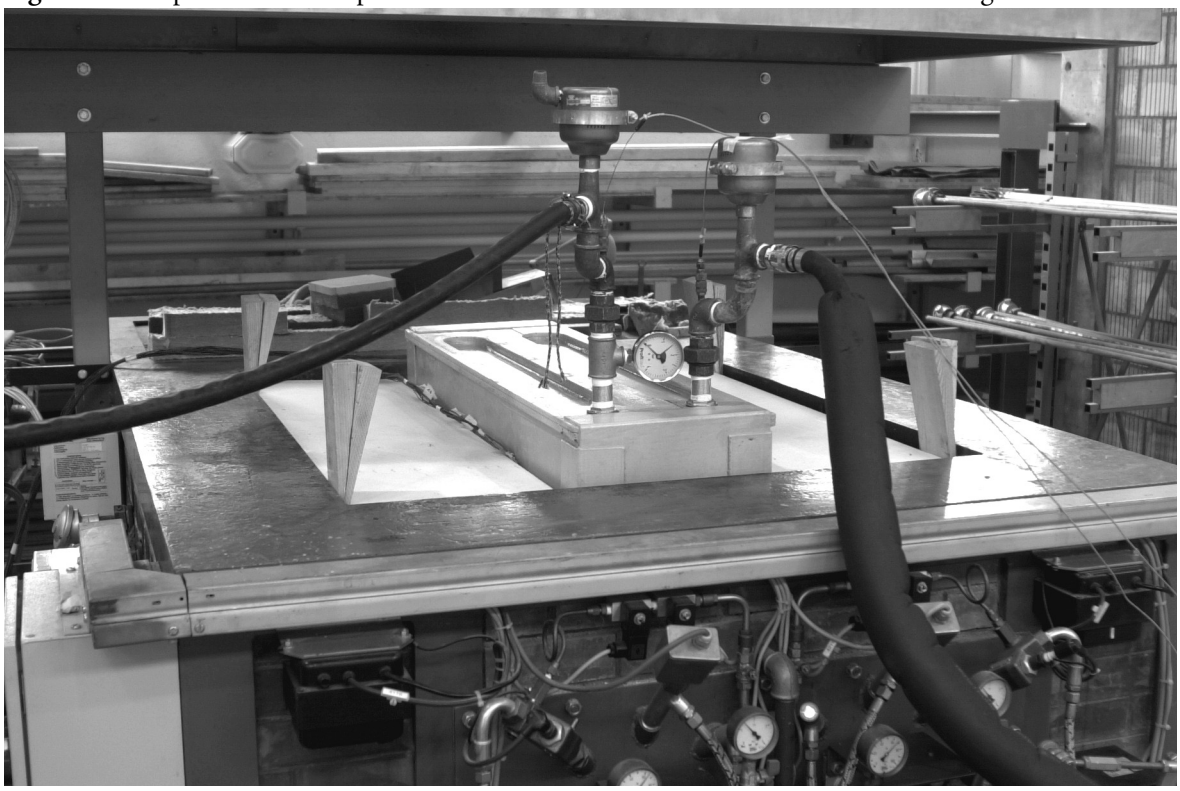

Figure B-7. Progression of damage across hot face of LC03 demonstrates the uneven heat flux applied by the oven

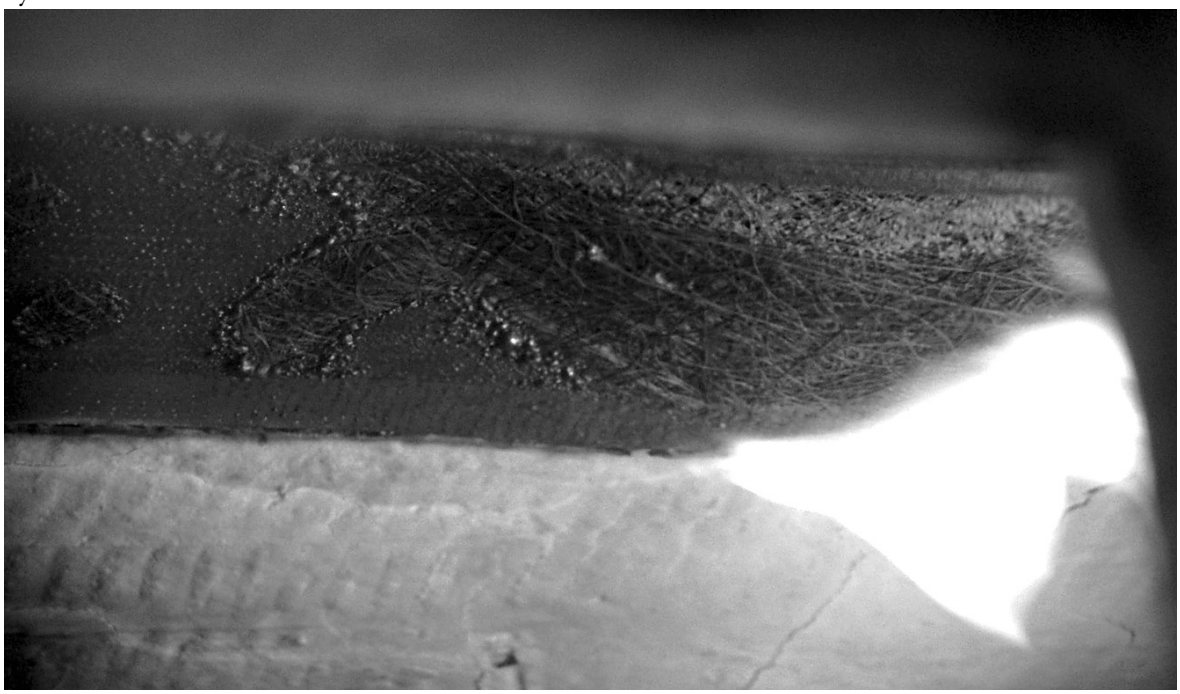

Figure B-8. Progression of damage across hot face of LC02

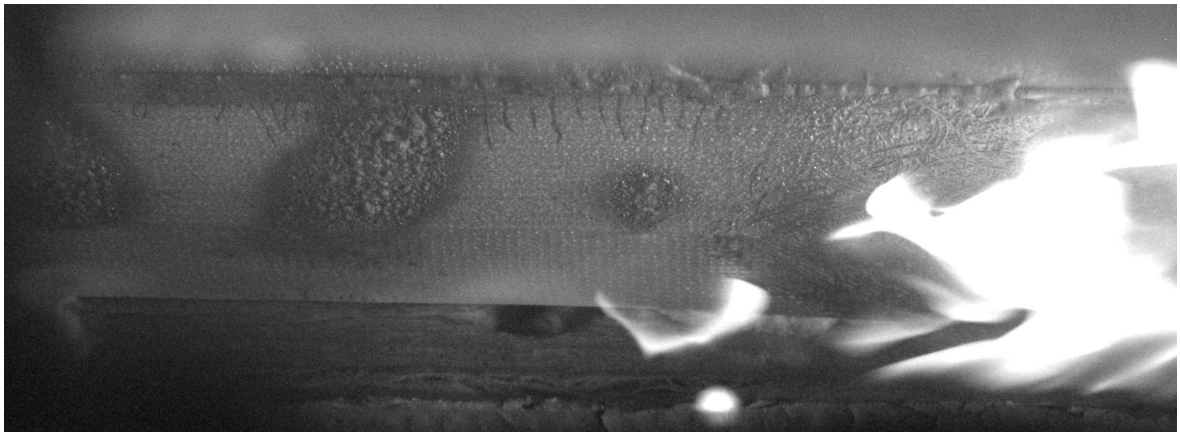

Figure B-9. Random mat whitened and bubbling into foam-like char in LC02

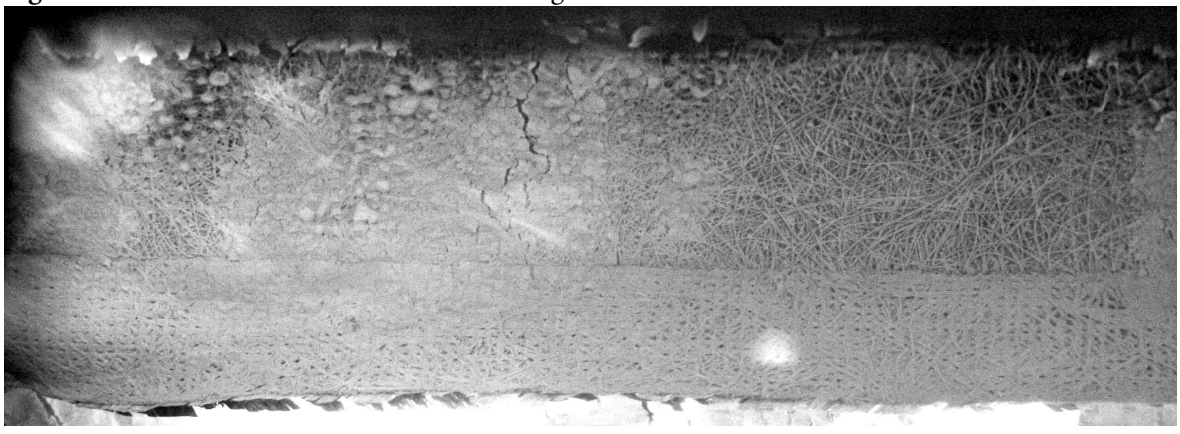

Figure B-10. Reinforcing fibers drooping down and oxidizing during LC03

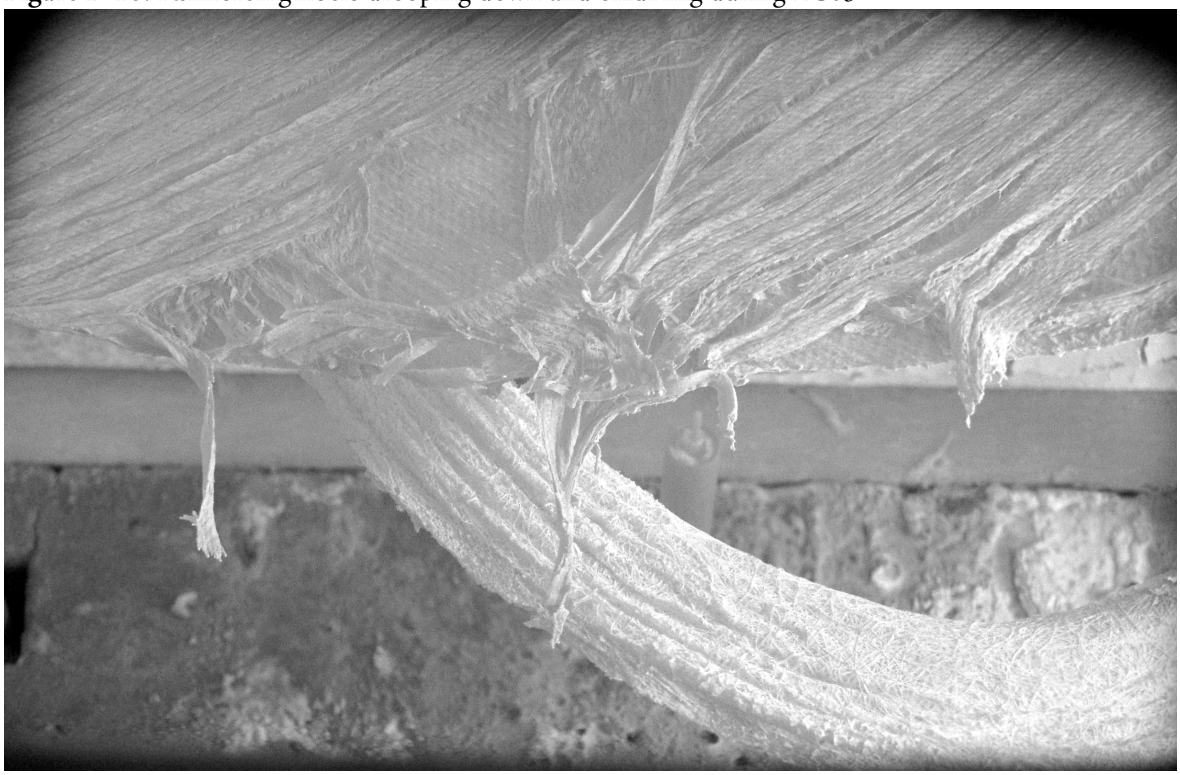

Figure B-11. Drooping reinforcement layers turning to foam-like char during LC03

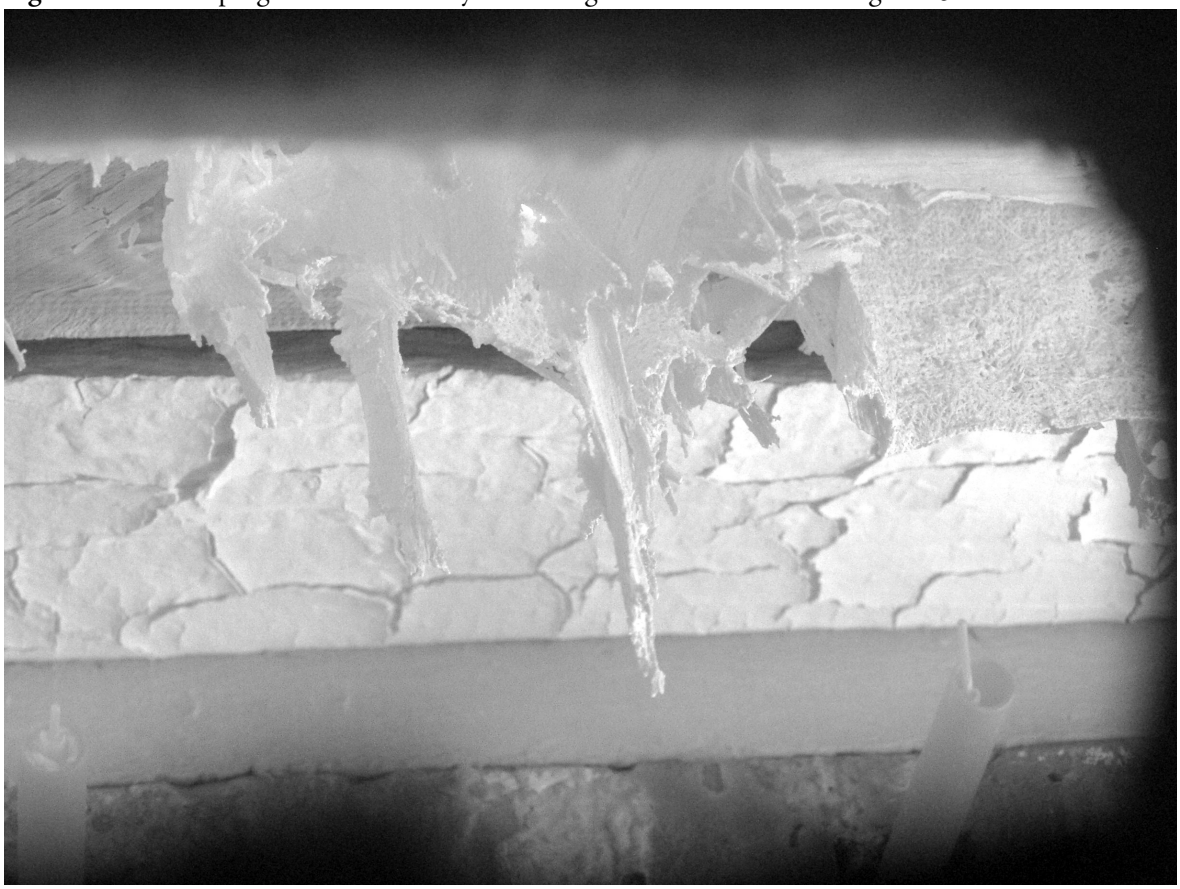

Figure B-12. High pressure in LC02 causes water to leak up through pinholes in the thin plates used to cover the access holes

Figure B-13. Post-experiment hot face of LC03

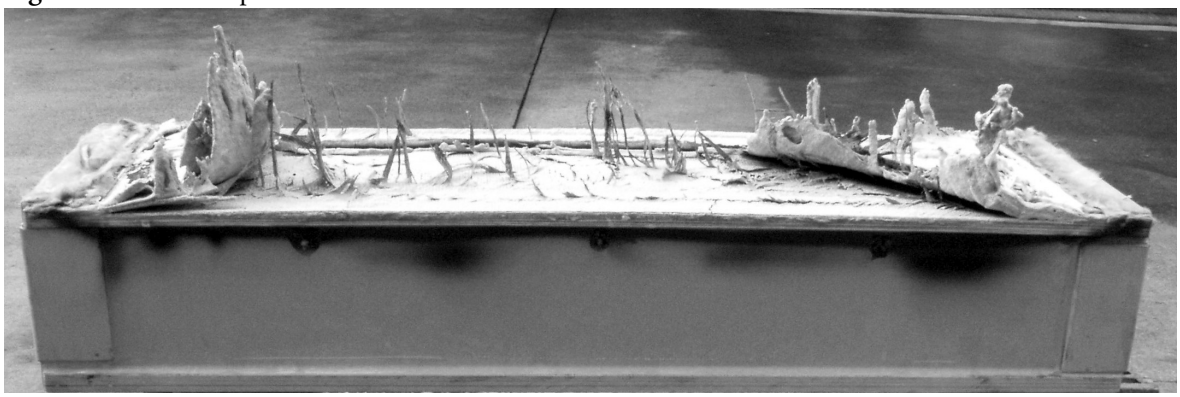

Figure B-14. Water temperature versus time - All LC Experiments

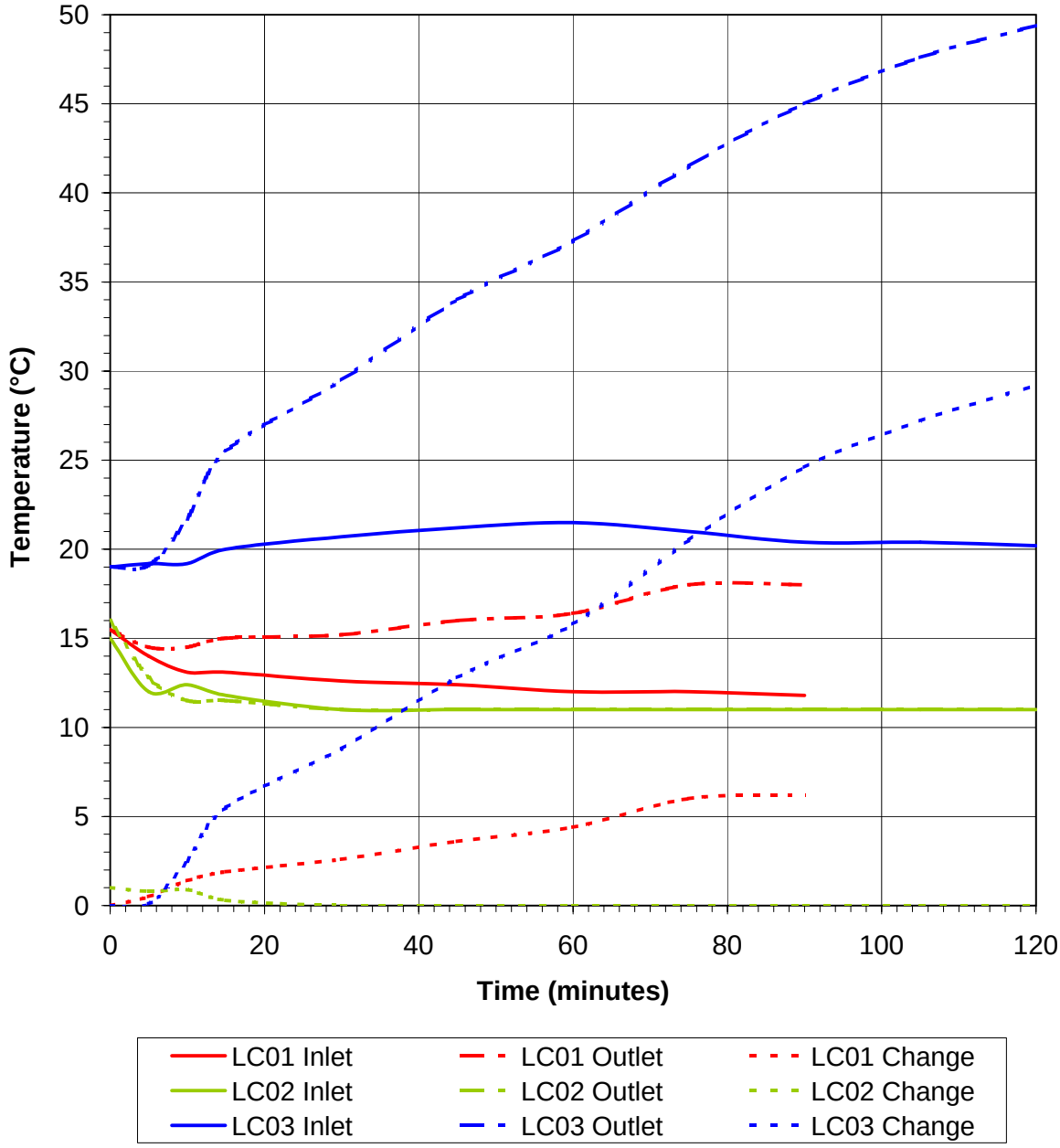

Figure B-15. Temperatures recorded during LC01 (numbers in boxes refer to thermocouple number and measured thickness of material below)

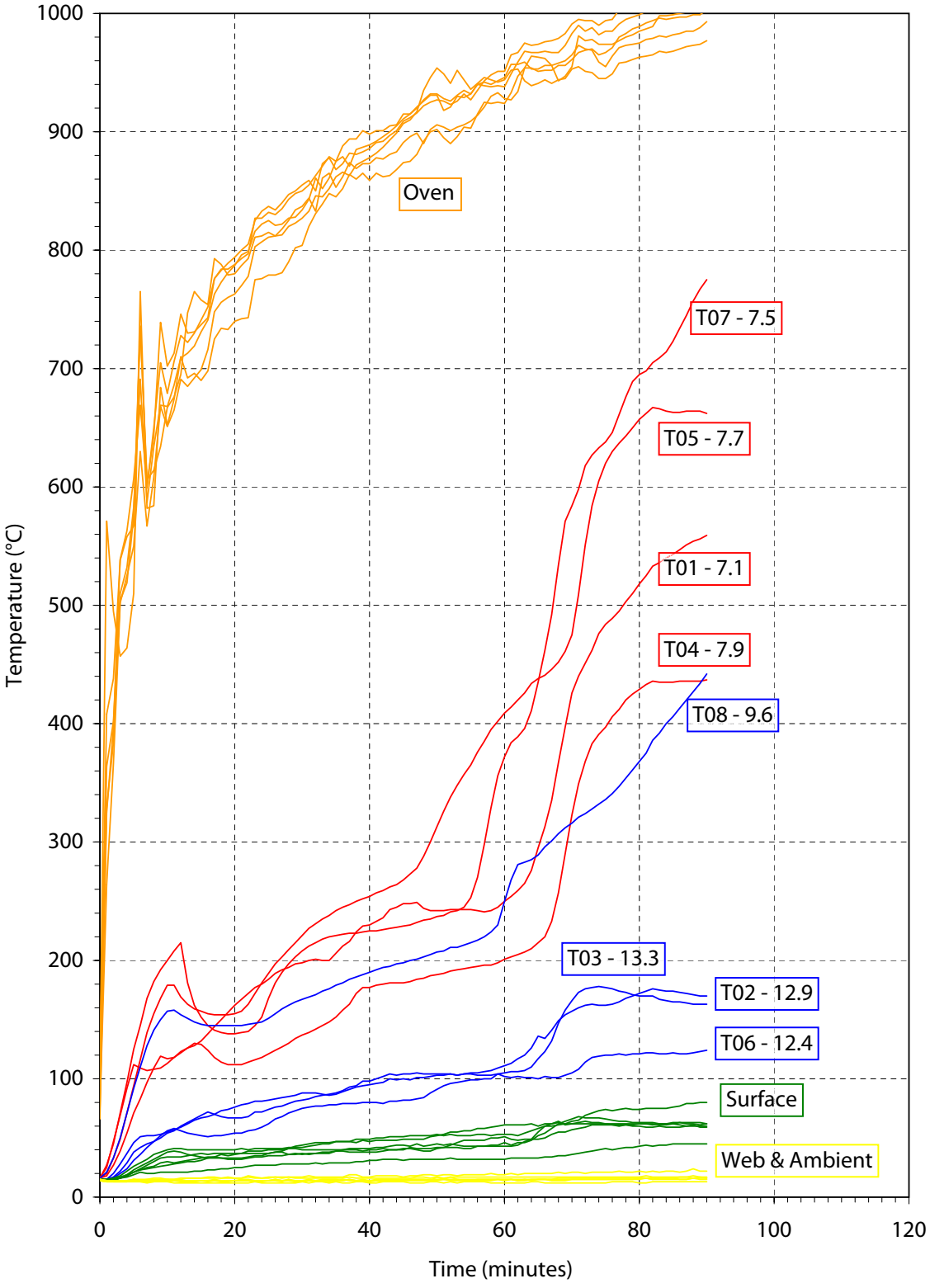

Figure B-16. Temperatures recorded during LC02 (numbers in boxes refer to thermocouple number and measured thickness of material below)

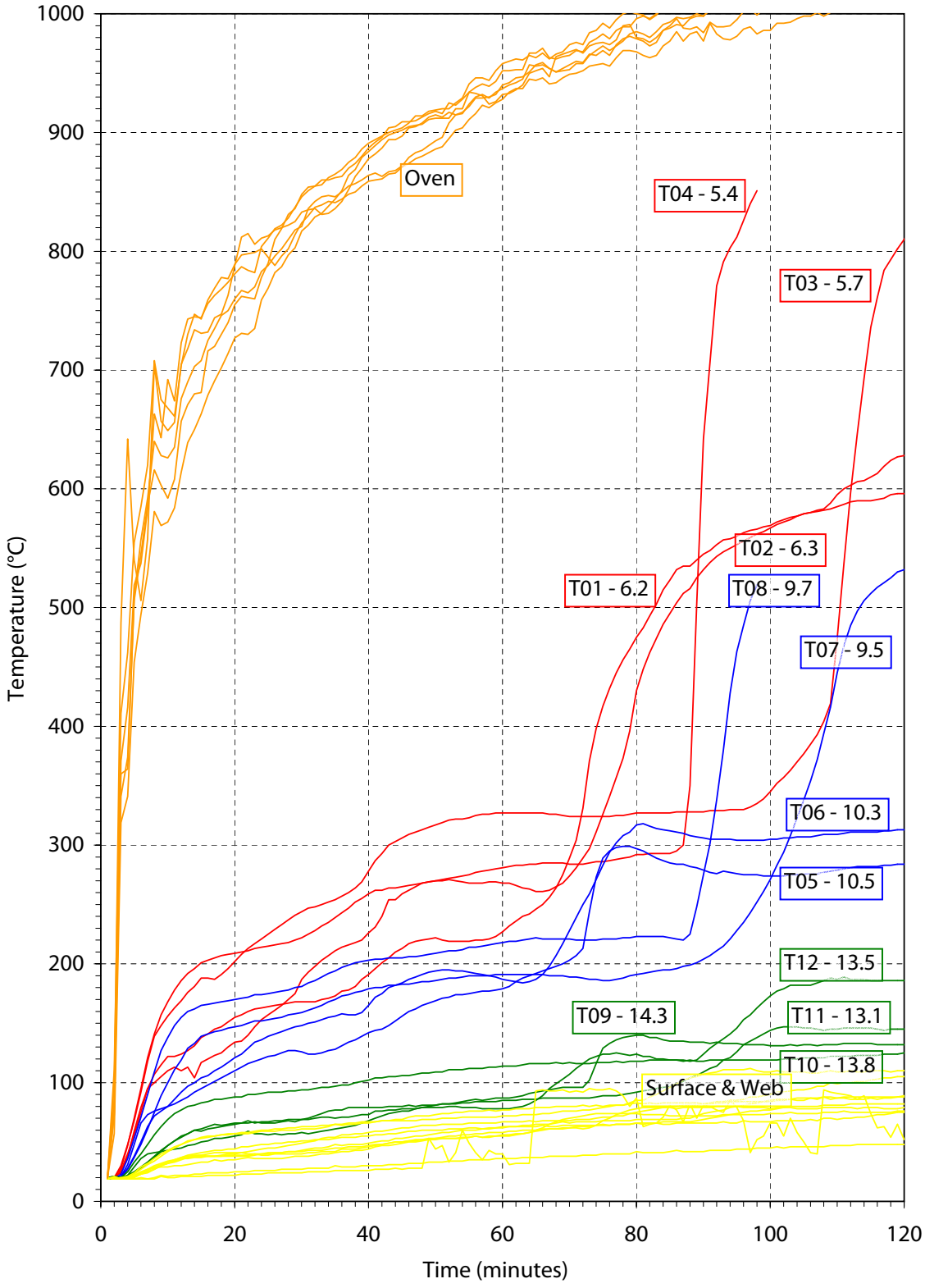

Figure B-17. Temperatures recorded during LC03 (numbers in boxes refer to thermocouple number and measured thickness of material below)

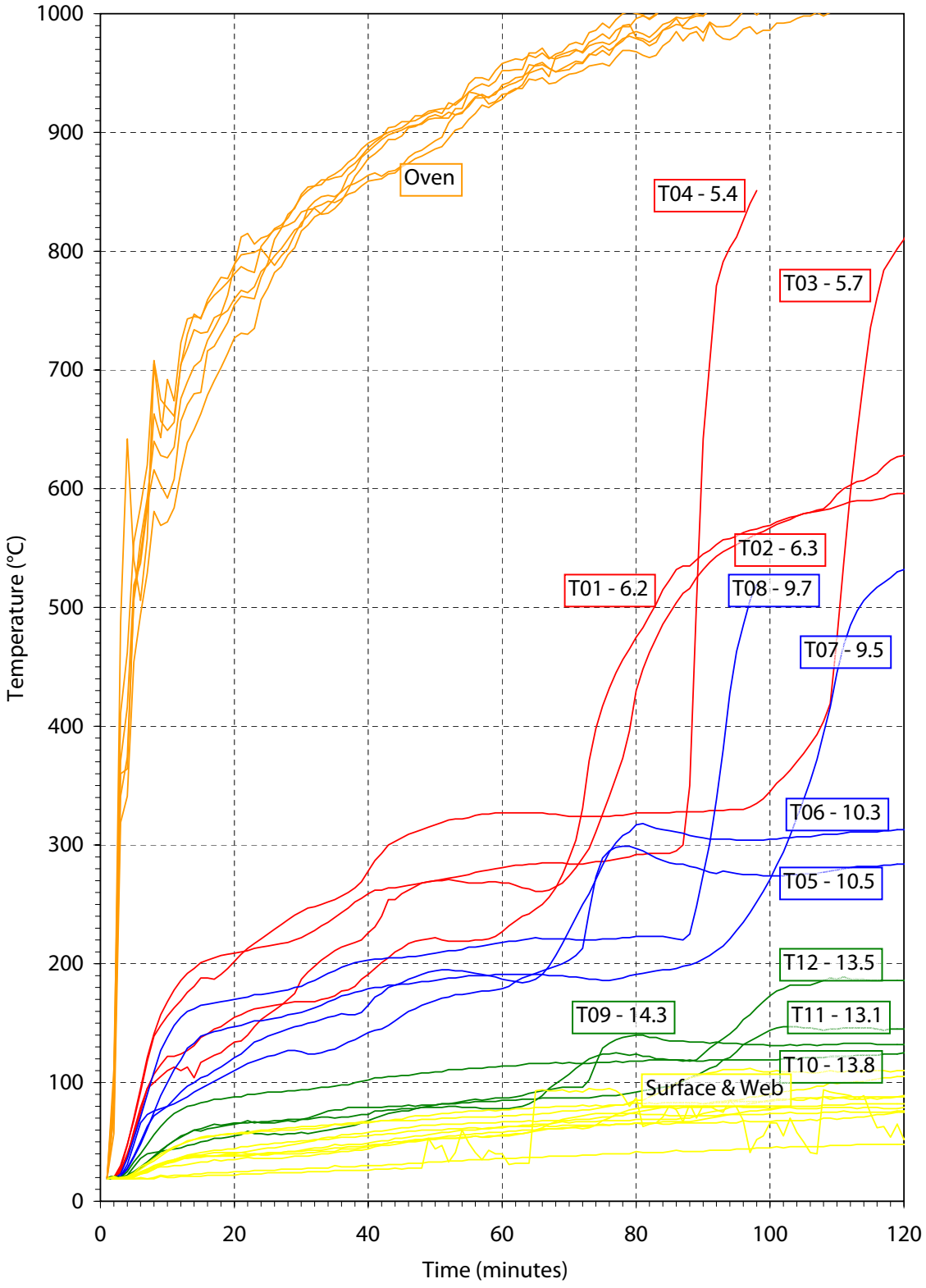

Figure B-18. Comparison of temperatures recorded during Charring and Liquid Cooling Experiments (temperatures are averages from all four instrument clusters)

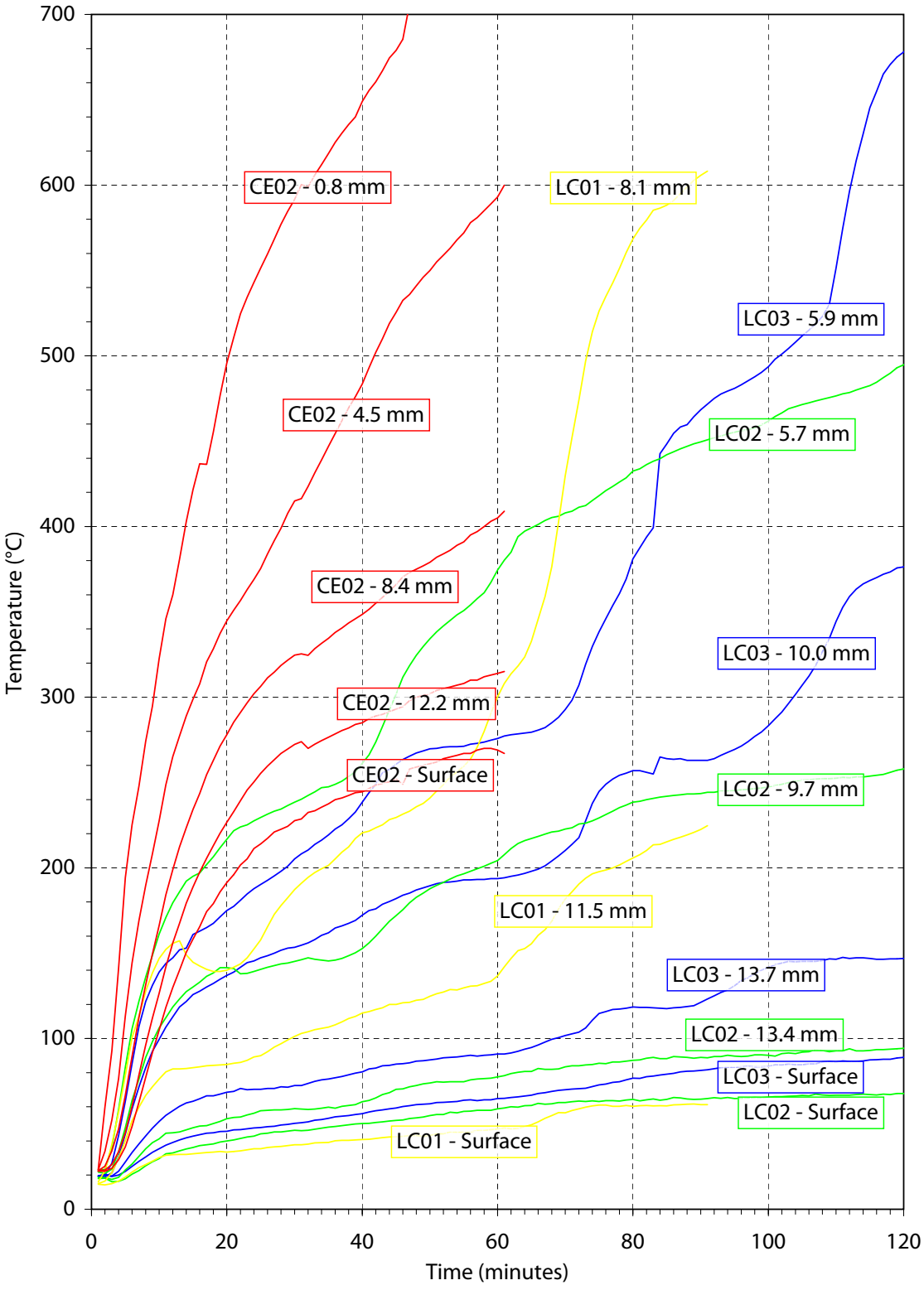

C

TECHNICAL REPORT

Structural Fire Endurance Experiments

Denoted herein as ***Structural Liquid Cooling Experiments SLC01-SLC03***

EPFL / CCLab - EMPA / Bauphysik - Craig Tracy - May 17th, 2004

Technical Report 2001.2/4

Structural Liquid Cooling Experiments (SLC01-SLC03)

Liquid-Cooled GFRP Panels on Large Horizontal Oven

1 Motivation and Summary

As final evidence of the feasibility of internal liquid cooling for the fire protection of fiber-reinforced polymer (FRP) panels, a series of experiments were performed on the large scale. Building upon the experiences from the Small-Scale Charring Experiments (CE01-CE03) (see Appendix A) and Small-Scale Liquid Cooling Experiments (LCE01-LCE03) (see Appendix B), the system was tested on the system level under structural as well as thermal loading. The techniques for introducing a constant flow of ambient-temperature water through the interior cells of the panels used in the LC experiments were improved for the SLC experiments. SLC01 and SLC02 were conducted with 2.00 m^3/hr and 1.00 m^3/hr, respectively, of water flowing through each of the three plumbing circuits. In light of the success of the first two experiments, SLC03 was conducted in the dry condition, e.g. with no liquid cooling, to provide a basis for comparison.

Three specimens of consisting of three pultruded sections each (3.50 m x 0.91 m) were individually tested. The specimens were loaded in four-point bending using twin 93 kN loads applied at roughly the third points of the 2.75 m simple span. This loading simulated the serviceability limit-state deflection (span/300) resulting from a evenly distributed load. The oven's oil burners were then ignited to bring the interior oven temperature along the ISO 834 cellulosic time-temperature curve. Under constant load, the deflections, strains, and temperatures were recorded as the fire slowly deteriorated the lower face sheets of the panels. SLC01 was prematurely concluded at 90 minutes due to a leakage of water, while SLC02

remained watertight and structurally sound for the full 120 minutes. SLC03, without the aid of liquid cooling, was concluded at 57 minutes due to structural failure.

2 Origin and Description of Specimens

2.1 Description of Materials

The specimens under investigation were samples of Martin Marietta Composites' DuraSpan® 766 bridge deck (see Figure C-1). The composite section is produced through the pultrusion process, where glass fiber reinforcement is wet-out by an isophthalic polyester resin and pulled through a heated die to cure into its final shape. Each pultruded shape consists of two relatively thick face sheets separated by three thinner webs, creating two internal cells. In order to facilitate alignment during adhesive bonding of adjacent shapes, tongue-and-groove connections are provided along the edges.

2.2 Origin of Specimens

The panels arrived in Lausanne in August of 2003 via airfreight and tractor-trailer from the United States. They were stored in an outdoor stockyard for roughly seven months. Approximately one month before experimentation, they were transported to the Swiss Federal Laboratories for Materials Testing and Research (EMPA) in Dübendorf. All of the preparation and instrumentation was completed at the EMPA's fire laboratory.

2.3 Preparation of Specimens

For all three of the SLC Experiments, panels consisting of three pultruded shapes were bonded together by the manufacturer using a flexible urethane adhesive (Pliogrip® from Ashland Chemical, USA). The finished panels measured 350 cm in length, 91.4 cm in width, and 19.5 cm in depth.

To maintain a constant face sheet thickness, the tongues from the unused exterior female connection were removed and bonded over the thin face-sheet portions of the exterior male connection on the opposite side (see Figure C-2). To allow the water to flow the length of one interior cell and then return in the adjacent cell, notches of roughly 100 cm^2 were cut into the webs separating the cells at the far of the panels. Finally, a watertight vessel was created by

bonding thin FRP channels to the ends of the panels using FRP angles for reinforcement. All bonds were made using Sikadur 330® epoxy adhesive from Sika AG of Switzerland.

2.4 Instrumentation

In order to measure the temperature profile through the lower face sheet, thermocouples were placed at various depths throughout the thickness. As in the LC Experiments, this was accomplished by cutting access hatches in the top face sheet and then machining slots into the lower face sheet. Slots of 4, 8, and 12 mm depths were routed into the lower face sheet below each of the four access hatches (see Figure C-6 and Figure C-7 for as-built dimensions of each slot). Strain gages and thermocouples were also placed on the interior surface of the lower face sheet. Though it would have been most desirable to place these instrument clusters towards the mid-span, it was decided that the portions of the upper face sheet that would need to resist bending through compression resistance should not be weakened by the cutting of the access hatches. Thus, the instrument clusters were located 30 cm from the supports, or roughly at the outer 1/10 points. Upon the completion of the instrumentation, thin FRP plates were screwed and bonded to the interior of the upper face sheets to close the hatches.

On the exterior surface of the upper face sheet, instrument clusters were placed at the same locations as the lower, as well as at the mid-span. In addition, displacement transducers were used to measure the vertical deflection at mid-span and at the loading axes. In all, 16 stain gages, 27 thermocouples, and 5 displacement transducers were employed for each experiment (see Figure C-5). Strains, deflections, and load were recorded at five second intervals while temperatures were recorded once each minute.

The thermocouple wires consist of two leads insulated by a fabric that is intended to resist fire but not moisture. Thus, the wires exposed to water inside the cells were waterproofed using a heat-shrink plastic housing. The cables entered the cells though a small hole in the upper face sheet, followed the interior surface down to the lower face sheet, and were bonded into the bottom of the machined slots. A paste made from Sikadur 330® epoxy and grindings from unused portions of the specimens was used to fill the slots over the thermocouple wires. Araldit® 5 Min. Rapid Epoxy from Ciba Speialitätenchemie AG of Switzerland was used to hold the wires in place and to seal their passage through the upper face sheet.

The strain gages were supplied by Hottinger Baldwin Messtechnik (HBM) GmbH of Germany and are designated type 6/120LY11. The gages are temperature compensated for steel, and have a recommended operating temperature range of -70°C to 200°C. The displacement transducers were also supplied by HBM and are designated type W20, with a maximum range of ±20 mm

and an accuracy of ±0.01 mm. The thermocouples were supplied by R. Wick AG of Switzerland and are designated type 24-K-GG (class II), with an accuracy of ±2.2°C or 0.75% of the measured temperature.

As foil strain gages measure elongation by the change in their electrical resistance, elongations due to changes in temperature must be compensated and separated from elongations due to structural loading. In typical structural experiments, this is achieved through a single compensation gage, which is subject to the same temperature conditions as the working gages but is not loaded. For the SLC experiments, however, the 16 different gages were subjected to widely differing temperature conditions. Thus, one compensation gage would not accurately represent all of the working gages.

To resolve this problem, an entirely different approach was taken. A sample of the FRP material was taken from the panels and instrumented with three strain gages. This sample was then placed in a small oven, where the temperature was slowly increased (over the course of many hours) from ambient to 100°C. The strains measured by the gages thus correspond to the elongation due to thermal expansion.

For the SLC experiments, a thermocouple was placed next to each strain gage. Therefore, the temperature of each gage was known at all times, allowing the elongation due to thermal expansion to be subtracted from the measurements after the experiment.

The insulation of normal strain gage wires is not suited to high-temperature operation. Thus, wires with Teflon® insulation were used in all cases. Due to their high cost, the wires were reused for each of the three experiments.

In addition to the many electronic methods used to quantify the experiment, a secondary manual method was employed. This method was used to verify the magnitude of the deflections recorded through the displacement transducers, as well as to provide some basic values in the case of a malfunction or loss of data. This manual method consisted of visually observing the movement of wooden rule fixed at the mid-span of the panels. Measurements were made at five minute intervals with the aid of binoculars.

For the control and measurement of the flowing water, calibrated and certified digital flow-rate meters were used for each of the three plumbing circuits. Water temperature was measured by special elbow joints fitted with thermocouples at the inlets and outlets of each cell.

3 Experimental Set-up

3.1 Oven Preparation and Support Conditions

Graduating from the small-scale experiments on the small horizontal oven, the Large-Scale Structural Liquid Cooling Experiments were conducted on the EMPA's large horizontal oven. The interior dimensions of the oven are 3.0 m x 4.9 m, with an internal volume of 25.5 m^3. As the panels only measured 3.5 m x 0.9 m, it was simplest to have them span in the oven's narrower direction. In this effort, a custom-built concrete frame was fabricated used special high-temperature concrete (see Figure C-3 and Figure C-4). This frame provided supports for the panels with a span of 2.75 m and protected the sides of the panels from fire. To create simple-support conditions, 25 mm steel plates were embedded at the support axes to accept steel rollers. Identical steel plates were attached to the undersides of the panels to reduce the bearing stresses over the rollers.

The remaining portions of the oven were enclosed using precast cellular concrete panels (Ytong® from Xella Porenbeton AG of Switzerland). The interior surfaces of these panels and of the concrete frame were covered with a layer of ceramic wool insulation. The floor of the oven beneath the concrete frame was tiled with cellular concrete blocks to absorb any water leakage, as the oven's lining consists of highly porous bricks that would be damaged by liquid water at that temperature.

As the concrete frame raised the panels a bit higher above the oven than normal, the oven's piloting thermocouples were moved such that they measured the gas temperature just below the lower face of the panels. These thermocouples, held in place by steel pipes, incidentally provided additional security by affording some support to the panels in the case of collapse.

3.2 Liquid Cooling System

As in the LC Experiments, water connections were all made at one end of the panels. Instead of using individual threaded nipples for each of the cells, however, custom-built steel adapters were used. These adapters consisted of a steel plate with holes drilled for each cell and threaded steel pipes welded above. Matching holes were cut into the upper face sheets of the panels. The adapters were then bolted and bonded to the upper face sheets, providing a durable and watertight connection.

Water was supplied by the fire hydrant outside of the laboratory using large-diameter flexible hoses borrowed from the local fire brigade. The three flow-rate meters were placed along the input lines to the panels. Fine adjustment of the flow rate was made using the valves of the flow meters such that the accuracy was assured to ±0.01 m^3/hr. Analog manometers were installed at the outlets of each plumbing circuit to verify that the internal water pressure was not too high. In summary, water flowed through each plumbing circuit in the following manner: fire hydrant → flexible fire hose → flow rate meter → flexible fire hose → thermocouple-equipped elbow joint → inlet (adapter) → outbound cell (cell II, IV, or VI, see XX) → return cell (cell I, III, or V, see XX) → outlet (adapter) → thermocouple-equipped elbow joint → manometer → flexible fire hose → drain.

3.3 Loading system

In order to best simulate an evenly distributed load using discrete hydraulic jacks, a four-point bending arrangement was selected. Two jacks at each of the third-points applied a force onto heavily-reinforced triple-web steel beams. A layer of rubber between the beams and the panels ensured that the load was evenly distributed across the three pultruded sections (see Figure C-3 and Figure C-4).

The jacks were driven by a single manually-controlled oil pump, whose single output hose split twice to feed all of the four jacks. The load was controlled through an analog pendulum manometer, which displayed the oil pressure on a dial and its corresponding jack force. In addition, the load was measured and recorded by a digital manometer. This manometer provided a voltage, which is then converted to a pressure, which corresponds to a jack force. The manometers and conversion factors were calibrated by the EMPA in April of 2004 (one month before testing) and are accurate to roughly ±2 kN. In any case, the experiments were performed at constant load (see Section 4.2), such that a highly accurate dynamic control system was not vitally linked to the quality of the results.

The analog pendulum manometer (with force graduations) was supplied by Roell Amsler (now Zwick GmbH & Co. KG of Germany), and is designated type PM with a maximum load of 150 kN per jack. The digital manometer was supplied by Hottinger Baldwin Messtechnik GmbH of Germany and is designated as type P8A. As of the 2004 calibration, its accuracy is quoted to be 0.03% + 60 mbar up to its capacity of 500 bar. The hydraulic jacks were supplied by Robert Bosch GmbH of Germany and apply a maximum force of 150 kN each.

4 Design of the Experiment

4.1 Selection of Flow Rates

Upon the post-experimental evaluation of the LCE specimens, it was found that even an extremely low flow rate of 0.16 m^3/hr permitted some portion of the lower flange to remain intact during a two-hour exposure (see Appendix B). Unsure that the scale-up and addition of structural loading would not produce a less favorable behavior, the SLC01 was conducted at a conservative flow rate of 2.00 m^3/hr. Gaining confidence from SLC01, SLC02 was conducted at 1.00 m^3/hr. With two good data sets and a satisfactory performance in the first two experiments, it was decided that SLC03 would provide the greatest contribution of knowledge if run as a control experiment. Thus, the third experiment received no liquid cooling and served as a basis for comparison.

4.2 Selection of Load

The load was calculated to impose a deflection that would normally limit the service load of such a panel in normal use. This deflection limit is equal to 1/300 of the clear span[1], L. The applied load is selected through the following calculations.

$$\delta = \frac{L}{300} = \frac{2750\,\text{mm}}{300} = 9.2\,\text{mm} \tag{C-1}$$

Thus, the panels should be loaded until a deflection of 9.2 mm is imposed at the mid-span. For a simply supported beam in four-point bending, the deflection is calculated according to the following equation.

$$\delta = \frac{PL^3}{24EI}\left(\frac{3\cdot a}{L} - \frac{4\cdot a^3}{L^3}\right) \tag{C-2}$$

Rearranging this equation to solve for P and inputting a = 900 mm (the distance from the supports to the loads), L = 2750 mm (the clear span), E = 26.96 GPa (supplied by the manufacturer - value is for the flanges), and I = 2.732 x 10^8 mm^4 (computed using AutoCAD), the load is calculated in the following equation.

1. The Swiss building code dictates a deflection limit of 1/350 for adequate rigidity, comfort, and functionality of concrete structures [167]. Relaxing this limit to 1/300 allows heavier loads, and thus, more conservative results.

$$P = \frac{24(9.2\text{ mm})\left(26{,}960\,\frac{\text{N}}{\text{mm}^2}\right)\left(2.732\times10^8\text{ mm}^4\right)}{(2750\text{ mm})^3\left(\frac{3\cdot900\text{ mm}}{2750\text{ mm}}-\frac{4\cdot(900\text{ mm})^3}{(2750\text{ mm})^3}\right)} = 92.9\text{ kN} \quad \text{(C-3)}$$

Because two jacks provided the load at each loading axis, the load applied by each jack was therefore one-half of the total load, or 46 kN.

4.3 Duration of Fire Exposure

In the LC Experiments, the occurrence of either of two events was used to determine the end of the experiment: the water leaking into the oven or the water boiling. For the SLC Experiments, some additional events were defined: the failure or rupture of the panel, the sudden increase in deflection (indicating a eminent collapse), and 30 mm of vertical deflection at mid-span (estimated to be roughly equivalent to the deflection of the panel with 10% of the lower face sheet in tact).

4.4 Temperature Loading

As in all of the small-scale experiments, the SCL Experiments were conducted according to the ISO 834 cellulosic time-temperature curve. The curve represents the most severe temperatures experienced in typical building fire over time. The curve closely resembles other curves used throughout the world such as the American ASTM E-119, the British BS 476, and the German DIN 4102. The logarithmic curve rapidly increases at first, surpassing 500°C after roughly 4 minutes. The temperature, T (in °C), is given as a function of time, t (in minutes), and initial oven temperature, T_0, in the following equation.

$$T - T_o = 345\log_{10}(8t+1) \quad \text{(C-4)}$$

4.5 Experimental Procedure

When applicable, the experiments began with the circulation of water through the cells. This was continued for at least 30 minutes so that thermal equilibrium was reached on the side of the water supply and within the panels. Next, the structural load was slowly applied to the panels. Ten minutes were then given for the deflection to stabilize.[2] Finally, the chronograph was started with the ignition of the oil burners.

Upon the occurrence of a failure criterion or after the planned 120 minutes of exposure, the burners were extinguished. As quickly as possible (roughly 5 minutes), the specimen and reaction frame were removed from the oven and placed outside of the laboratory to cool. After sufficient time to allow the specimen to assume ambient temperature, loading was once again applied up to the capacity of the test equipment.

4.6 Experimental Notes

4.6.1 SLC01 Notes

Because the panel was recessed slightly within the custom-built concrete frame, it was not possible to directly view the panels from the oven's four observation windows. Thus, a glass mirror was placed within the oven to the provide a fleeting glimpse of the panels' undersides. The glimpse was fleeting because high temperatures within the oven first oxidized the silver coating on the back of the mirror and then melted the glass. The mirror was a puddle of liquid in under 20 minutes.

Despite the loss of the mirror, the flames consuming the underside of the panel were clearly visible. Large flames reaching more than one meter below the specimen were fanned by the strong exhaust system of the oven. A prevailing gas current was visible as it caused much larger flames towards the northern side of the oven (specimen inlet/outlet side - see Figure C-10).

The first actual view of the underside of the specimen was not until the first reinforcement layers broke free from the surface and drooped down. Layers of glass rovings became clearly visible at 45 minutes (see Figure C-11).

At roughly 86 minutes, a steady stream of water vapor was observed to be leaking through the urethane joint between cells II and III, towards the northern side of the oven. At 92 minutes, this leakage increased to an even flow of liquid water onto the floor of the oven. This leakage absorbed large amounts of energy though evaporation and was therefore accompanied by a severe drop in oven temperature and an increase in oven pressure (decrease in negative pressure). Thus, the experiment was concluded with the extinction of the oil burners. As quickly as possible afterwards, the instrument cables and water hoses were disconnected from the specimen. A large crane was then used to move the entire oven reaction frame, including the concrete frame, cellular concrete panels, and hydraulic jacks off of the oven and outside of the laboratory (see Figure C-12).

2. Experience at the CCLab in other experiments involving the same type of panels has shown that creep occurs during the first few minutes after loading, but then quickly stabilizes.

The specimen and reaction frame were given several hours to cool ambient temperature. After this cooling, the specimen was slowly loaded in the effort of determining ultimate load. Unfortunately, the 150 kN capacity of the jacks (300 kN per loading axis) proved insufficient to cause a failure. Thus, the resistance was proven to at least that load, and the post-fire stiffness can be compared to that of the untested condition.

4.6.2 SLC02 Notes

It was not possible to run SLC01 for the full 120 minutes because of the local breach and leakage of the watertight vessel; the specimen still provided adequate structural resistance and may have been able to support the load for much longer. The augmentation of the water flow rate in SLC02 would not necessarily impede the occurrence of local burn-through's, as the existence of small hot spots in the oven appears unavoidable. Thus, little information would be gained by augmenting the water flow rate for SLC02. On the contrary, decreasing the water flow rate would help define the influence of liquid cooling rate on structural resistance. The water flow rate for SLC02 was therefore chosen to be one-half that of SLC01, or 1.00 m^3/hr.

Just before the ignition of the oven for the commencement of the experiment, it was noted that the flow rates of the three outlet hoses were not equal. By turning off the flow of water to some plumbing circuits and running others, it was determined that insufficiently flat surfaces at the ends of the panels lead to incomplete bonding of the end channels, and thus leakage between the plumbing circuits. The different levels of resistance to flow exerted by the different paths of the flexible fire hoses caused an uneven pressure between the circuits. The water was able to follow the path of least resistance by leaking to the circuits with lower pressure. As the utility of the experiment hinged upon the knowledge of exact water flow rates, SLC02 was aborted pending repairs.

The repair consisted of making a shallow vertical cut along the webs that separate the circuits using a portable circular saw. Epoxy adhesive was then used to bond a rectangle of FRP material into these vertical cuts. Water-tightness trials proved this to be an entirely successful method of stopping the leakage between the plumbing circuits.

With a newly watertight vessel, SLC02 was conducted approximately one week later. The experiment ran much the same as SLC01, though no leakage was observed. At the completion of 120 minutes, the temptation was strong to continue the fire exposure until some sort of failure occurred. This temptation was resisted, however, because it would have made impossible the testing of the specimen for residual strength after cooling.

As in SLC01, the specimen and frame were allowed to cool for several hours. Slowly increasing the load on the specimen, the 150 kN capacity of the hydraulic jacks was reached without any structural failure of the specimen.

4.6.3 SLC03 Notes

In light of the success of SLC02, which was conducted at a fairly low flow rate, it was decided that SLC03 would provide the most information if run as control experiment, i.e. without liquid cooling. All details of the specimen preparation were identical to the previous experiments such that the element was watertight. The cells were only open to the atmosphere through the pipes of the metal adapter. This had the effect of preventing the buoyant convection of ambient air across the hot interior face of the lower flange. When the quantity of smoke pouring from these pipes into the laboratory increased to unhealthy levels, rags were used to plug them up as well.

The first 45 minutes of SLC03 proceeded much the same as the first two experiments, though on an accelerated time scale. Unlike the first two experiments, deflections increased steadily rather than slowing down over time. The deflection at 45 minutes was higher than that observed for 120 minutes in SLC02.

Also unlike the first two experiments, a structural failure occurred. Surprisingly, the failure did not occur in the fire-exposed lower face sheet. While this face sheet continued to lose roving layer after layer into the oven, it was the upper face sheet that eventually failed. A compression failure occurred in the upper face sheet after 57 minutes of fire exposure. Upon recognition of the failure, the load was removed, the oven was extinguished, and the entire apparatus was moved outside of the laboratory. No post-fire loading was performed.

5 Post-Fire Inspection of Specimens

All of the specimens were cut into four sections using a large diamond saw. This greatly facilitated the study of the layer-wise status and remaining thickness of the specimens. Cuts were made at the ends of the fire-exposed portion and at the mid-span. In general, uniformity of fire damage was observed between the three locations of each specimen. Thus, the observations and images of the sections originate from any of the locations, depending only on practical factors such as lighting conditions.

5.1 SLC01

Two of the four roving[3] layers became delaminated from the lower face sheet and had partially fallen away from the panel. Damage was beginning to occur at the third roving layer, as shown in Figure C-20 and C-23). In this third roving layer, the regions directly below the webs were more severely damaged than the regions below the open cells (see Figure C-18). This stands to reason, as the heat applied directly below the webs was required to pass through a greater thickness of material before it reached the cooling effect of the flowing water.

All fibers that drooped down into the oven were decomposed into a white foam-like char. Though quite flexible and string-like at high temperatures, this char became very brittle upon cooling. As was observed in the CE and LCE series, the damage from the hot face inwards in the following progression: whitish fiber char alone → brittle black fibers in black powdery resin char → slightly ductile black fibers in black resin char → very ductile fibers in partially degraded yellowed resin → undamaged fibers in undamaged resin.

An inspection of the hot face of the specimen did not reveal any clear path for the water leakage. The fourth roving layer was not compromised in any region, which suggests that the leakage passed instead through one of the thermocouple slots. It is possible that the damage to the hot face proceeded to the depth of one of the thermocouples, and that water leaked down around the thermocouple wire into the bottom of the slot. During the experiment, the water appeared to be coming from the bonded joint between cells II and III, but this may just be result of the water flowing around the delaminated layers of reinforcement and out at the edges.

At roughly 16 mm, the deflection after unloading was approximately 3 mm greater than was measured at the beginning of the fire loading. This corresponds to a deflection-to-span ratio of 1/170. The roughly 60 mm of deflection (ratio 1/46) imposed by the post-fire loading was completely recovered after unloading.

5.2 SLC02

The damage incurred by the lower face sheet of the specimen was very similar to that of SLC01, though the third deepest roving layer (counting from the hot face) was in slightly better condition (see Figure C-21 and C-24). No leakage of water was found. The sides and upper face sheet appeared to be in perfect condition. In the rush to disconnect all of the cables and

3. "Rovings" are the longitudinal bundles of glass fibers that constitute the majority of the fiber volume and are most important in resisting longitudinal tensile and compressive stresses (such as those resulting from bending) on the pultruded element.

hoses after extinction of the oven's burners, the displacement transducers were unplugged before the specimen was fully unloaded. Thus, the permanent deflection could not be determined. As in SLC01, the deflection imposed by the post-fire loading was completely recovered after unloading.

5.3 SLC03

The damage to the lower face sheet was more severe than in the previous two experiments. All four roving layers were completely delaminated (see Figure C-22 and C-25). As the face sheet warped and delaminated, the connection to the webs was broken in some areas. Overall, only a 1-2 mm thin layer containing the inner surface veil and stitched mat remained partially intact, which indicates that the webs eventually provided all of the tensile resistance in bending. Without the bracing effect of the lower face sheet, lateral torsional buckling of the webs would probably have occurred if the upper face sheet had not first failed in local buckling.

Though the lower face sheet was more severely damaged than in the two previous experiments, it was the damage to the upper face sheet clearly differentiates the specimen from that of SLC01 and SLC02. The sheet buckled along a nearly strait line running across all three of the pultruded elements and between the two loading axes. The buckle resembled the collision of continental plates at a subversion fault, with one side vertically displacing 3 to 4 mm above the other. From the side view, the buckle followed a roughly 45° angle through the upper face sheet (see Figure C-16 and C-17).

6 Discussion of Results

6.1 Measurement of Deflections

An evaluation of the load versus deflection revealed that the displacement transducers did not function properly at the lower load levels. The "as-recorded" load vs. deflection graphs show a non-linear behavior – a behavior that has never been observed in the extensive group of structural tests conducted on the deck by other researchers within the CCLab and elsewhere. The obvious conclusion is that the transducers where initially operating outside of their recommended range, but then began to function correctly when the load caused adequate deflections to bring the transducers within their proper range.

To remedy this problem, a correction factor was introduced for each displacement transducer for each experiment. By projecting the linear regression of the most linear portion of the load vs. deflection curve onto the x-axis, an intercept is found. If all is functioning properly, this intercept should be close to zero. Due to the erroneous initial readings of the transducers, however, this intercept was found to be as far off as -25.5 mm. The magnitude of this intercept for each device in each experiment was added to the "as-recorded" deflection values at all load levels. Finally, the values recorded in the erroneous range were removed to form the "adjusted" data set. The data sets shown in Figure C-36 to C-38 are "adjusted". Figure C-35 shows the "as-recorded" data sets plotted on the same graph as the "adjusted" data sets for SLC01. The fit of the linear regressions is far better for the "adjusted" data sets.

6.2 Prediction of Initial Deflections

As described in Section 4.2, the experimental load of 92.9 kN was selected to impose a deflection to span ratio of 1/300, or 9.2 mm. In the actual experiment, the deflection under the 92.9 kN load was initially measured at 10.0 mm (see Figure C-29). At the time that the experiment was conducted, this appeared to be an excellent agreement between measured and predicted values. In light of the previous section, however, it is now clear that this agreement was the result of several inaccuracies having inverse influences and effectively cancelling each other's effects:

- The first inaccuracy refers to the measurement of deflections and is described in the previous section. When the adjustment is made to the measured values, a deflection of 11.97 mm, 12.02 mm, and 12.34 mm correspond to a 92.9 kN load in experiments SLC01, SLC02, and SLC03, respectively. The average of these values is 12.1 mm and the standard deviation is 0.20 mm.
- The Young's Modulus used in the prediction calculation was inaccurate. The value initially chosen (29.96 GPa) originated from the deck manufacturer's published values in the year 2000. The manufacturer later reduced this value in a 2001 publication to 21.24 GPa. Further, this value applies only to the flanges. The modulus of elasticity of the webs is lower at 17.38 GPa. A more accurate deflection prediction can be made by using the E that corresponds to each component rather than assigning the E of the flanges to everything.

- The moment of inertia used in the first calculation was computed based on the cross-section of the specimen without the glued-on strips at the stepped portions. The addition of these strips increases the moment of inertia from $2.73\text{x}10^8$ to $2.90\text{x}10^8$ mm^4.
- Shear deflections were not considered in the prediction calculations. Equation 2 only accounts for deflections resulting from bending, neglecting the deflections due to shear deformation. Although this term is often neglected in steel and concrete design, it is can be more important in FRP structures and especially FRP sandwich structures[4].

The calculations in Section 4.2 are repeated with the changes outlined above. The total deformation is therefore:

$$\delta_{\text{TOTAL}} = \delta_{\text{SHEAR}} + \delta_{\text{BENDING}} \tag{C-5}$$

Using the method of virtual forces, this becomes:

$$\delta_{\text{TOTAL}} = \frac{aP}{GA}\left(\frac{L-2a}{L}\right) + \frac{PL^3}{24EI}\left(\frac{3a}{L} - \frac{4a^3}{L^3}\right) \tag{C-6}$$

where a is the distance between the load and support, P is the load, A is the cross-sectional area of the webs, G is the shear modulus, E is the Young's Modulus, and I is the revised moment of inertia. To consider the different stiffness moduli over the cross-section, the combined value called the *rigidity*, EI, is calculated as the sum of the contributions of each part of the cross section:

$$\begin{aligned} EI &= E_w I_w + 2E_f I_f \\ &= \left(17380\frac{\text{N}}{\text{mm}^2}\right)\left(4.66\text{x}10^7\ \text{mm}^4\right) + 2\left(21240\frac{\text{N}}{\text{mm}^2}\right)\left(1.21\text{x}10^8\ \text{mm}^4\right) \\ &= 5.98\text{x}10^{12}\ \text{N}\cdot\text{mm}^2 \end{aligned} \tag{C-7}$$

where I_w is the moment of inertia of all of the webs combined and I_f is the value for one flange. This value is used in Equation 6 to provide the improved deflection prediction.

4. Though the panels are not truly sandwich structures, the flexible webs often result in a similar behavior.

$$\delta_{\text{TOTAL}} = \frac{900\text{ mm}\cdot 92{,}900\text{ N}}{4{,}140\ \frac{\text{N}}{\text{mm}^2}\cdot 11{,}206\text{ mm}^2}\left(\frac{2{,}750\text{ mm}-2\cdot 900\text{ mm}}{2{,}750\text{ mm}}\right) + \frac{92{,}900\text{ N}\left(2{,}750\text{ mm}\right)^3}{24\left(5.98\times 10^{12}\text{ N}\cdot\text{mm}^2\right)}\left(\frac{3\cdot 900\text{ mm}}{2{,}750\text{ mm}}-\frac{4\cdot\left(900\text{ mm}\right)^3}{\left(2{,}750\text{ mm}\right)^3}\right)=12.0\text{ mm} \quad \text{(C-8)}$$

Thus, recalculating Equation 2 with the revised values and the same load results in a predicted deflection of 12.0 mm. The consideration of shear deformations increases the predicted deflection by roughly 0.4 mm alone. With all of the improvements and changes to the calculation, the prediction is very good at 3% below the average measured deflection of 12.1 mm.

6.3 Strains

Figures C-26 through C-28 show the measured axial strains on the outer surface of the upper face sheets at mid-span and at 30 cm from the supports. Also shown are the axial strains on the inner surface of the lower face sheets at 30 cm from the supports. As previously described, it was not possible to apply strain gages on the lower face sheet at mid-span. The axial strains shown represent only the portion from structural loading. The axial strains due to thermal expansion were subtracted from the total strains measured.

The axial strain vs. time curves show trends similar to the deflection vs. time curves shown in Figure C-29. The axial strains at the ignition of the burners were the same in all specimens. The strains in the compression-stressed upper face sheets were approximately 15% higher than in the tension-stressed lower face sheets due to the cross-sectional geometry. After ignition of the burners, the strains in the liquid-cooled specimens rapidly increased for approximately 10-20 minutes, particularly in the lower face sheets, and then stabilized at an almost constant value until the end of the experiments.

In this phase of almost constant strains, the tensile strains were approximately 300% higher than the compression strains. This was due to two factors: the reduction of lower face sheet thickness (which moved the neutral axis upward), and the thermal expansion of the reinforcement layers at the tensile face. This second phenomenon resulted from the fact that the elongation of the fibers due to thermal expansion was greater than the elongation caused by bending. The hottest reinforcement layers towards the lower face, which would normally be in tension at ambient temperatures, actually elongated so much more than the cooler, deeper reinforcement layers that they were forced into compression. The inner fibers, therefore,

needed to resist the stress imposed by bending and by the expanding outer reinforcement layers, and thus exhibited much higher strains than the upper face sheets. This behavior was confirmed through ongoing thermomechanical finite element analysis.

The axial strains in the compressed upper face sheet of the non-liquid cooled specimen were almost the same as in the liquid-cooled specimens. The strains on the tension-stressed lower face sheet, however, rapidly increased up to failure. The slight decrease of the strains between 5 and 10 minutes was attributed to the softening of the approximately 2 mm thick protective epoxy layer applied over the strain gages. This layer was applied to protect the gages from water in the liquid-cooled experiments and was repeated in SLC03 for consistency.

The pre-fire and post-fire strains corresponding to the fire test load level are compared in Figure C-39. The shift of the neutral axis is shown through the assumption that the section remains plain and the distribution is linear. As the material is heated and delaminates away from the hot face, the neutral axis moves upward.

6.4 Stiffness Reduction

To investigate the loss of stiffness due to the fire exposure, the experimental mid-span deflections, δ, are plotted against load, P (see Figure C-36 to C-38). The slope of the linear regression of this data set is the bending stiffness, S. The following table provides these values for the three experiments.

Table C-1. Bending stiffness, S (kN/mm), resulting from measured mid-span deflections

	SLC01		SLC02		SLC03	Average
	Pre-Fire	Post-Fire	Pre-Fire	Post-Fire	Pre-Fire	Pre-Fire
δ transducer 1	7.72	4.76	7.61	4.41	7.75	-
δ transducer 2	7.27	4.55	7.31	4.17	7.41	-
δ transducer 3	7.77	4.82	7.55	4.53	7.86	-
Average	**7.59**	**4.71**	**7.49**	**4.37**	**7.67**	**7.58**

The bending stiffness is defined as follows:

$$S = \frac{P}{\delta} \tag{C-9}$$

where E is the Young's Modulus, I is the moment of inertia, L is the length of the beam, and c and d are constants that depend on the loading and support conditions. Substituting S into

Equation 6 and solving for *EI*, the rigidity of the section can be derived from the measured bending stiffness.

$$EI = \frac{aAGLS\left(3L^2 - 4a^2\right)}{24\left[AGL + aS(2a - L)\right]} \quad \textbf{(C-10)}$$

where *a* is the distance between the load and support, *A* is the cross-sectional area of the webs, *G* is the shear modulus, and *E* is the modulus of elasticity. To illustrate the calculation, the values that correspond to SLC01 are inserted into Equation 10 in the following.

$$EI = \frac{(900\,\text{mm})(11206\,\text{mm}^2)\left(6670\,\frac{\text{N}}{\text{mm}^2}\right)(2750\,\text{mm})\left(7590\,\frac{\text{N}}{\text{mm}}\right)\left[3(2750\,\text{mm})^2 - 4(900\,\text{mm})^2\right]}{24\left\{(11206\,\text{mm}^2)\left(6670\,\frac{\text{N}}{\text{mm}^2}\right)(2750\,\text{mm}) + (900\,\text{mm})\left(7590\,\frac{\text{N}}{\text{mm}}\right)\left[2(900\,\text{mm}) - (2750\,\text{mm})\right]\right\}} \quad \textbf{(C-11)}$$

The results of this calculation are shown in the following table for each specimen.

Table C-2. Rigidity, *EI* (N·mm^2), resulting the experimental bending stiffness, *S*.

SLC01		SLC02		SLC03	Average
Pre-Fire	Post-Fire	Pre-Fire	Post-Fire	Pre-Fire	Pre-Fire
5.71x10^{12}	3.50x10^{12}	5.64x10^{12}	3.25x10^{12}	5.78x10^{12}	5.71x10^{12}

The theoretically calculated and experimentally derived rigidities match very well. The average pre-fire value listed above is 4.7% lower than the theoretical value (5.98x10^{12} N·mm^2) calculated through Equation 7 in Section 6.2. Comparing the pre and post-fire rigidities, reductions of 39% and 42% are seen for the specimens of SLC01and SLC02, respectively.

6.5 Loss of Cross-Section

6.5.1 Two-Layer Model

A simple two-layer model can be used to simulate the bending behavior of the post-fire specimen [137]. The section is divided into a fully-degraded region that has no remaining stiffness, and a virgin region, where the stiffness remains at the pre-fire value. The depth at which this division is made, d_c, can be chosen based on one of two criteria:

- the depth at which the temperature reached *Tg* in the last minutes of the fire exposure
- by physical inspection of the specimen after cooling.

The first criterion makes the assumption that any material is heated above T_g has no residual strength, and all material that remained below T_g experienced no loss of stiffness. The second criterion is more approximate because visual inspection can only reveal the depth at which there is no more decomposition. When all of the loose fibers are removed a solid surface is encountered, the investigation can go no farther. The depths at which the stiffness is degraded but the resin has not decomposed cannot be measured. Thus, the second criterion tends to produce less conservative predictions than the first criterion.

From the post-fire inspection of the specimens, the depth of the fully-degraded region was found to be roughly 9.5 mm deep for both SLC01 and SLC02. Judging instead by the temperature profiles, the depths are found to be 11.7 mm for SLC01 and 13.5 mm for SLC02.

The calculation of the rigidity, *EI*, proceeds the same as would for any beam bending analysis.

- The section is transformed according to the moduli of elasticity.
- The depth of neutral axis is found by setting the sum of the moments of the areas about the neutral axis equal to zero.
- The moment of inertia of each component is then calculated about the neutral axis.
- Finally, the rigidity of the post-fire section is found by summing the rigidities of the individual components (similar toEquation 7).

The results of this calculation are shown in the following table.

Table C-3. Rigidity predictions by the 2-layer model

Experiment	Criterion	d_c (mm)	*EI* from 2-Layer Model N·mm^2	*EI* from Measured *S* N·mm^2	Disparity[a] %
SLC01	visual inspection	9.5	4.15×10^{12}	3.50×10^{12}	+18
SLC01	temp. profile	11.7	3.58×10^{12}	3.50×10^{12}	+2
SLC02	visual inspection	9.5	4.15×10^{12}	3.25×10^{12}	+28
SLC02	temp. profile	13.5	3.07×10^{12}	3.25×10^{12}	-6

a. Disparity = (calculated - measured) / measured

6.5.2 Three-Layer Model

Slightly more complex than the two-layer model, the three-layer model includes a region with degraded mechanical properties in addition to the fully-degraded and virgin zones. The border between the fully-degraded region and the partially degraded region is denoted d_{Td} and is defined as the deepest layer to have been heated to the onset of decomposition, $T_{d,onset}$. The

border between the partially degraded region and the virgin region is denoted d_{Tg}, and is defined as the deepest layer to have been heated to the onset of glass transition, $T_{g,onset}$.

Because the stiffness of the partially-degraded layer, E_d, is unknown, the rigidity, *EI*, can only be found as a function of E_d. Using the rigidities found through Equation 10, however, it is possible to solve for E_d. Because this analytical calculation would employs experimental results, though, there is no comparison that can be made to judge the accuracy of the prediction. A more useful approach is to assume a percent reduction of E_d and then solve for the *EI*. This calculation proceeds as follows:

- E_d is assumed to be 30% of E pre-fire. This assumption is based on the idea that the stiffness drops of sharply after T_g and then changes little as the temperature approaches T_d.
- The depth of neutral axis is found by setting the sum of the moments of the areas about the neutral axis equal to zero.
- The rigidity is found by summing all of the rigidities of the individual components, similar to Equation 7.

The results of this calculation are shown in the following table.

Table C-4. Stiffness of the partially degraded region according to the 3-layer model

Experiment	d_{Tg} (mm)	d_{Td} (mm)	*EI* from 3-Layer Model N·mm^2	*EI* from Measured *S* N·mm^2	Disparity %
SLC01	13.8	7.9	3.39×10^{12}	3.50×10^{12}	-3.1
SLC01	15.1	8.9	3.05×10^{12}	3.25×10^{12}	-6.6

Thus, the three-layer model provides a better approximation of the rigidity of the post-fire sections.

6.6 Leakage of SLC01

The breach in the watertight envelope of SLC01 forced the conclusion of experiment. A local hot spot within the oven caused a small burn-through in the lower face sheet, which lead to water leakage and a severe drop in oven temperature. In the laboratory, this phenomenon was undesirable because it posed a danger to the test equipment. In true fire conditions, however, this exact behavior could be quite beneficial. Similar to a fire sprinkler, local burn-through's could provide the best defense against unwanted fire at the locations where it is most needed.

The concept requires development, but is mentioned to explain why the leakage of the specimen should be regarded as a strength to be developed rather than a weakness to be eliminated from the proposed liquid cooling system.

6.7 Failure of SLC03

Without liquid cooling, significant amounts of heat were transferred from the lower to the upper face sheet. This transfer was partially made by conduction through the webs, but also through radiation and convection within the cells. This quickly brought the temperature through the webs and much of the upper face sheet above the glass transition temperature. As the upper face sheet was resisting compression and relied on the resin to maintain the alignment of the glass fibers, it was extremely vulnerable to thermal insult. The lower face sheet, however, was in nearly pure tension. Because the fibers remained anchored outside of the heated area, it remained able to resist its load even after all of the resin had decomposed. This explains why the relatively cooler upper face sheet failed before the lower.

6.8 Liquid Cooling

The efficacity of liquid cooling has already been demonstrated on the small scale. In additional to supporting this evidence through the addition of structural loading on full-sized specimens, the experiments provide a new and unexpected argument for liquid cooling. Prior to SLC03, it was assumed that damage to the lower flange would lead to the structural failure of the panels. Testing in the dry condition under structural load showed that heat transfer from the lower face sheet can quickly bring the opposite face sheet above the glass transition temperature. This is equally important for panels in the vertical orientation, where design might require 50% of a column section to remain intact in order to support its load. Without liquid cooling, such columns would be subject to the same failure seen in SLC03.

6.9 Experimental Set-up and Procedure

6.9.1 Areas for Improvement

Displacement transducers with a range of ±20 mm were employed for the measurement of deflections more by default than by choice. Instruments with a larger range of ±25 mm would have been a better choice but were not available. The result was that the gages exceeded their recommended operational ranges in several cases, though the data appears to be valid. Still, the

exact placement of the gages remained an endless inconvenience throughout the testing and should be avoided whenever possible.

The hydraulic jacks employed were also selected by default rather than choice. As the laboratory's only loading equipment suited for use above the oven, the limitation of 150 kN per jack was unavoidable. The situation was mitigated by the use of two jacks at each loading axis rather than one alone. Despite this limitation, it was still possible to demonstrate the strength and safety of the panels up to 320% of the service load.

SLC02 was delayed by approximately one week because of a leakage between the plumbing circuits. This leakage can be traced back to the lack of flatness of the ends of the panels, though the manufacturer cannot be blamed because he had no knowledge of the end-use or the need for water-tightness. The repair implemented was fairly simple and completely successful, though it would have been better still to have avoided the problem in the first place.

6.9.2 Successful Innovations

The method of removing the entire reaction frame, concrete cap, and specimen after fire loading proved very successful in protecting the specimen from further exposure without the need to remove and reinstall the specimen and gages for post-fire loading. This procedure proposed by the laboratory technicians saved untold hours of labor and probably improved the accuracy of the measurements.

The metal adapters fabricated to make the connection between the panels and the hoses was also highly successful. The many leakages encountered in the LC Experiments around the individual nipple connections were completely avoided. The adapters also employed larger diameter pipes, which reduced the head loss and therefore the water pressure within the panels. With respect to the global design concept of the eventual building system, such connections could prove quite useful.

Finally, a major improvement was made in the method of clamping the access hatch covers for the curing of the epoxy. The method replaced the complex system of bar clamps and timber beam used for the LC specimens with a simple set of pre-aligned screws. Not only was this method quicker, easier, and more reliable, but allowed the placement of hatch covers without access through ends of the cells. This sort of technique could be important in many repairs or unusual connection conditions in the eventual building system where access through the end cells will be impossible.

7 Conclusions

The following conclusions can be made from the SLC Experiments:

1. With the aid of liquid cooling, FRP panels supporting structural loads can resist the extreme temperatures presented by severe fire conditions for at least 120 minutes.
2. Panels exposed to such conditions deflect significantly within the first 10 minutes. While the control panel continued the trend until failure, the deflection of the liquid-cooled panels approached a nearly steady-state condition, deflecting more in the first 10 minutes (8 mm) than in the following 80 minutes (6 mm).
3. No significant difference was noted between the thermal-mechanical performance of the two liquid-cooled specimens.
4. The post-fire bending stiffness of the specimens showed a decrease of 39% and 44% for the 2.00 m^3/hour and 1.00 m^3/hour specimens, respectively. This reduction is attributed to the reduction of the moment of inertia due to the loss of material from the lower face sheet and to a reduction in the Young's Modulus of regions that were heated above T_g.
5. The predictions of a three-layer model matched well with experimentally measured values.
6. Effective and efficient methods have been developed to make water-tight plumbing connections and access hatches for cellular FRP panels.
7. Based on these experiences with an unretarded, non-charring resin and from the perspective of structural fire resistance, no fire retardants or charring agents are needed to protect FRP components from fire when liquid cooling is employed.
8. FRP elements and parts of FRP elements in compression are far more vulnerable to temperature-induced failure than those in tension. The protection of such components is where liquid cooling can make the most valuable contribution.

8 Appendix

Table C-5. Post-experimental layer-wise status of specimens

Reinforcement Layer	Status		
	SLC01	**SLC02**	**SLC03**
surface veil (Hot Face)	delaminated/consumed	delaminated/consumed	delaminated/consumed
stitched mat (+45°/90°/-45°/random)	delaminated/consumed	delaminated/consumed	delaminated/consumed
0° roving	delaminated/consumed	delaminated/consumed	delaminated/consumed
stitched mat (+45°/90°/-45°/random)	delaminated/consumed	delaminated/consumed	delaminated/consumed
0° roving	delaminated/consumed	delaminated/consumed	delaminated/consumed
stitched mat (+45°/90°/-45°/random)	delaminated/consumed	delaminated/consumed	delaminated/consumed
0° roving	delaminated/consumed	delaminated/consumed	delaminated/consumed
stitched mat (+45°/90°/-45°/random)	mostly intact	mostly intact	delaminated/consumed
0° roving	intact	intact	delaminated/consumed
stitched mat (+45°/90°/-45°/random)	intact	intact	partially intact
surface veil (Cold Face)	intact	intact	intact

Figure C-1. Martin Marietta DuraSpan® 766 bridge deck

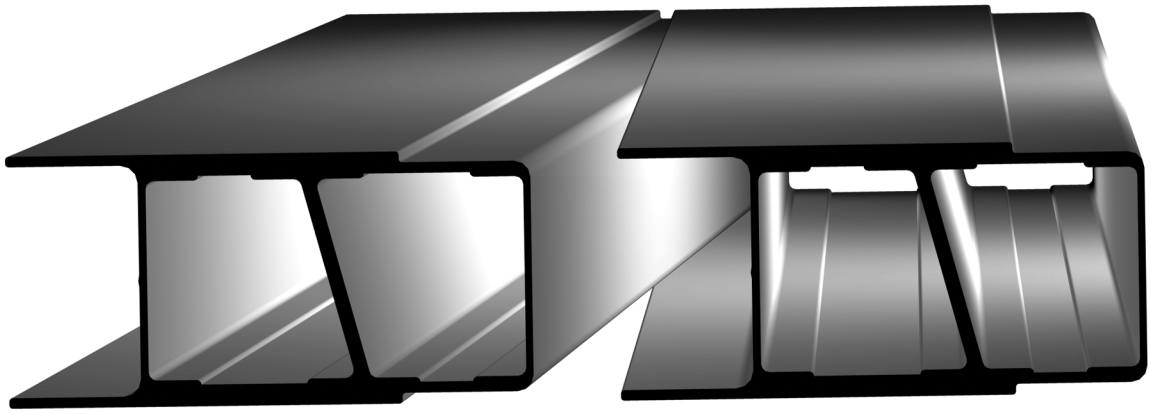

Figure C-2. Removal and placement of specimen tails for constant face sheet thickness

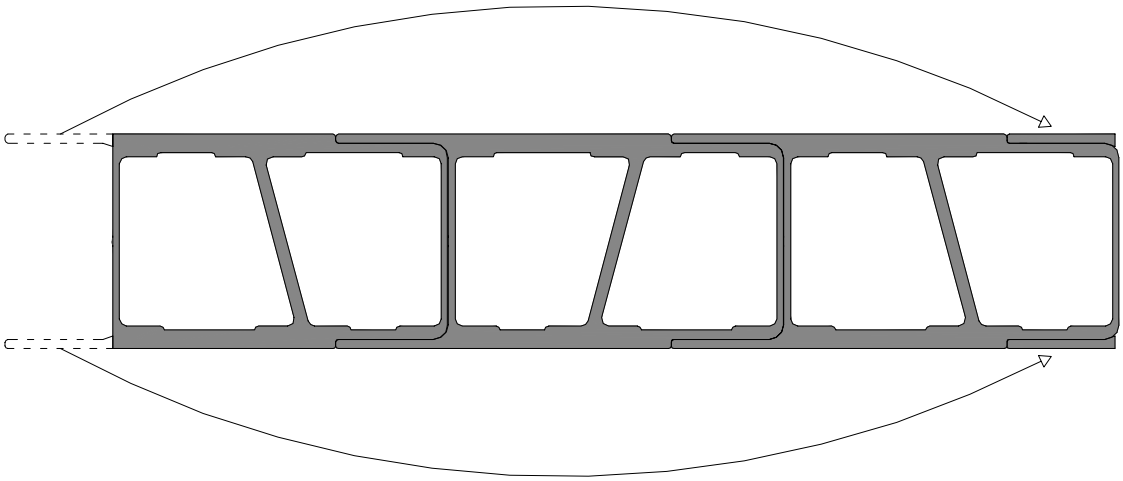

Figure C-3. End view of large horizontal oven and experimental set-up (not to scale)

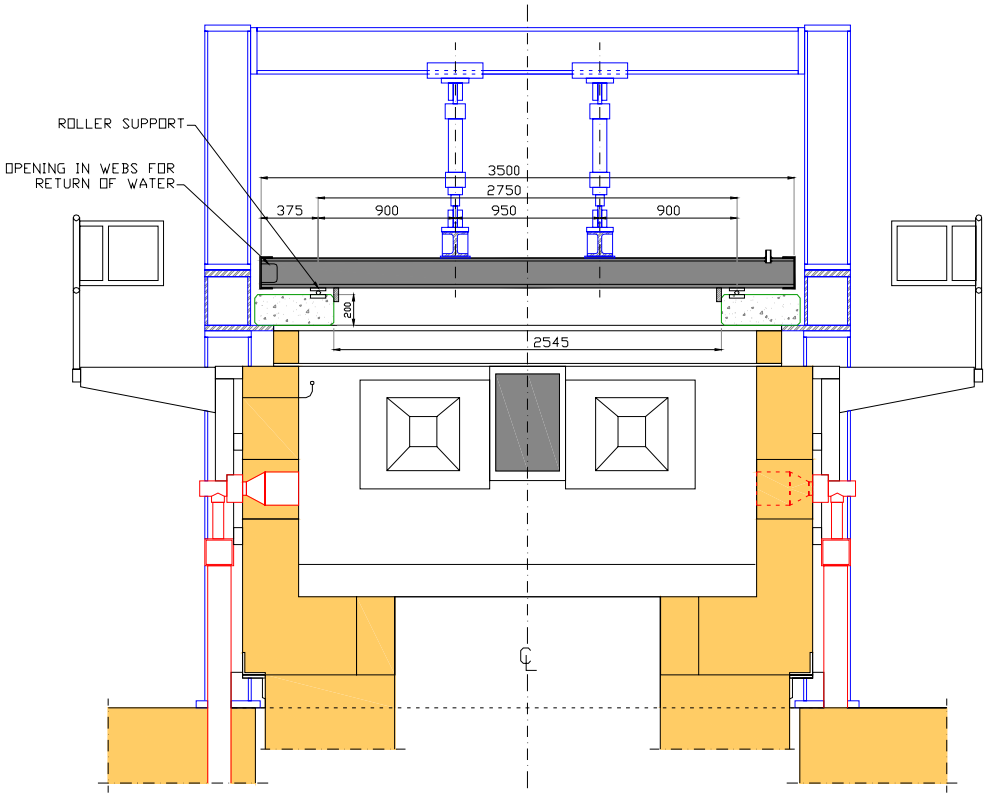

Figure C-4. Side view of large horizontal oven and experimental set-up (not to scale)

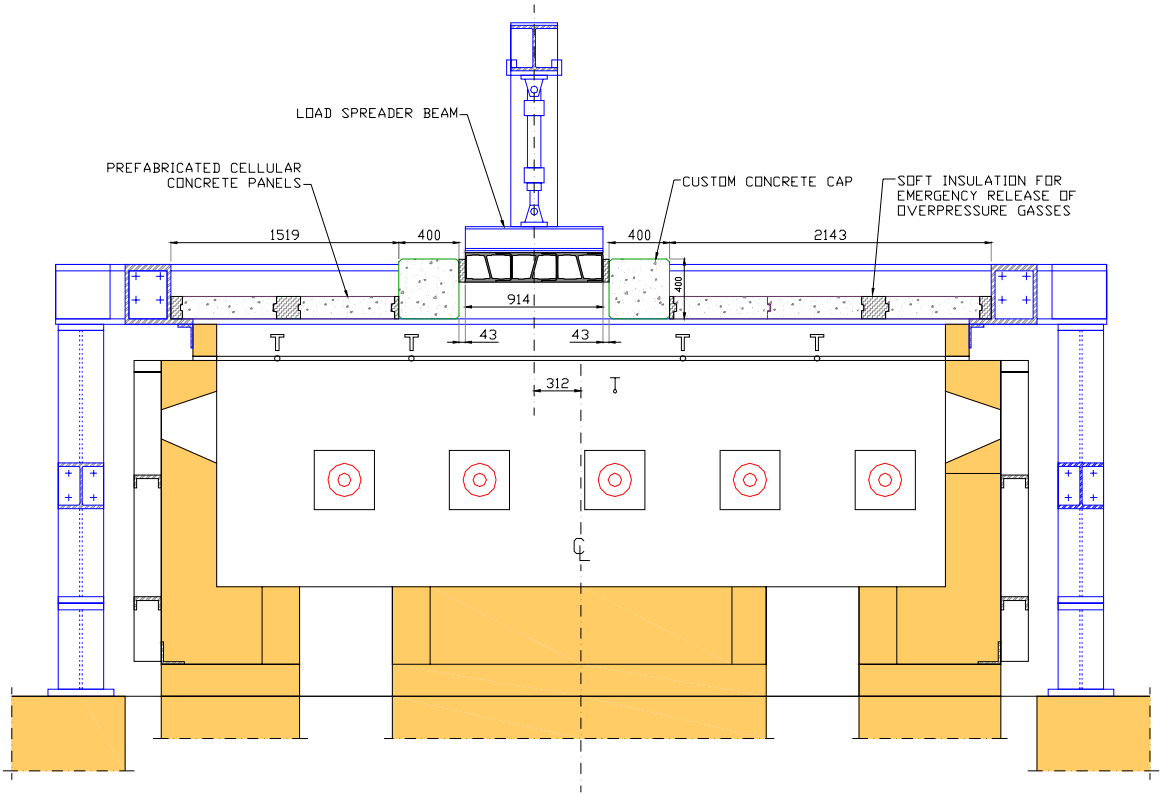

Figure C-5. Instrumentation of upper face sheet of specimens

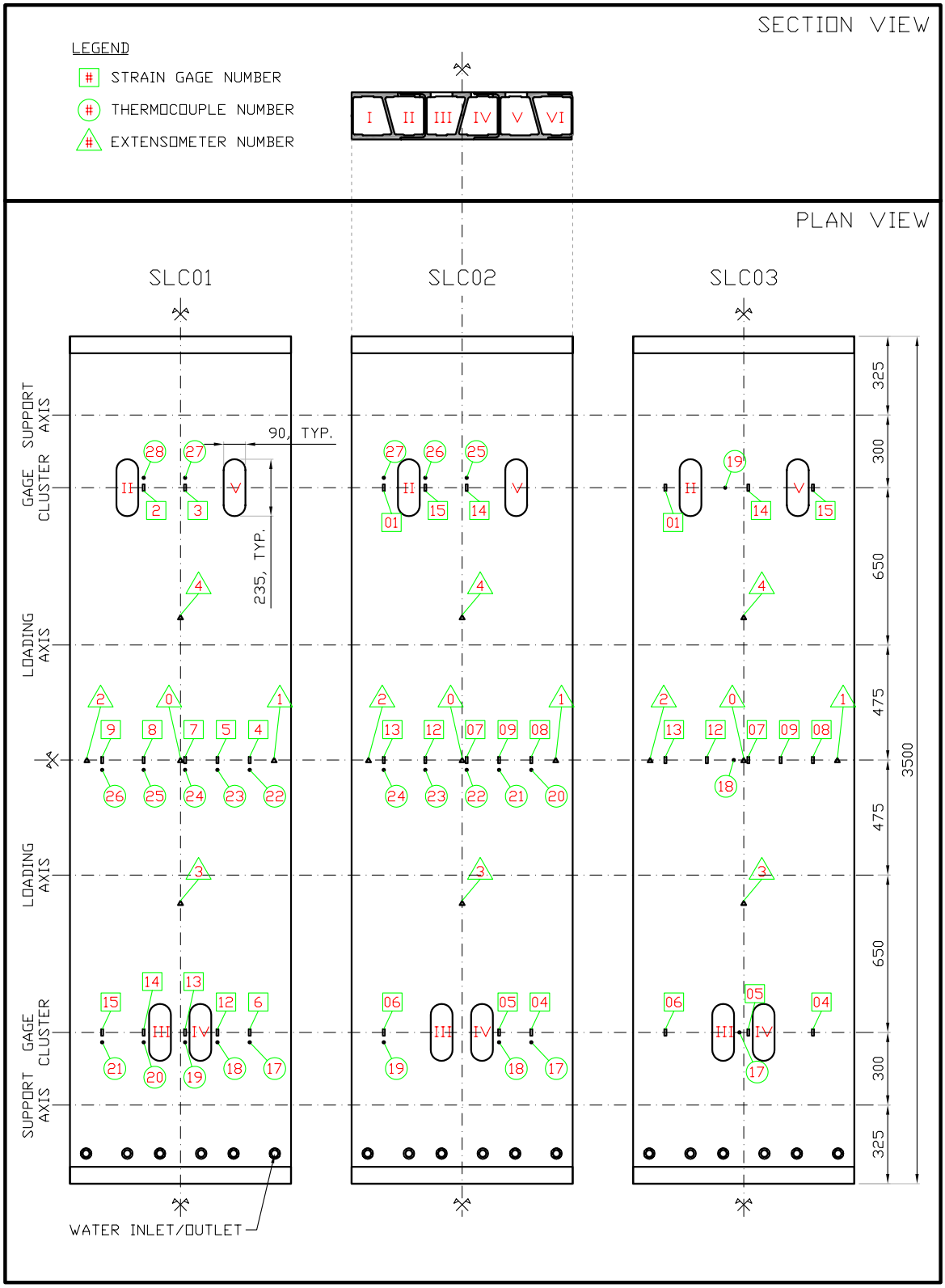

Figure C-6. Instrumentation and as-built dimensions of lower face sheet (Cells II-III)

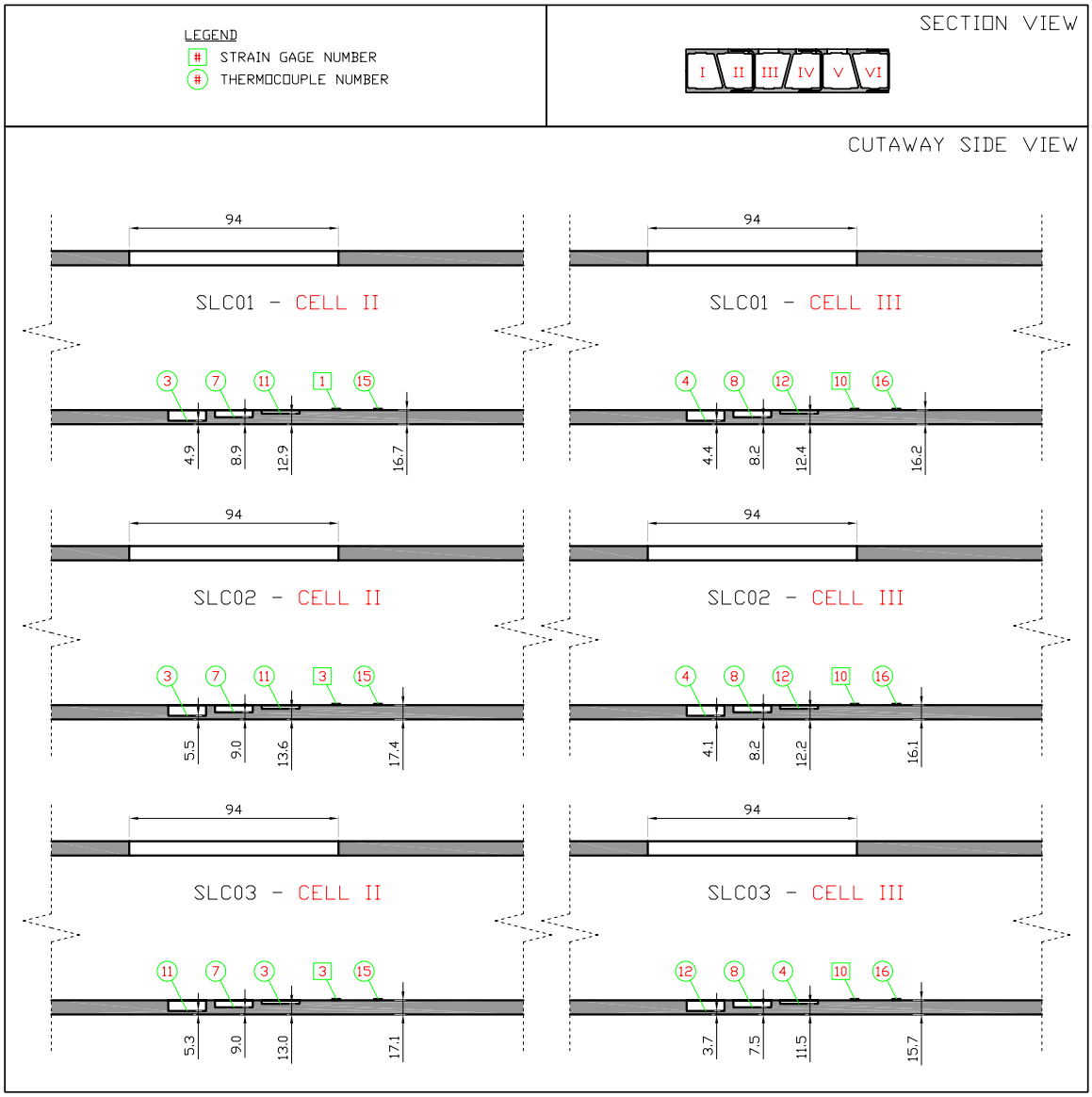

Figure C-7. Instrumentation and as-built dimensions of lower face sheet (Cells IV-V)

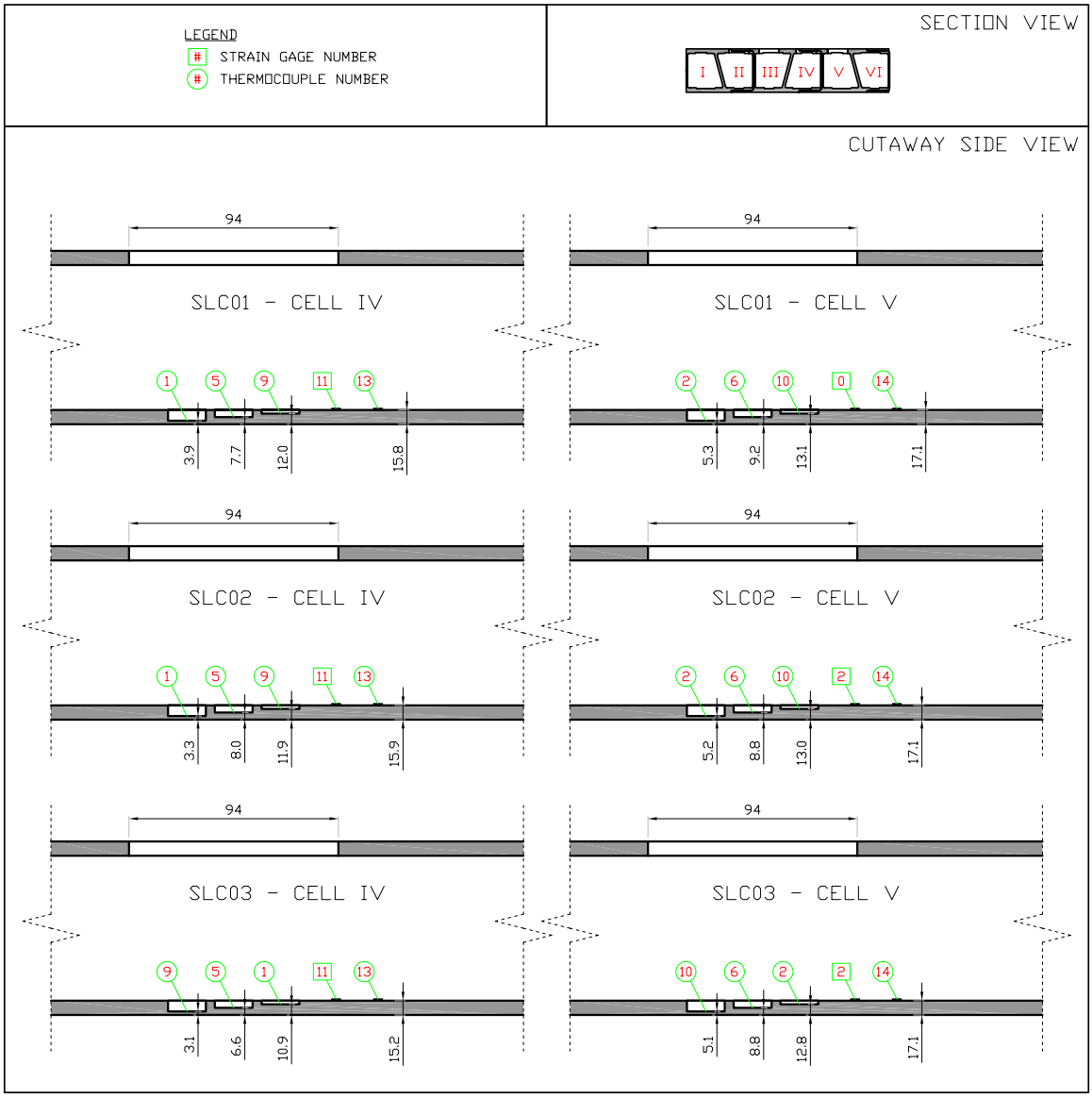

Figure C-8. SLC01 - Experimental set-up

Figure C-9. SLC02 - Experimental set-up

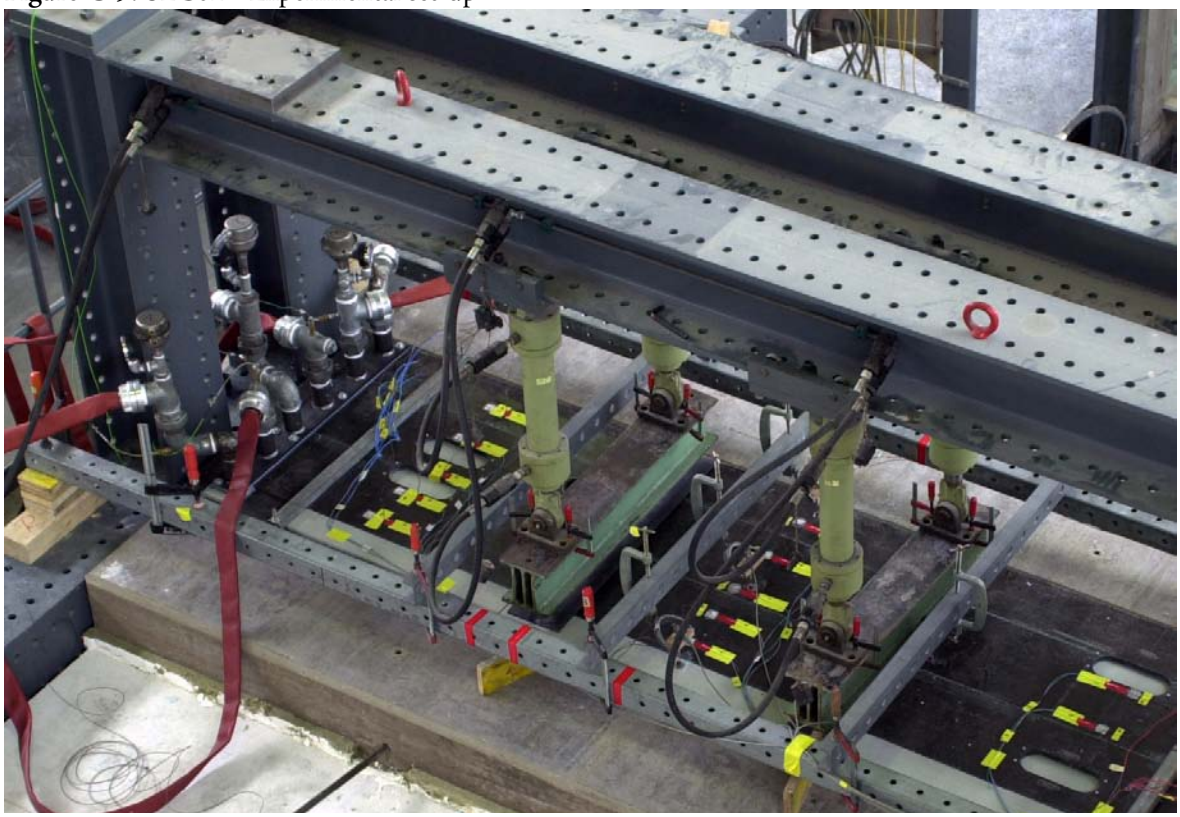

Figure C-10. SLC02 - After approx. 30 minutes of thermal loading (uneven heating evident)

Figure C-11. SLC01 - After approx. 70 minutes of thermal loading (broken rovings visible)

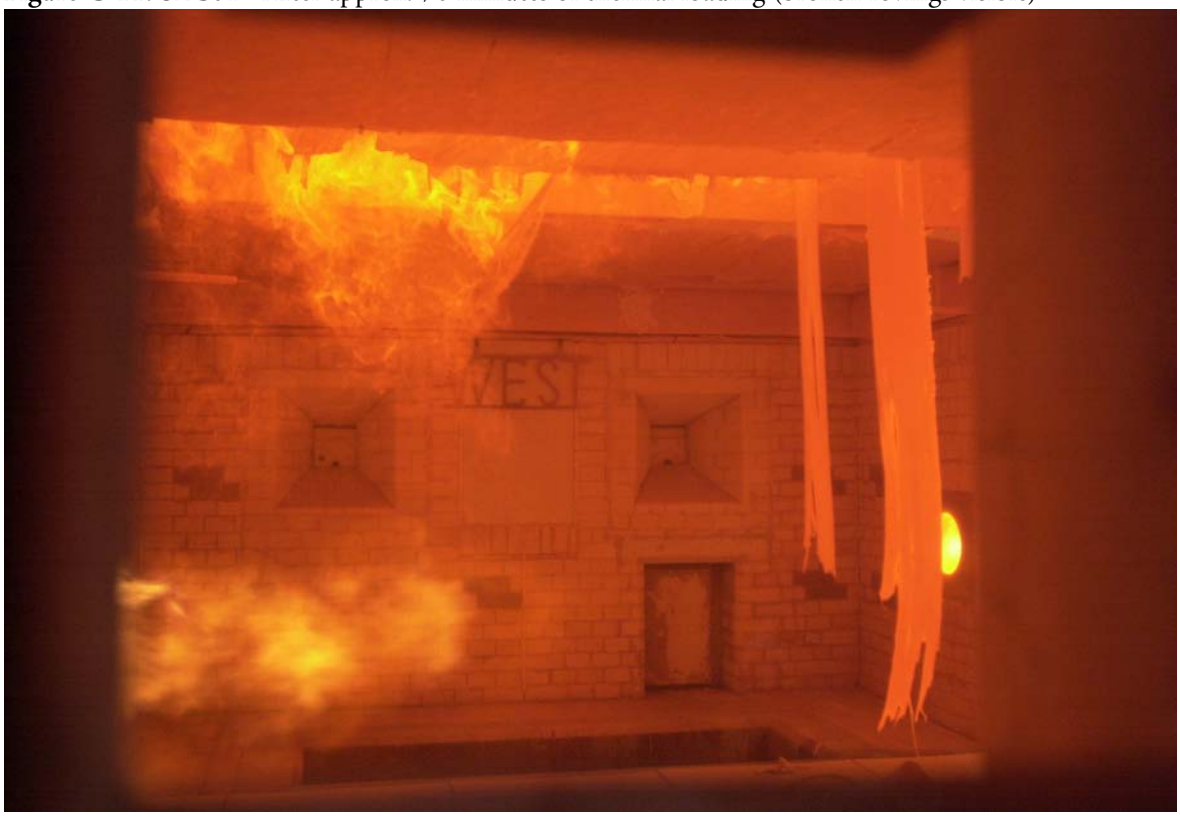

Figure C-12. SLC01 - Removal of specimen and reaction frame at conclusion of experiment

Figure C-13. SCL01 - Hot face of specimen directly after conclusion of experiment

Figure C-14. SLC03 - Smoke and steam escaping through steel adapter pipes

Figure C-15. SLC03 - Location of failure in upper face sheet

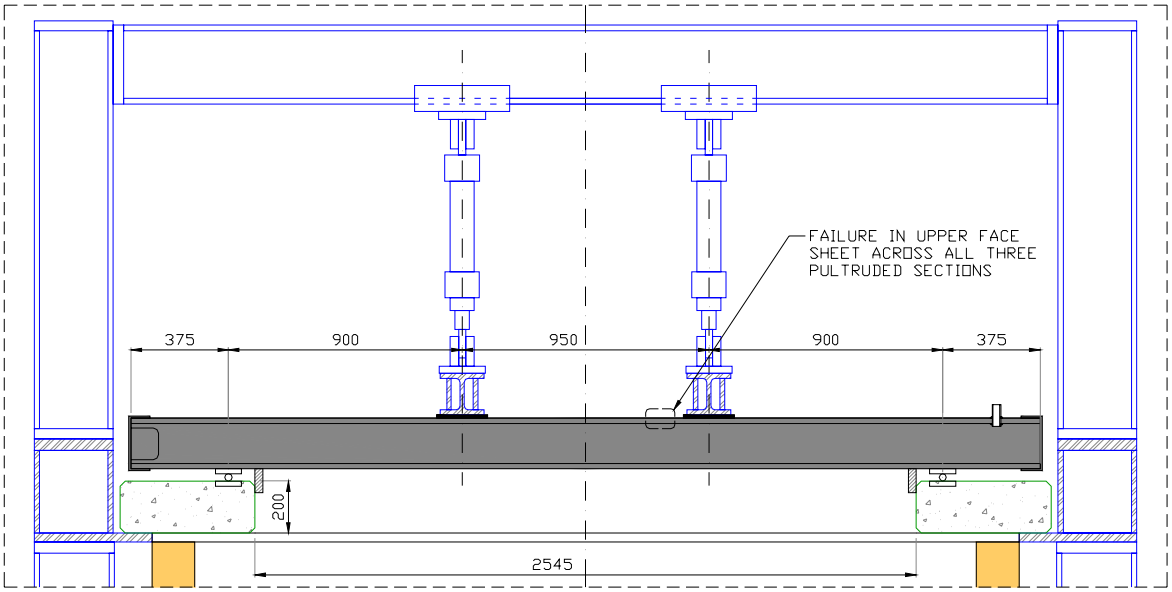

Figure C-16. SLC03 - Failure of upper face sheet

Figure C-17. SLC03 - Close-up view of failure in upper face sheet

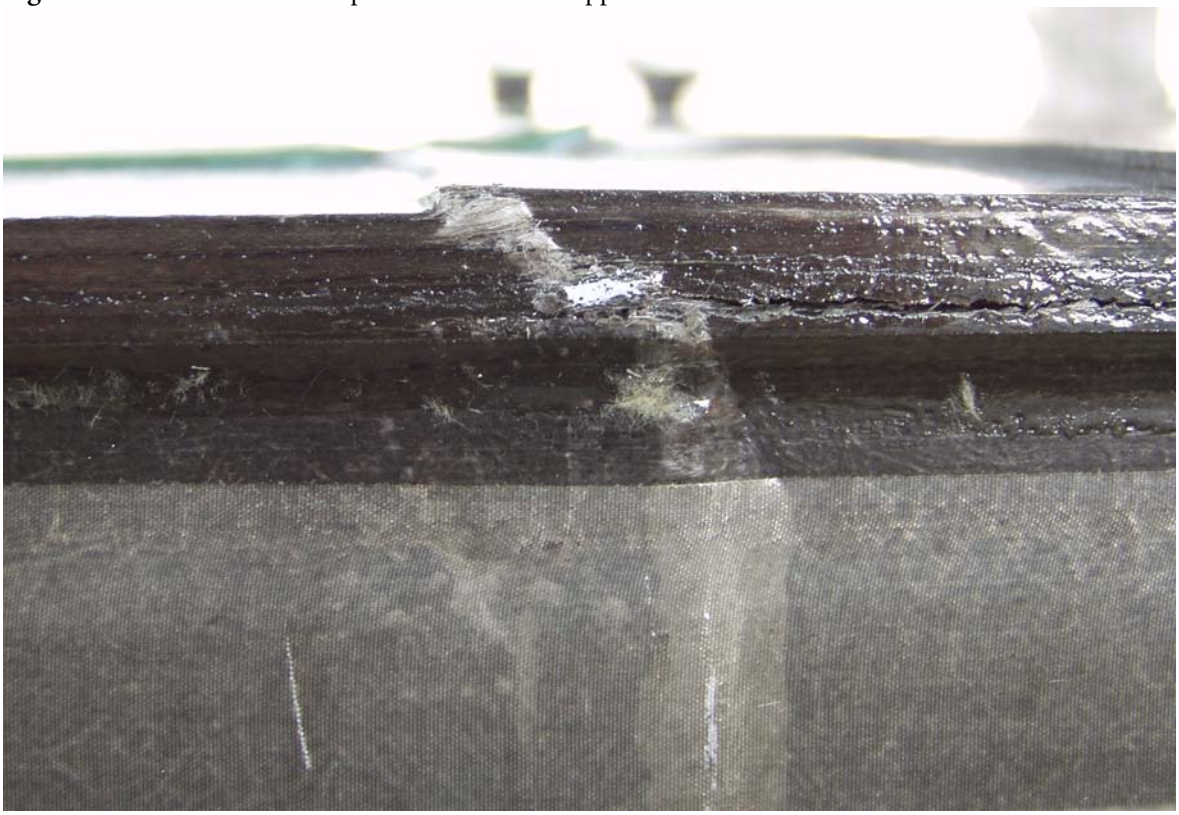

Figure C-18. Depth of fire damage

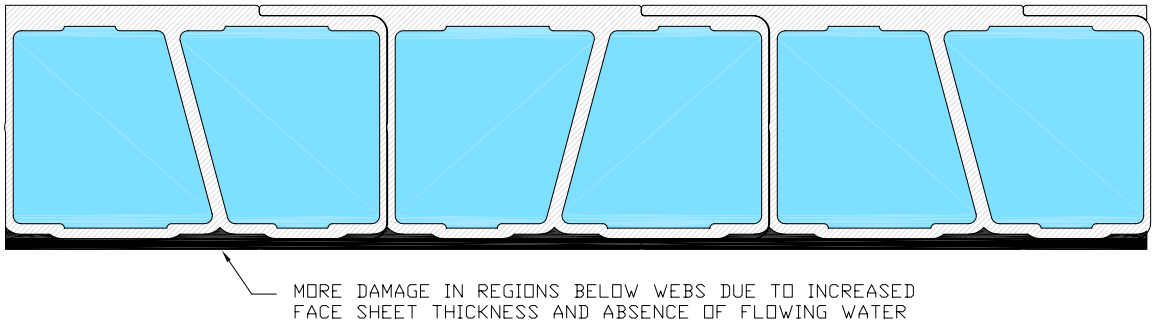

Figure C-19. Specimens post-experiment, quartered to allow layer-wise inspection

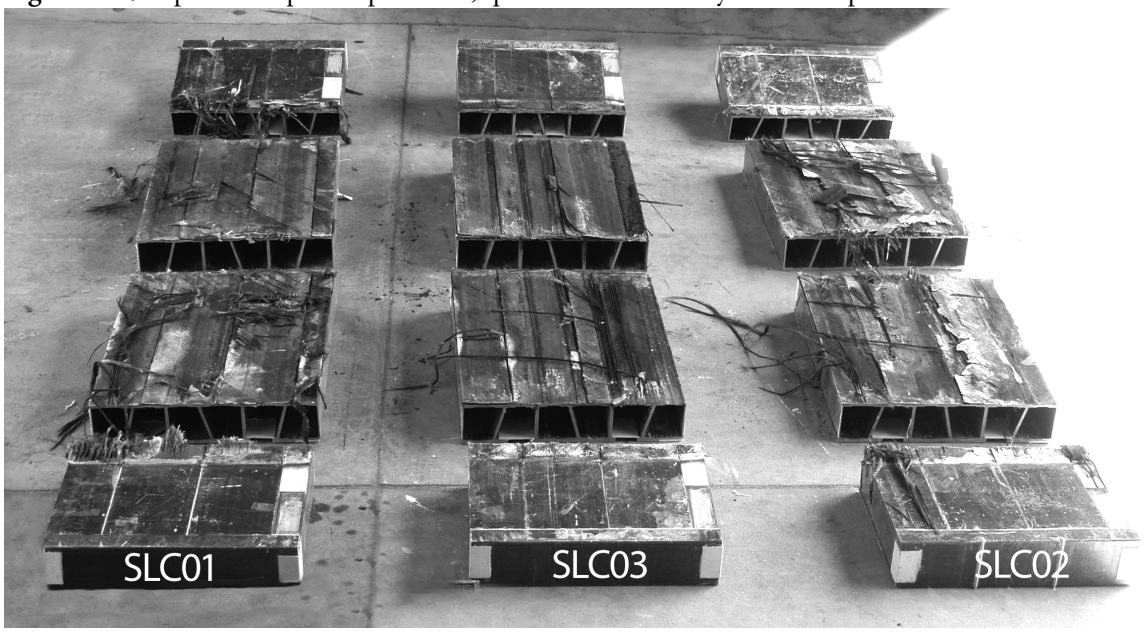

Figure C-20. SLC01 remaining lower face sheet thickness

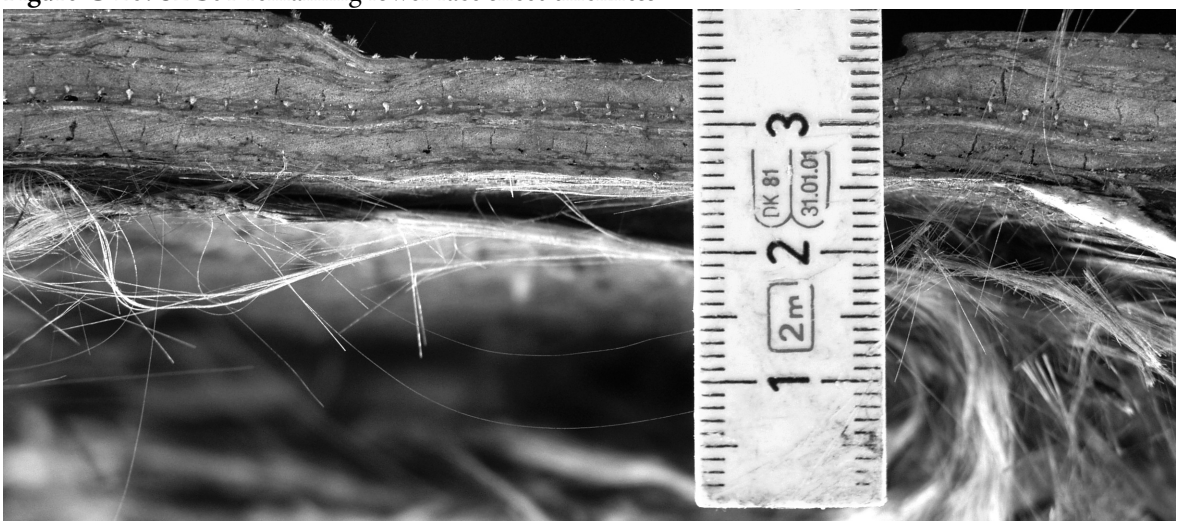

Figure C-21. SLC02 remaining lower face sheet thickness

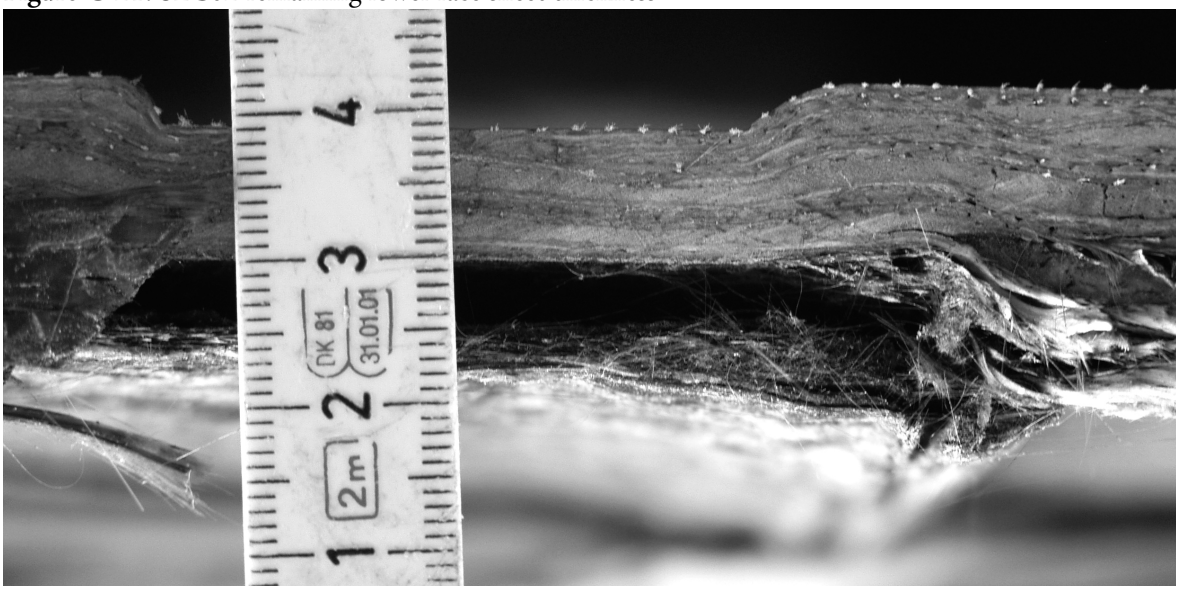

Figure C-22. SLC03 remaining lower face sheet thickness

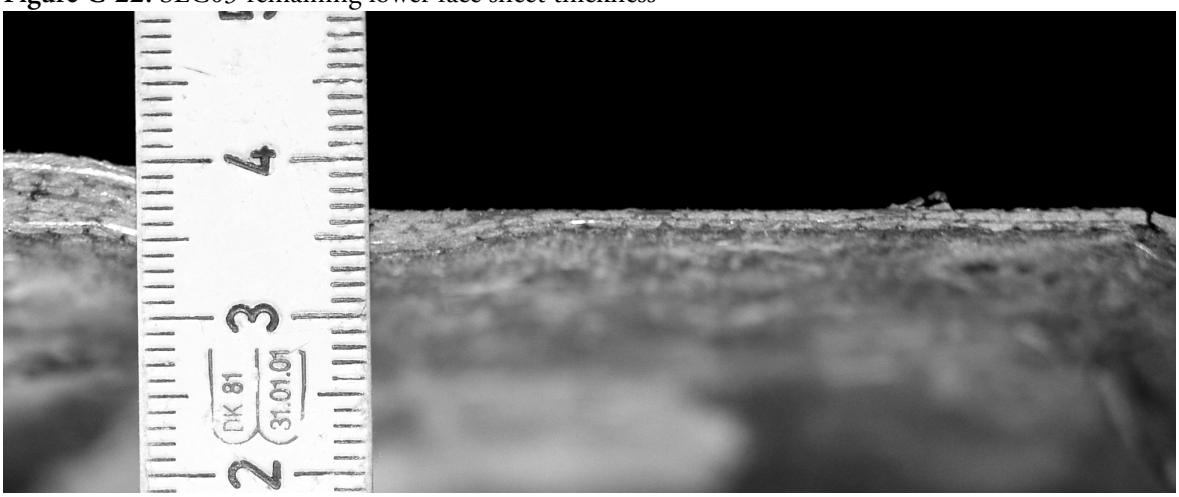

Figure C-23. SLC01 delamination

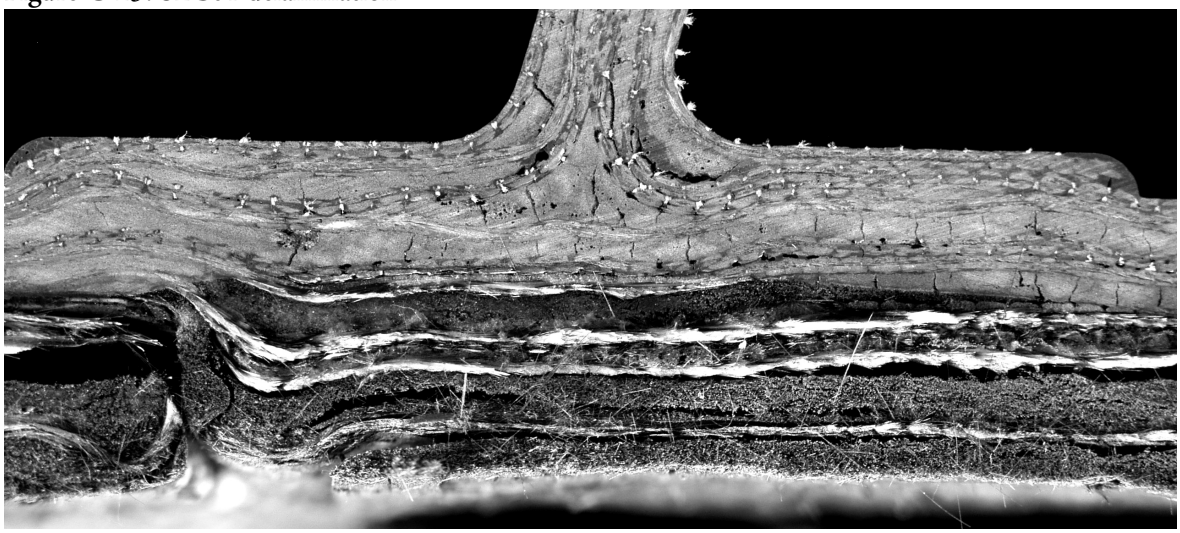

Figure C-24. SLC02 delamination

Figure C-25. SLC03 delamination

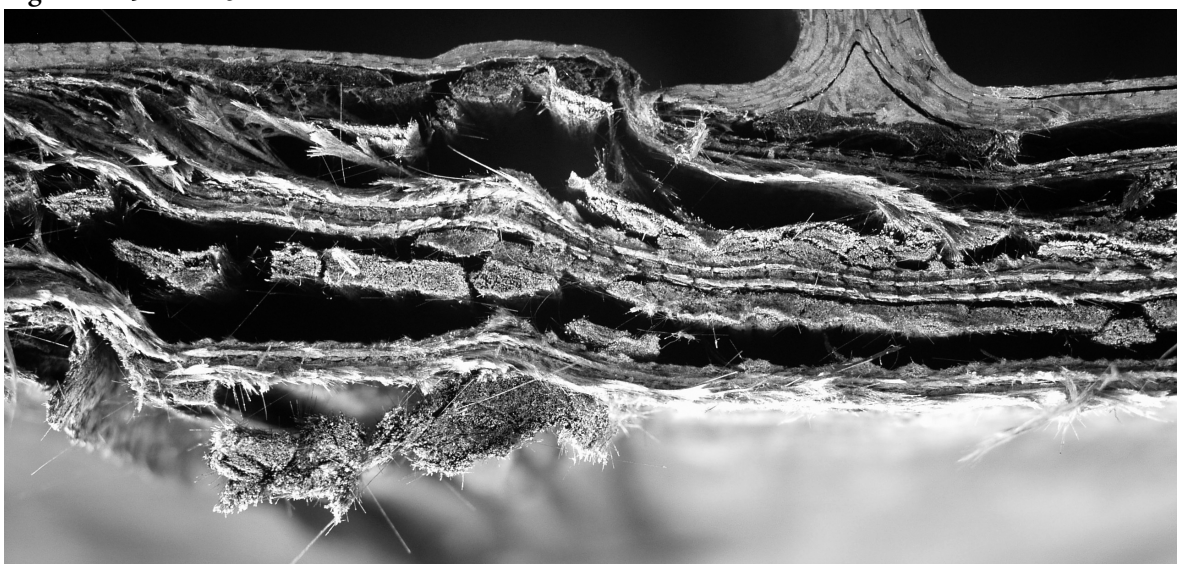

Figure C-26. SLC01 - Strain vs. time

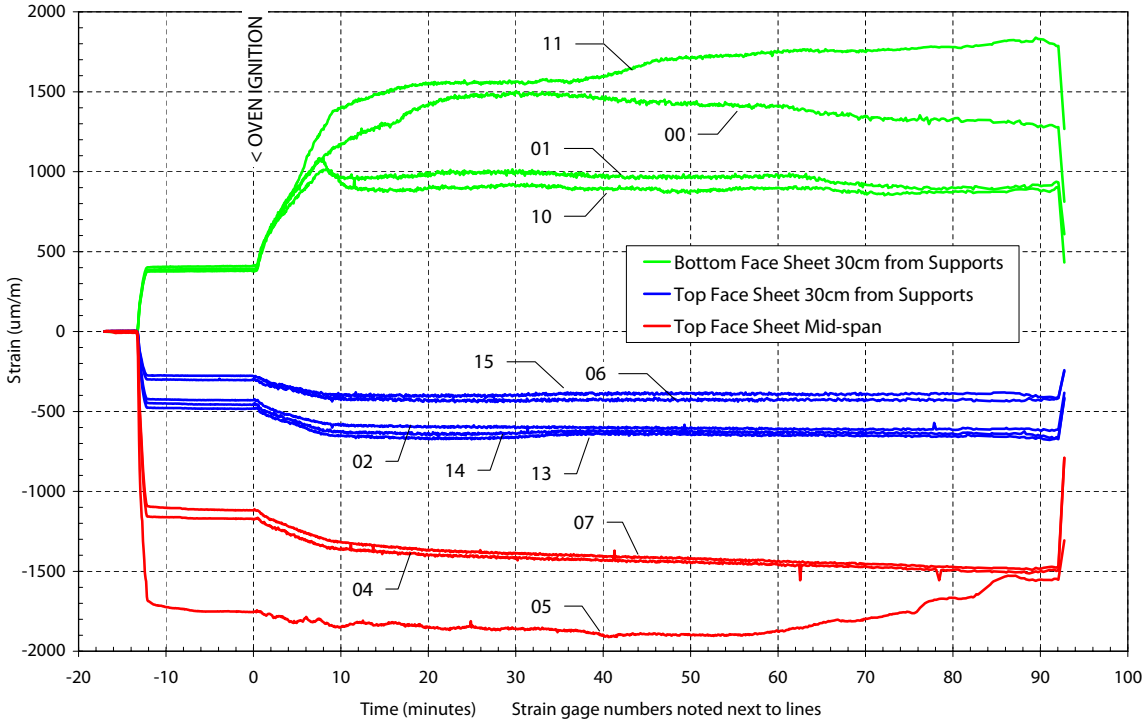

Figure C-27. SLC02 - Strain vs. time

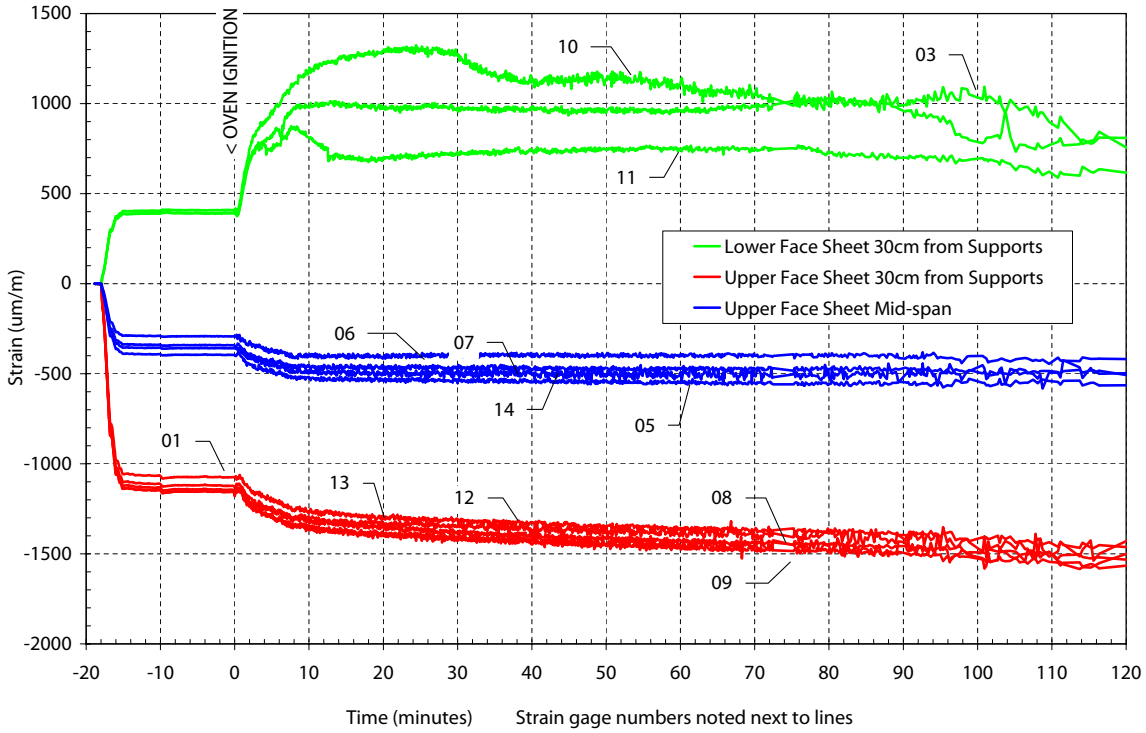

Figure C-28. SLC03 - Strain vs. time

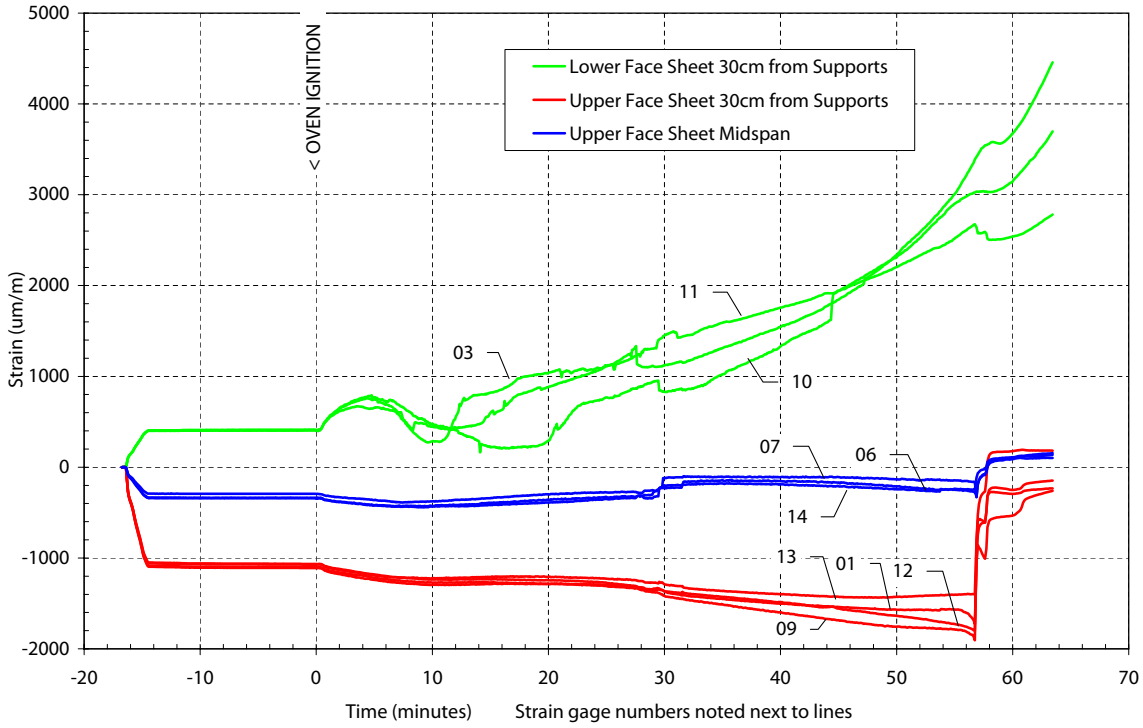

Figure C-29. All SLC Experiments - Average adjusted mid-span deflection vs. time

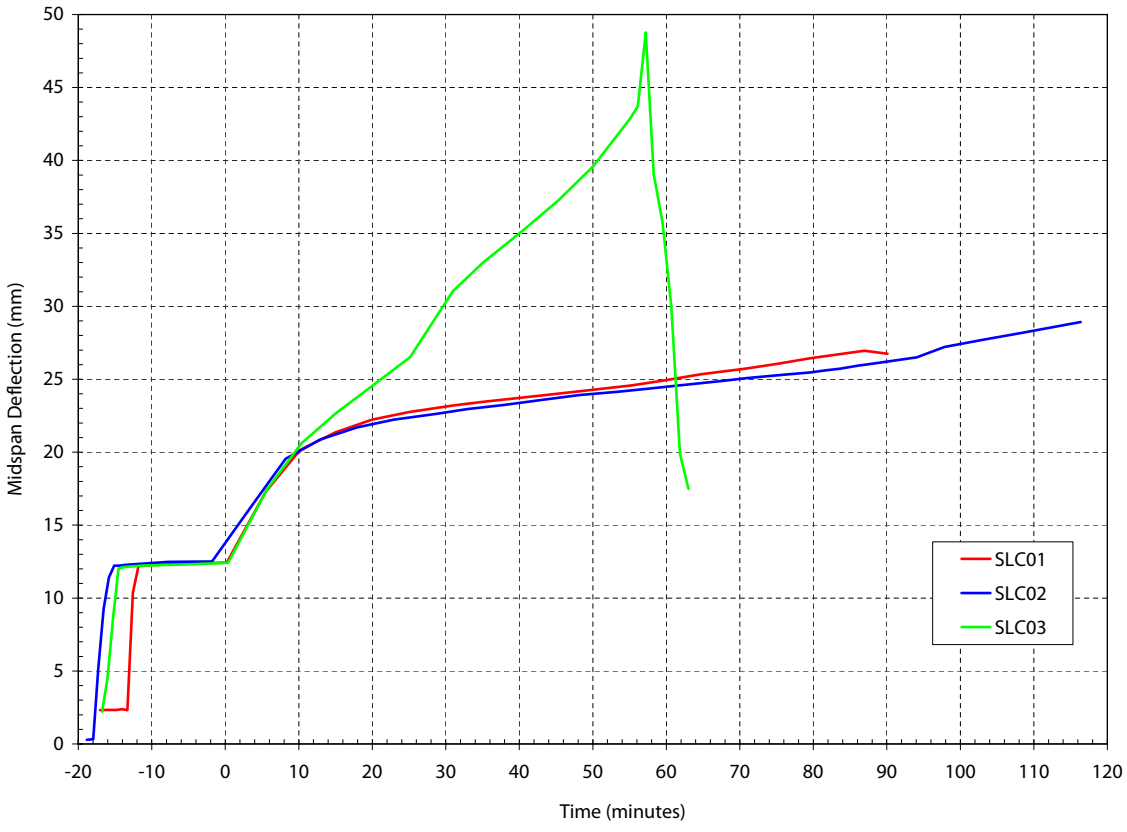

Figure C-30. All SLC Experiments - Change in water temperature vs. time (T_{outlet} - T_{inlet})

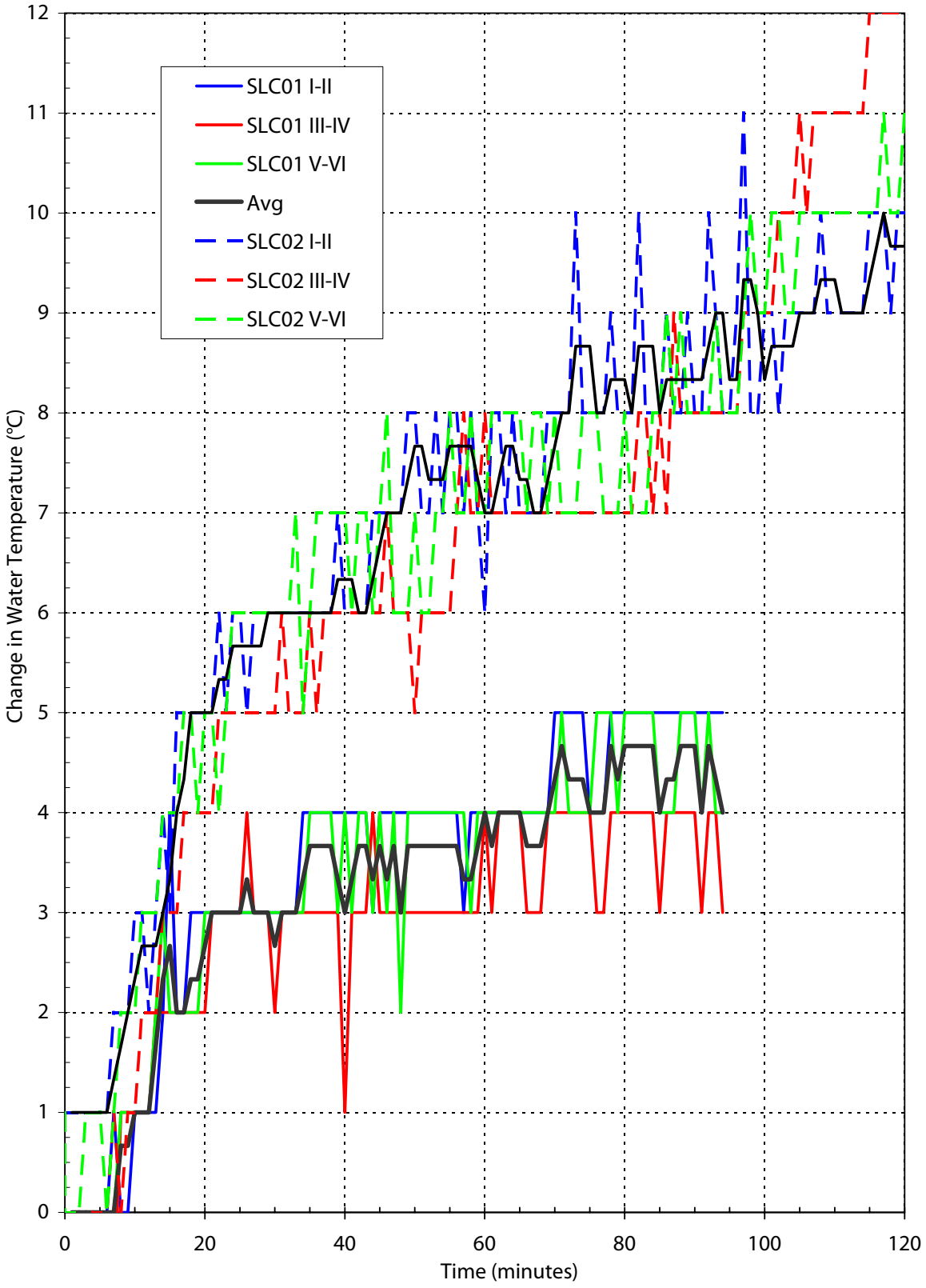

Figure C-31. SLC01 - Temperature vs. time (measurements in legend refer to distance from hot face)

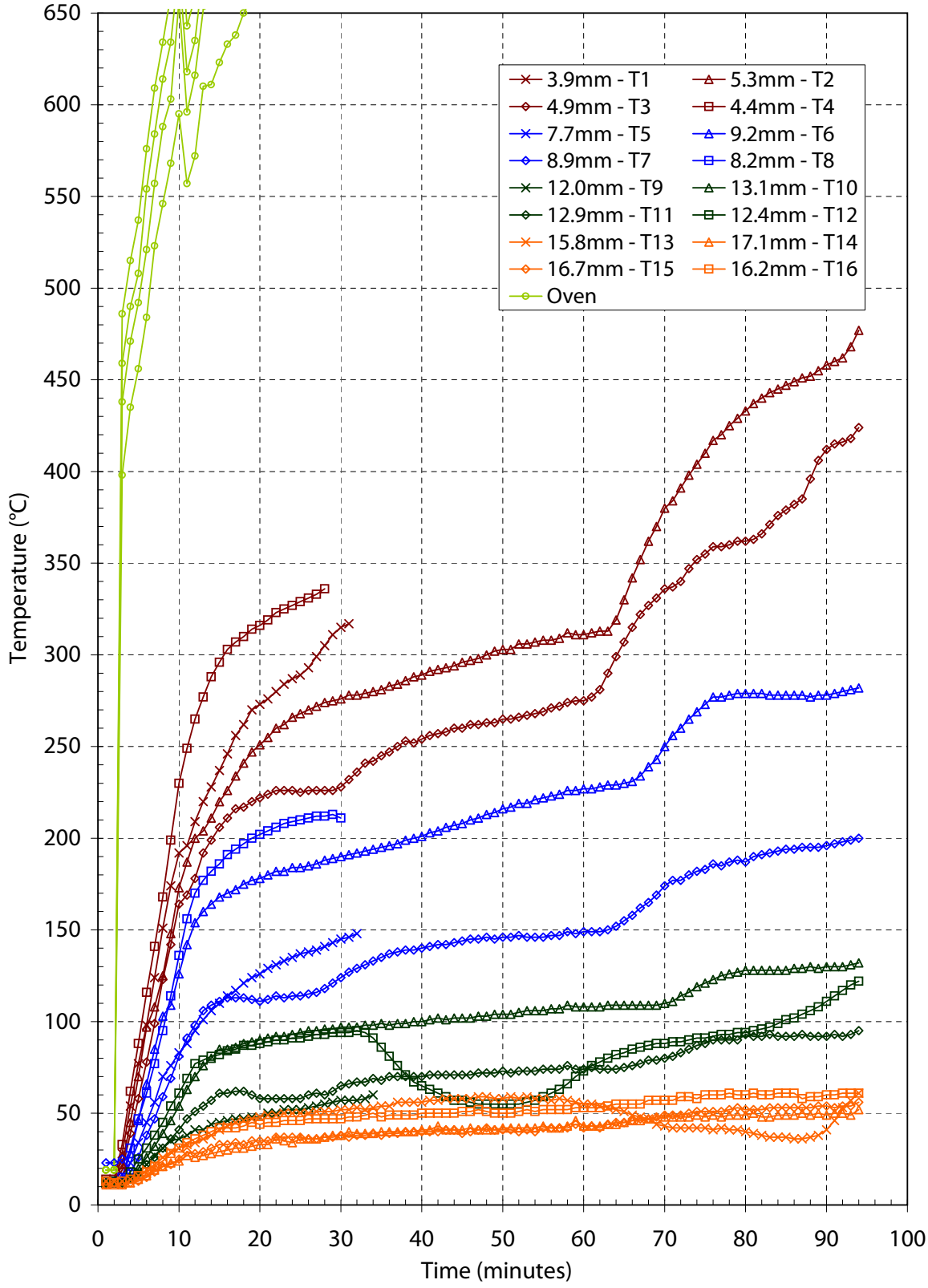

Figure C-32. SLC02 - Temperature vs. time (measurements in legend refer to distance from hot face)

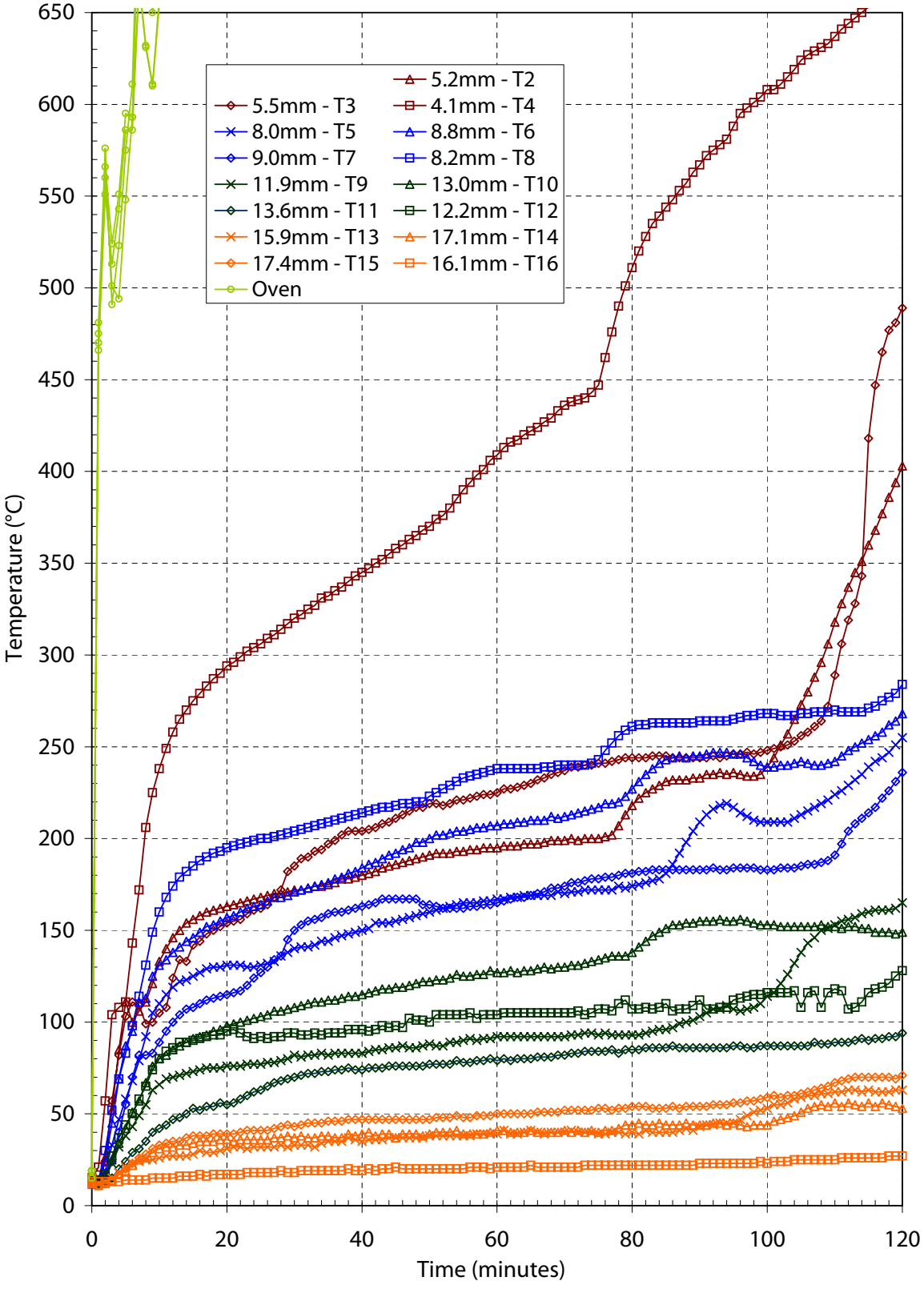

Figure C-33. SLC03 - Temperature vs. time (measurements in legend refer to distance from hot face)

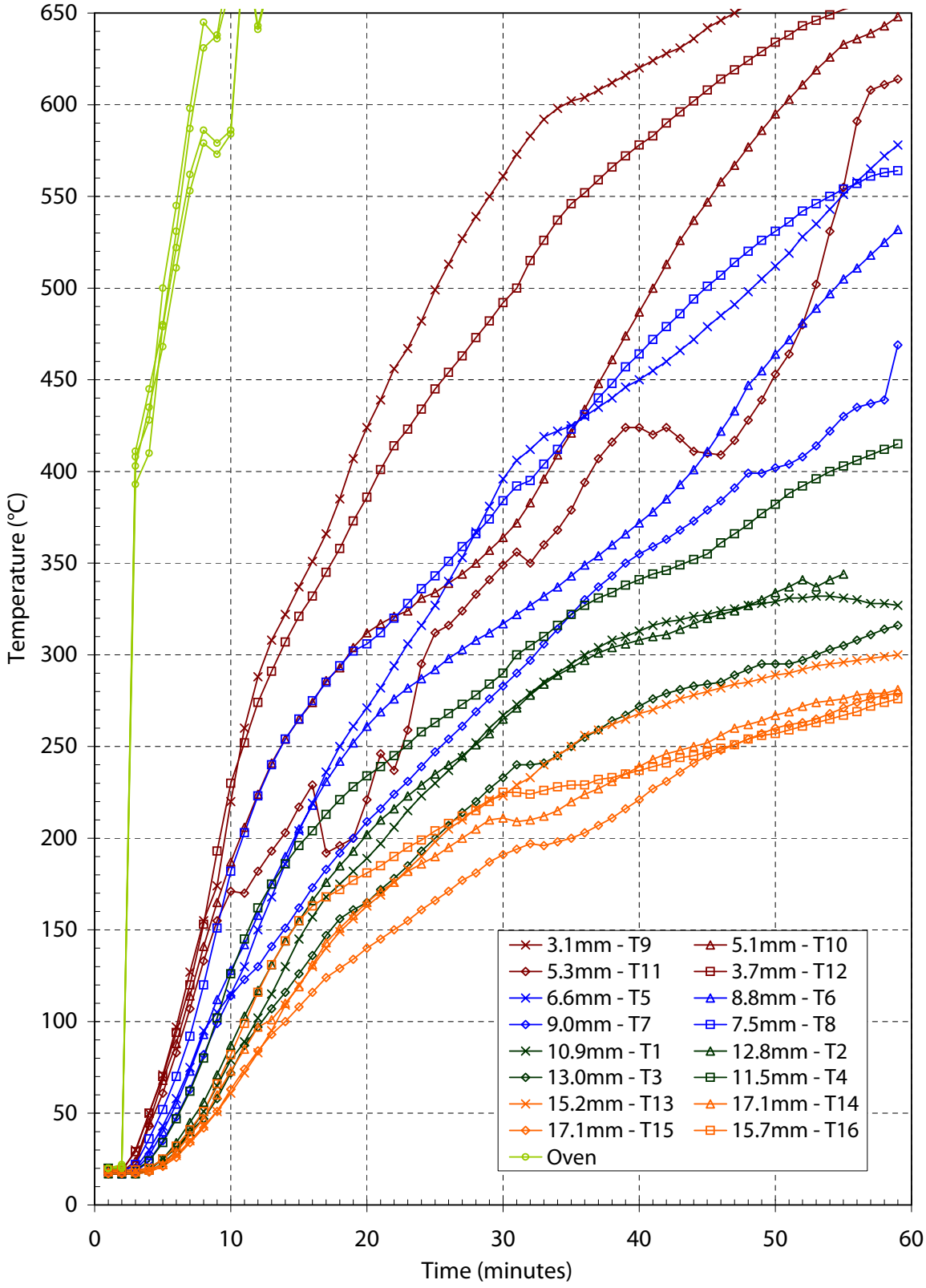

Figure C-34. Average temperature profiles through lower face sheet at selected times

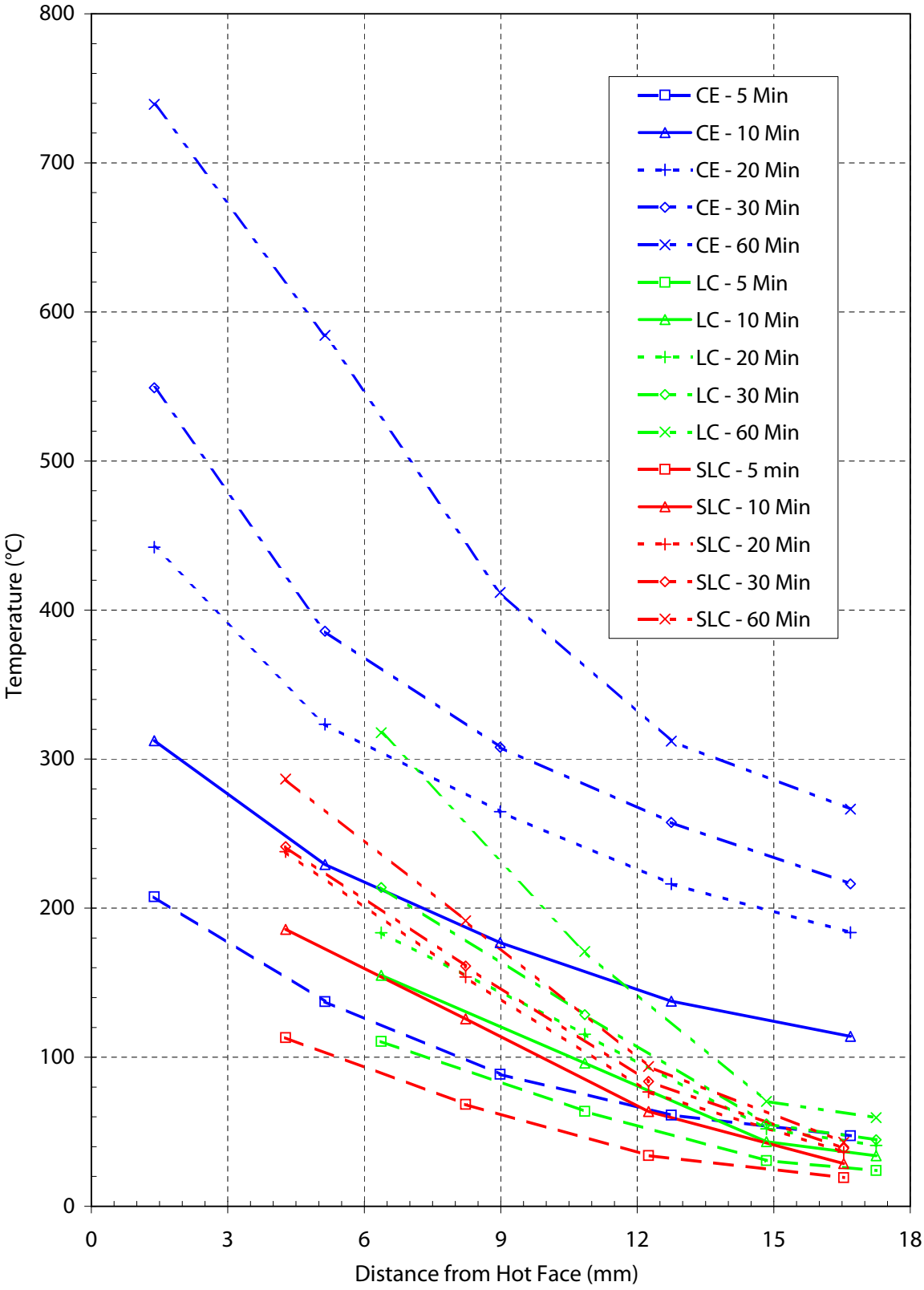

Figure C-35. SLC01 - Illustration of corrections made to "As-recorded" deflections

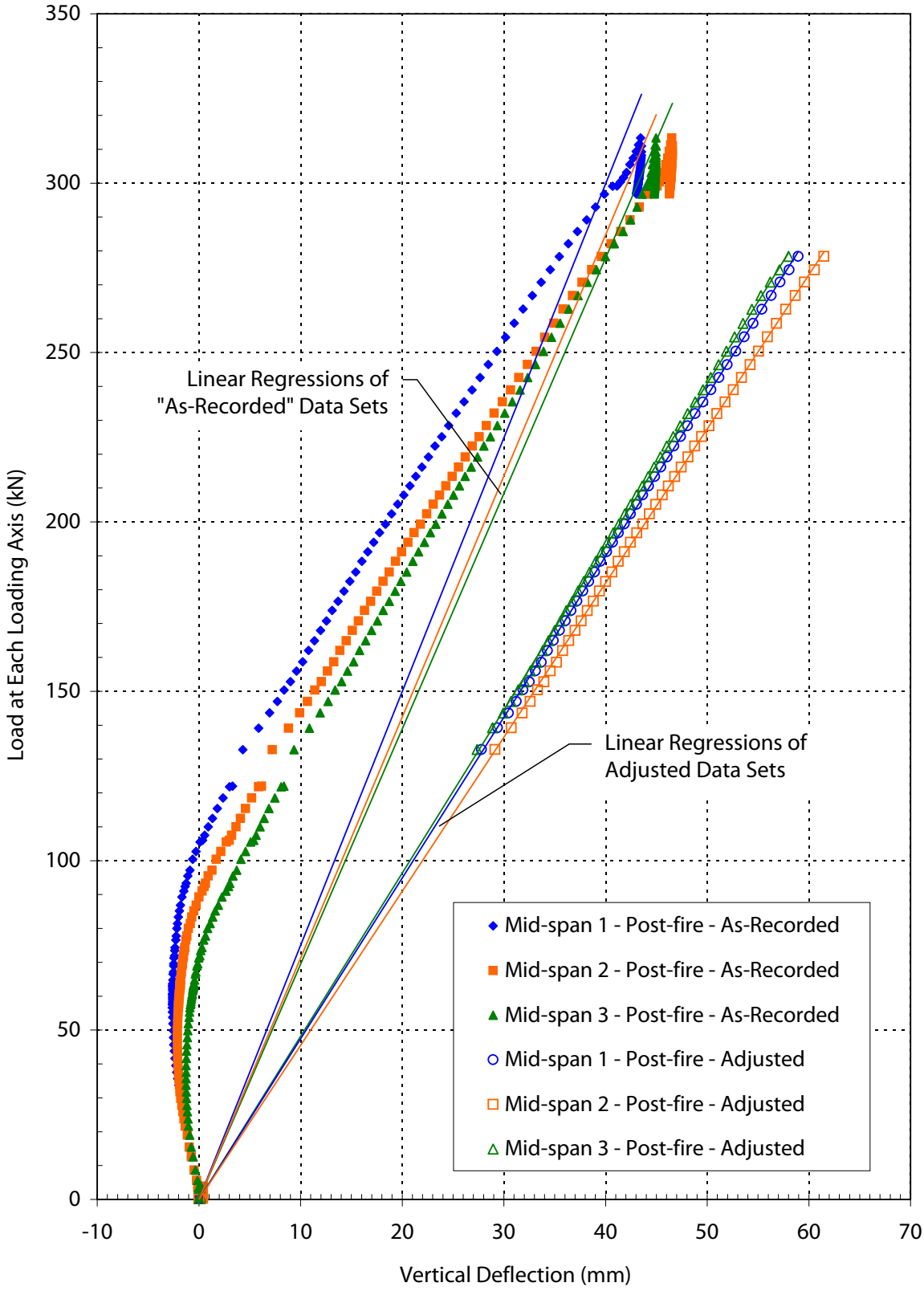

Figure C-36. SLC01 - Deflection vs. time (adjusted values - see text)

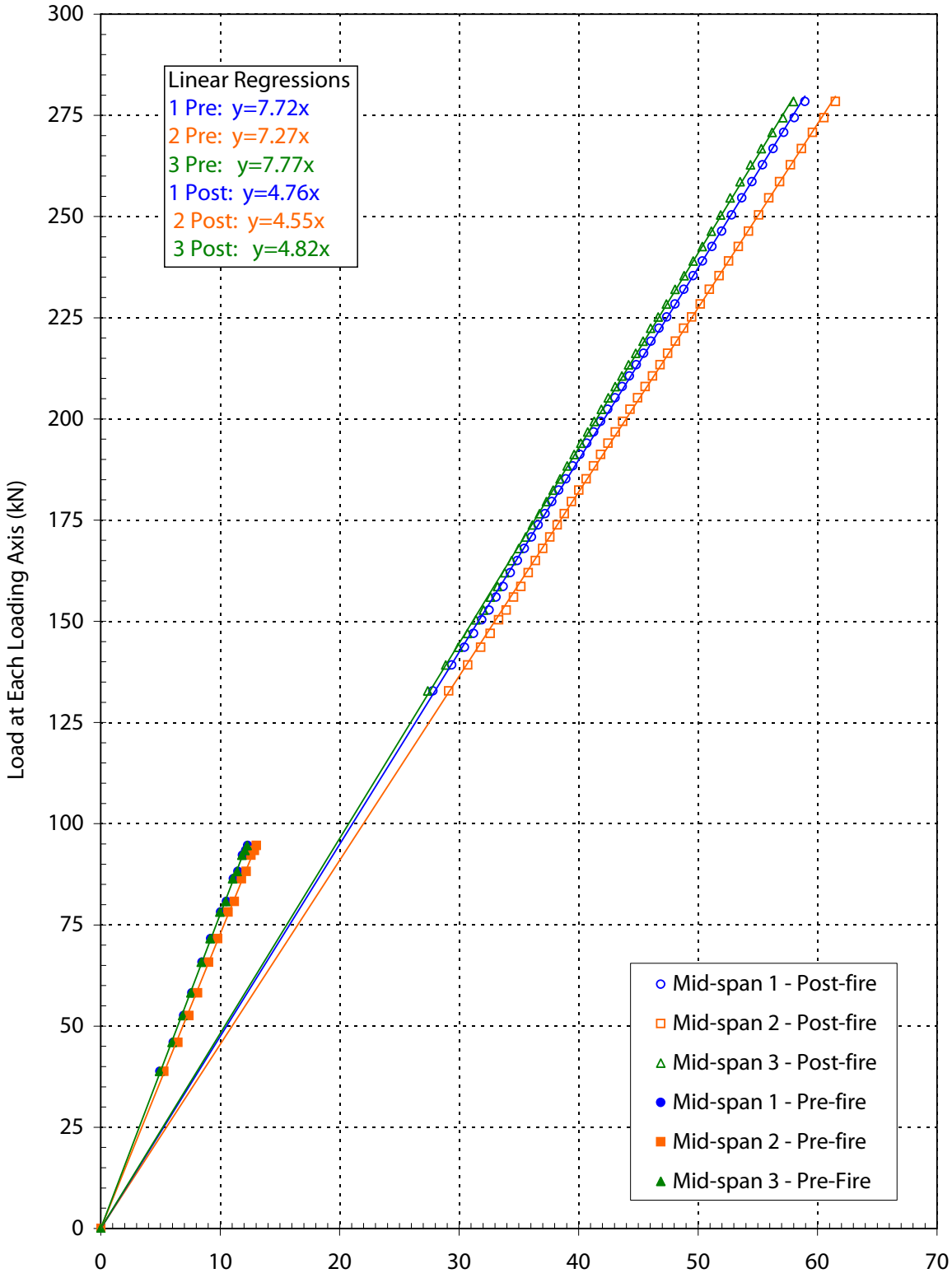

Figure C-37. SLC02 - Deflection vs. time (adjusted values - see text)

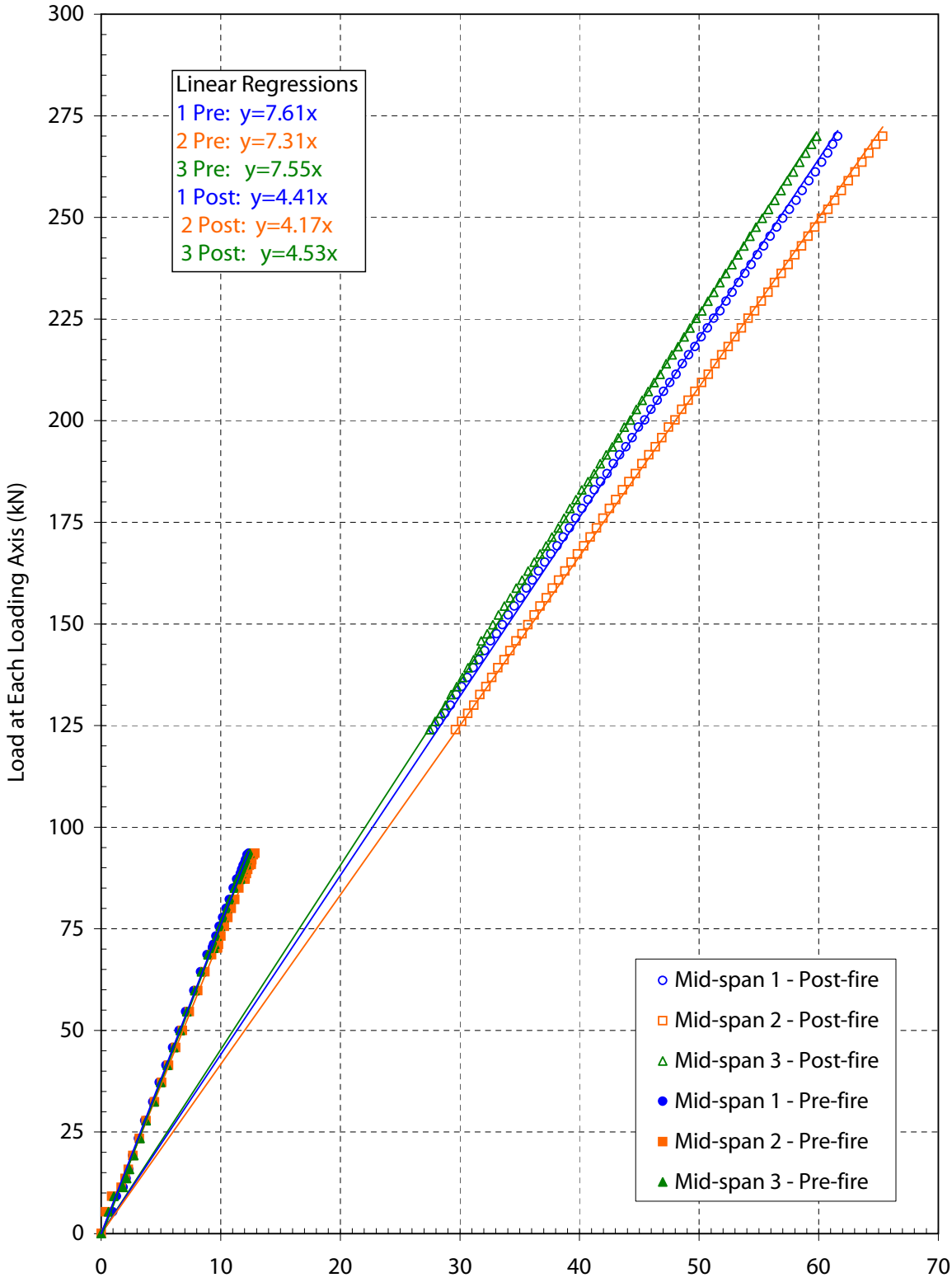

Figure C-38. SLC03 - Deflection vs. time (adjusted values - see text)

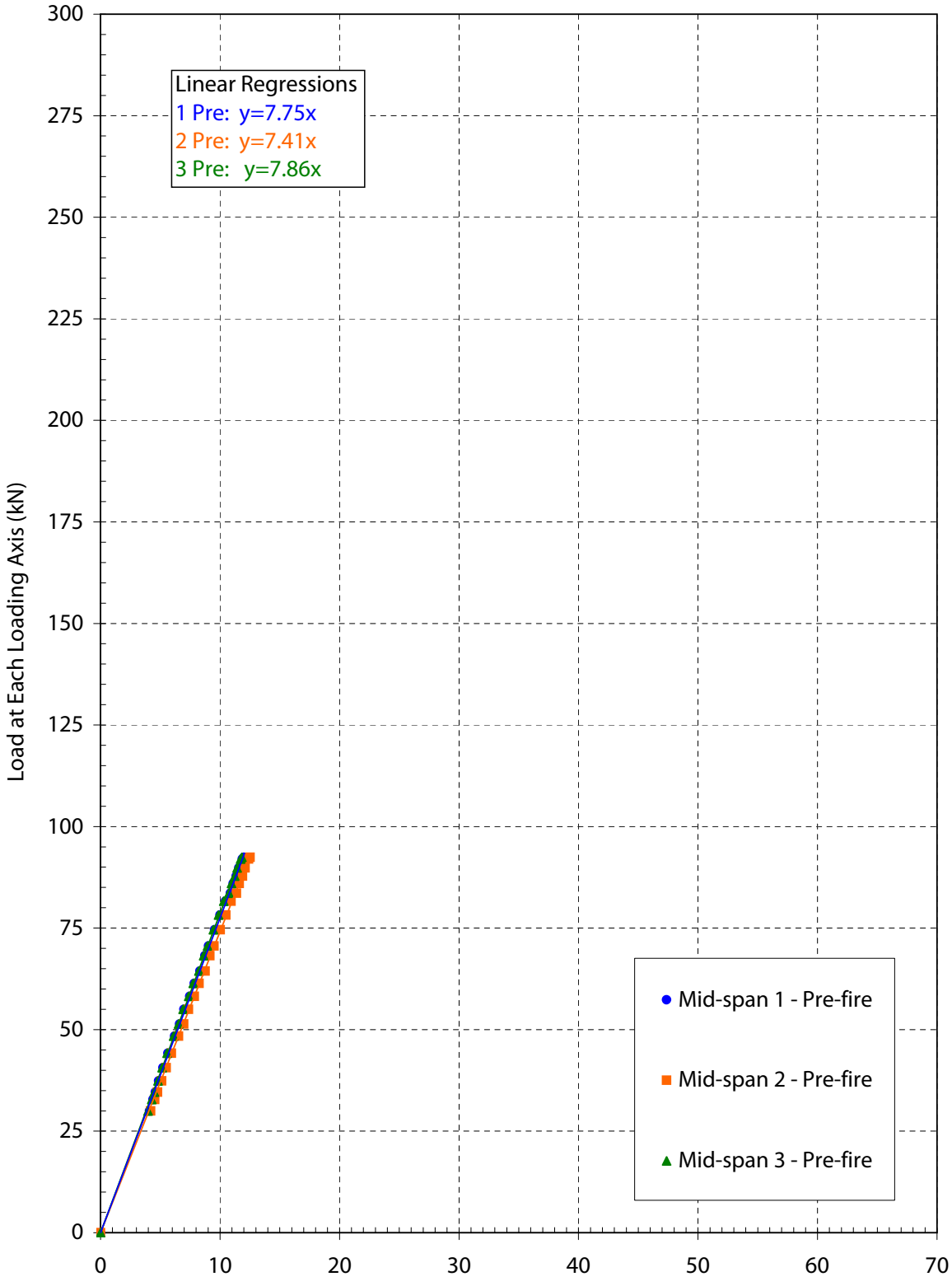

Figure C-39. All SLC Experiments - Strain distributions at 30 cm from supports (units: μm/m)

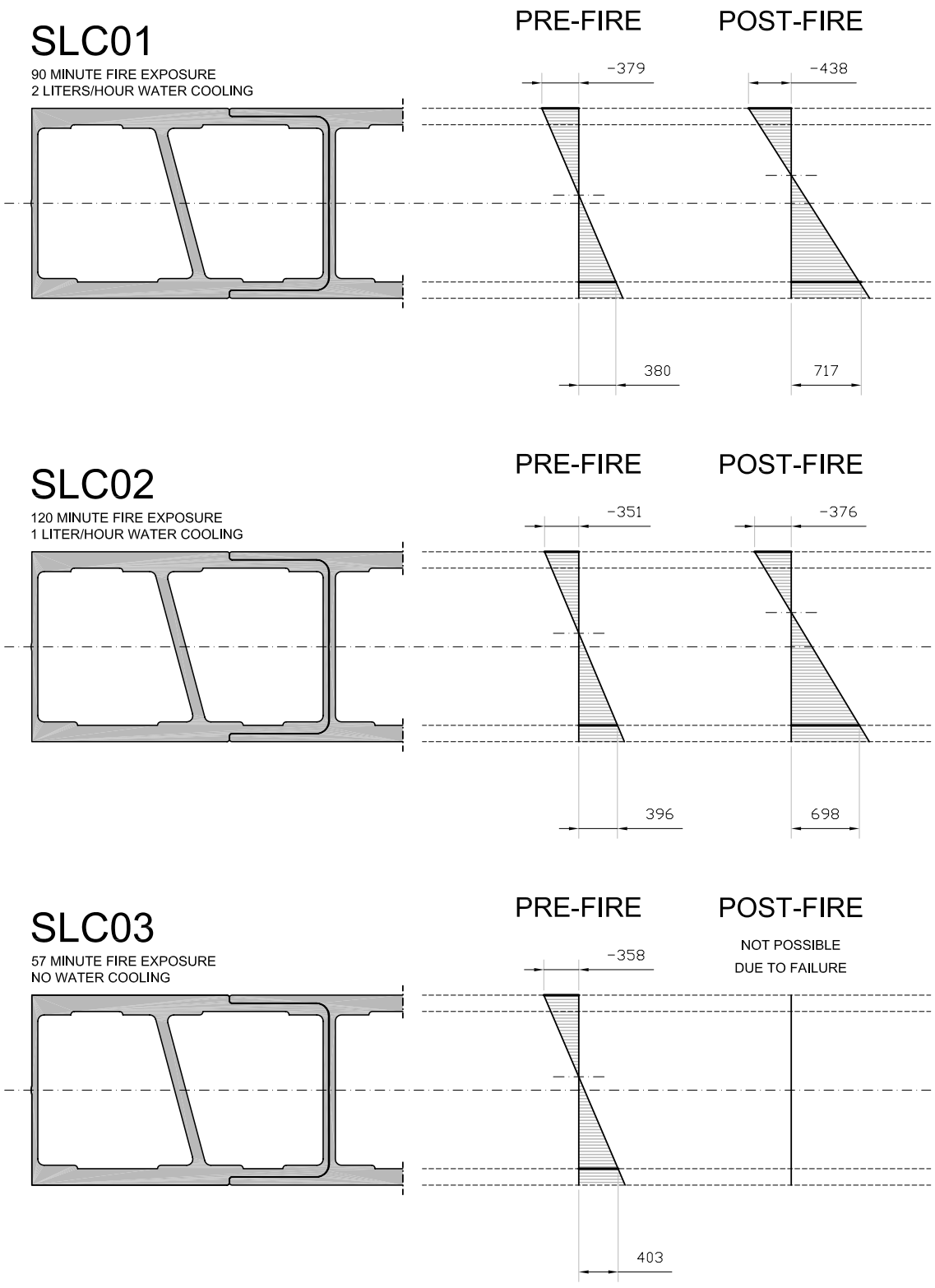

D

Numerical Model Source Code

Text Input Files for the Thermochemical and Thermomechanical Models

1 Themochemical Model Source Code for *ANSYS 7.0*

```
/title,Thermochemical_Model_(142w)

!--------------------------- VARIABLES AND CONSTANTS ---------------------------

/PREP7
/UNITS,SI
TOFFST,274                !  Conversion from Kelvin to Celsius
                          !  Units:  m, °C, kg, s, J, Pa

       !  NOTE: “hfint” IS THE ONLY VALUE THAT DIFFERS
       !        BETWEEN THE LIQUID-COOLED AND DRY CONDITIONS

*SET,hfint ,  200         !  Convection film coef at internal water interface

*SET,bftint,   16         !  Water temperature

*DIM,hfhot,TABLE,4,,,TEMP  !  Convective film coef at hot face
hfhot(1,0)=20,1000
hfhot(1,1)= 5,  50
                          !  ISO 834 curve - oven gas temperature
*DIM,bftbot,TABLE,12,,,TIME
bftbot(1,0)= 60,180,360,600,1200,1800,2400,3600,5400,7200
bftbot(1,1)=349,502,603,678, 781, 842, 885, 945,1006,1049

*SET,totaltime,7200       !  Time at end of fire exposure
*SET,timestep,20
*SET,numstep,360
*SET,minsteps,1
*SET,maxsteps,1000
*SET,iters,10
*SET,apprate,timestep

ET,1,PLANE55              !  2D thermal element
ET,2,SURF151,,,,1,1       !  2D thermal surface effects element
KEYOPT,2,5,1
KEYOPT,2,6,0
KEYOPT,2,8,2
KEYOPT,2,9,1              !  Radiation option

                          !  X is width, Y is depth
                          !  Material 1 is for face sheets, 2 for webs

MPTEMP
MPTEMP,    1,  20,  90, 100, 110, 250, 270
MPTEMP,    7, 300, 550, 600
MPDATA,C,1,1,1170,1170,2300,1170,1170,1482
MPDATA,C,1,7,1950,1950,1170
MPDATA,C,2,1,1170,1170,2300,1170,1170,1482
MPDATA,C,2,7,1950,1950,1170

MPTEMP
MPTEMP,    1,    20, 250, 300, 330, 500, 700
MPTEMP,    7,   850, 900
MPDATA,KXX,1,1,0.35,0.40,0.15,0.12,0.10,0.10
MPDATA,KXX,1,7,0.40,0.80
MPDATA,KXX,2,1,0.35,0.40,0.15,0.12,0.10,0.10
```

```
MPDATA,KXX,2,7,0.40,0.80

MPTEMP
MPTEMP,         1,  20,  40,  90, 150, 250, 270
MPTEMP,         7, 330, 370, 390, 480, 550, 600
MPTEMP,        13, 850, 870
MPDATA,DENS,1, 1,1890,1888,1886,1881,1871,1852
MPDATA,DENS,1, 7,1673,1506,1472,1419,1378,1229
MPDATA,DENS,1,13,1172,1096
MPDATA,DENS,2, 1,1890,1888,1886,1881,1871,1852
MPDATA,DENS,2, 7,1673,1506,1472,1419,1378,1229
MPDATA,DENS,2,13,1172,1096

MPTEMP
MPTEMP,         1,  20,1200
MPDATA,EMIS,1, 1,0.75,0.95
MPDATA,EMIS,2, 1,0.75,0.95

!------------------------------ DEFINE GEOMETRY --------------------------------

K,1, 0     ,0     ,,
K,2, 0.0469,0     ,,
K,3, 0.1288,0     ,,
K,4, 0.2166,0     ,,
K,5, 0.2572,0     ,,
K,6, 0.3041,0     ,,
K,7, 0.3041,0.0204,,
K,8, 0.3041,0.0921,,
K,9, 0.2980,0.0921,,
K,10,0.2980,0.0204,,
K,11,0.2572,0.0204,,
K,12,0.2572,0.0168,,
K,13,0.2166,0.0168,,
K,14,0.2166,0.0204,,
K,15,0.1785,0.0204,,
K,16,0.1592,0.0921,,
K,17,0.1476,0.0921,,
K,18,0.1669,0.0204,,
K,19,0.1288,0.0204,,
K,20,0.1288,0.0168,,
K,21,0.0469,0.0168,,
K,22,0.0469,0.0204,,
K,23,0.0061,0.0204,,
K,24,0.0061,0.0921,,
K,25,0     ,0.0921,,
K,26,0     ,0.0204,,

A,1,2,21,22,23,26
A,2,3,20,21
A,3,4,13,14,15,18,19,20
A,4,5,12,13
A,5,6,7,10,11,12
A,10,7,8,9
A,18,15,16,17
A,26,23,24,25

LGLUE,ALL

LSEL,S,LINE,,2                  !  Concatenate lines for mapped meshing
```

```
LSEL,A,LINE,,3
LCCAT,ALL
LSEL,ALL
LSEL,S,LINE,,4
LSEL,A,LINE,,5
LCCAT,ALL
LSEL,ALL
LSEL,S,LINE,,11
LSEL,A,LINE,,12
LCCAT,ALL
LSEL,ALL
LSEL,S,LINE,,13
LSEL,A,LINE,,14
LSEL,A,LINE,,15
LCCAT,ALL
LSEL,ALL
LSEL,S,LINE,,16
LSEL,A,LINE,,8
LCCAT,ALL
LSEL,ALL
LSEL,S,LINE,,22
LSEL,A,LINE,,23
LCCAT,ALL
LSEL,ALL
LSEL,S,LINE,,24
LSEL,A,LINE,,18
LCCAT,ALL
LSEL,ALL
LSEL,S,LINE,,1
LSEL,A,LINE,,7
LSEL,A,LINE,,10
LSEL,A,LINE,,17
LSEL,A,LINE,,20
LCCAT,ALL

ALLSEL,ALL

!------------------------------------ MESH ----------------------------------

MAT,1                           !  Use material number 1
TYPE,1                          !  Use type 1 elements
MSHKEY,1                        !  Use mapped meshing (0 for free)
MSHAPE,0,2D                     !  Use quadrilaterals (1 for triangles)
ESIZE,0.001                     !  Max element edge length
AMESH,1,5                       !  Mesh selected areas
ESIZE,0.002
AMESH,6,8

EPLOT

NUMMERG,NODE,0.0001,0.0001      !  Merge redundant nodes
NUMMERG,KP,0.0001,0.0001        !  Merge redundant kp's, lines, and areas

!-------------------- APPLY LOADS AND BOUNDARY CONDITIONS --------------------

TUNIF,20                        !  Uniform initial temperature

TYPE,2
REAL,2
```

```
MAT,1

ALLSEL,ALL
NSEL,S,LOC,Y,0
ESLN,S
N,100000,0.1521,-0.1             !  Extra “space” node for radiation
ESURF,100000                     !  Generate SURF151 surface effect elements

ESEL,S,TYPE,,2
SFE,ALL,1,CONV,0,%hfhot%         !  Convection on hot face

D,100000,TEMP,%bftbot%           !  Temp boundary at “space” node for radiation

ALLSEL,ALL
LSEL,S,LINE,,27
LSEL,A,LINE,,23
LSEL,A,LINE,,24
LSEL,A,LINE,,19
LSEL,A,LINE,,12
LSEL,A,LINE,,13
LSEL,A,LINE,,28
LSEL,A,LINE,,30
LSEL,A,LINE,,15
LSEL,A,LINE,,16
LSEL,A,LINE,,9
LSEL,A,LINE,,3
LSEL,A,LINE,,4
LSEL,A,LINE,,31
NSLL,S,1

SF,ALL,CONV,hfint,bftint         !  Apply convection load to water interface

ALLSEL,ALL
FINISH

!----------------------- NONLINEAR TRANSIENT SOLUTION -------------------------

/SOLU

SOLCONTROL,ON
ANTYPE,TRANS                     !  Transient analysis
TIMINT,ON,THERM                  !  Activate thermal effects
CNVTOL,HEAT,,1E-5,2,5E-8         !  Set convergence tolerance limits
NEQIT,100                        !  Maximum number of iterations
NSUBST,numstep                   !  Number of substeps
KBC,1                            !  Stepped loading (0 for ramped)
TIME,totaltime                   !  Time at end of fire exposure
AUTOTS,OFF                       !  Automatic time stepping off
OUTPR,ALL,ALL
OUTRES,ALL,ALL

SOLVE

FINISH
END
```

2 Thermomechanical Model Source Code for *ANSYS 7.0*

```
/title,Thermomechanical_Model_(142w)

!--------------------------- VARIABLES AND CONSTANTS ---------------------------

/PREP7
/UNITS,SI
TOFFST,274                !  Conversion from Kelvin to Celsius

                          !  Units:  m, °C, kg, s, J, Pa

ACEL,0,0,-9.81            !  Gravity

*SET,tc,0.00494           !  Depth of mid-layer temperature boundary condition
*SET,d1,0.325             !  Dist from end of panel to edge of support
*SET,d2,0.100             !  Width of support (X direction)
*SET,d3,0.760             !  Dist from edge of support to edge of loading patch
*SET,d4,0.180             !  Width of loading patch
*SET,d5,0.385             !  Dist from edge of loading patch to center of panel
*SET,numdiv1,10           !  Number of elements in X-direction for d1
*SET,numdiv2, 6           !  Number of elements in X-direction for d2
*SET,numdiv3,28           !  Number of elements in X-direction for d3
*SET,numdiv4, 8           !  Number of elements in X-direction for d4
*SET,numdiv5,16           !  Number of elements in X-direction for d5

*SET,bfttop,20            !  Bulk fluid temp at FRP cold face (room temp)

! Thermal boundary conditions from Themochemical Model - particular values shown
are from simulation of liquid-cooled specimen

*DIM,thotface,  TABLE,14,,,TIME
thotface(1,0)=   1,60,120,300,600,1200,1800,2400,3000,3600,5400,7200
thotface(1,1)=  20,57, 85,177,325, 543, 640, 699, 738, 762, 825, 862

*DIM,tmidlayer, TABLE,14,,,TIME
tmidlayer(1,0)=  1,60,120,300,600,1200,1800,2400,3000,3600,5400,7200
tmidlayer(1,1)= 20,26, 38, 87,179, 246, 271, 292, 317, 348, 450, 564

*DIM,tcoldface1,TABLE,14,,,TIME  ! At the thinner portion of the face sheet
tcoldface1(1,0)= 1,60,120,300,600,1200,1800,2400,3000,3600,5400,7200
tcoldface1(1,1)=16,16, 16, 17, 20,  24,  25,  26,  26,  27,  28,  29

*DIM,tcoldface2,TABLE,14,,,TIME  ! At the thicker portion of the face sheet
tcoldface2(1,0)= 1,60,120,300,600,1200,1800,2400,3000,3600,5400,7200
tcoldface2(1,1)=16,16, 16, 17, 19,  22,  24,  24,  25,  25,  26,  27

*SET,totaltime,7200       ! Time at end of fire exposure
*SET,timestep,120
*SET,numstep,60
*SET,minsteps,1
*SET,maxsteps,100
*SET,iters,10
*SET,apprate,timestep

ET,1,MESH200,6            !  Unsolved element type for 2D mesh, quad 4-node
ET,2,SOLID5               !  Main element
ET,3,BEAM4                !  Element used to allow rotational freedom at support
```

```
!  X is the pultrusion direction, Y is width, Z is depth
!  Material 1 for the face sheets, 2 for the webs, 3 for the steel support

MP,KXX,1,0.35
MP,KXX,2,0.35

MP,  C,1,1170
MP,  C,2,1170

MPTEMP
MPTEMP,1,           20,     117,     200,     400,    600,850
MPDATA, EX,1,,21.240E9,21.240E9,18.959E9,12.018E9,4.509E9,1E6
MPDATA, EY,1,,11.790E9,11.790E9,10.524E9, 6.671E9,2.503E9,1E6
MPDATA, EZ,1,, 4.140E9, 4.140E9, 3.695E9, 2.343E9,0.879E9,1E6
MPDATA,GXY,1,, 5.580E9, 5.580E9, 4.981E9, 3.157E9,1.185E9,1E6
MPDATA,GYZ,1,, 4.140E9, 4.140E9, 3.695E9, 2.343E9,0.879E9,1E6
MPDATA,GXZ,1,, 4.140E9, 4.140E9, 3.695E9, 2.343E9,0.879E9,1E6
MPDATA, EX,2,,17.380E9,17.380E9,15.514E9, 9.834E9,3.689E9,1E6
MPDATA, EY,2,, 9.650E9, 9.650E9, 8.614E9, 5.460E9,2.048E9,1E6
MPDATA, EZ,2,, 4.140E9, 4.140E9, 3.695E9, 2.343E9,0.879E9,1E6
MPDATA,GXY,2,, 7.170E9, 7.170E9, 6.400E9, 4.057E9,1.522E9,1E6
MPDATA,GYZ,2,, 4.140E9, 4.140E9, 3.695E9, 2.343E9,0.879E9,1E6
MPDATA,GXZ,2,, 4.140E9, 4.140E9, 3.695E9, 2.343E9,0.879E9,1E6

MPTEMP
MPTEMP,        1,  10,  40,  90, 150, 250, 270
MPTEMP,        7, 330, 370, 390, 480, 550, 600
MPTEMP,       13, 850, 870
MPDATA,DENS,1, 1,1890,1888,1886,1881,1871,1852
MPDATA,DENS,1, 7,1673,1506,1472,1419,1378,1229
MPDATA,DENS,1,13,1172,1096
MPDATA,DENS,2, 1,1890,1888,1886,1881,1871,1852
MPDATA,DENS,2, 7,1673,1506,1472,1419,1378,1229
MPDATA,DENS,2,13,1172,1096

MP,ALPX,1,12.6E-6
MP,ALPY,1,21.8E-6
MP,ALPZ,1,37.0E-6
MP,PRXY,1,0.32
MP,PRXZ,1,0.30
MP,PRYZ,1,0.30
MP,ALPX,2,12.7E-6
MP,ALPY,2,37.0E-6
MP,ALPZ,2,21.3E-6
MP,PRXY,2,0.30
MP,PRXZ,2,0.32
MP,PRYZ,2,0.30

MP,RSVX,1,1
MP,MURX,1,1
MP,RSVX,2,1
MP,MURX,2,1
MP,RSVX,3,1
MP,MURX,3,1

MP,EX  ,3,210E9
MP,KXX ,3,10
MP,PRXY,3,0.3
```

```
MP,C   ,3,10000
MP,DENS,3,7850

!---------------------------- DEFINE GEOMETRY ---------------------------------

N,1,0,0.3041,-1
N,2,0,0     ,-1
N,3,0,0.3041,-0.02
N,4,0,0    ,-0.02
N,5,0,0.076025,-0.02
N,6,0, 0.15205,-0.02
N,7,0,0.228075,-0.02

K,1,-0.375 ,0     ,0
K,6,-0.375 ,0.3041,0
K,7,-0.375 ,0.3041,0.0204
K,8,-0.375 ,0.3041,0.1742
K,9,-0.375 ,0.3041,0.1946
K,10,-0.375,0.2572,0.1946
K,11,-0.375,0.1753,0.1946
K,12,-0.375,0.0875,0.1946
K,13,-0.375,0.0469,0.1946
K,14,-0.375,0     ,0.1946
K,15,-0.375,0     ,0.1742
K,16,-0.375,0     ,0.0204

K,17,-0.375,0.0061,0.0204
K,18,-0.375,0.0469,0.0204
K,19,-0.375,0.0469,0.0168
K,20,-0.375,0.1288,0.0204
K,21,-0.375,0.1288,0.0168
K,22,-0.375,0.1669,0.0204
K,23,-0.375,0.1785,0.0204
K,24,-0.375,0.2166,0.0204
K,25,-0.375,0.2166,0.0168
K,26,-0.375,0.2572,0.0204
K,27,-0.375,0.2572,0.0168
K,28,-0.375,0.2980,0.0204
K,29,-0.375,0.0061,0.1742
K,30,-0.375,0.0469,0.1778
K,31,-0.375,0.0469,0.1742
K,32,-0.375,0.0875,0.1778
K,33,-0.375,0.0875,0.1742
K,34,-0.375,0.1256,0.1742
K,35,-0.375,0.1372,0.1742
K,36,-0.375,0.1753,0.1778
K,37,-0.375,0.1753,0.1742
K,38,-0.375,0.2572,0.1778
K,39,-0.375,0.2572,0.1742
K,40,-0.375,0.2980,0.1742

K,41,-0.050,0     ,0
K,42, 0.050,0     ,0
K,43, 0.050,0.3041,0
K,44,-0.050,0.3041,0
K,45,-0.050,0     ,-0.02
K,46, 0.050,0     ,-0.02
K,47, 0.050,0.3041,-0.02
K,48,-0.050,0.3041,-0.02
```

```
K,49,0     ,0     ,0
K,50,0     ,0.3041,0
K,51,0     ,0.3041,-0.02
K,52,0     ,0     ,-0.02

K,53,-0.375 ,0     ,tc
K,54,-0.375 ,0.0469,tc
K,55,-0.375 ,0.1288,tc
K,56,-0.375 ,0.2166,tc
K,57,-0.375 ,0.2572,tc
K,58,-0.375 ,0.3041,tc

A,16,17,29,15
A,22,23,35,34
A,28, 7, 8,40
A, 1, 6,58,57,56,55,54,53
A,53,54,19,18,17,16
A,54,55,21,19
A,55,56,25,24,23,22,20,21
A,56,57,27,25
A,57,58, 7,28,26,27
A,15,29,31,30,13,14
A,30,32,12,13
A,33,34,35,37,36,11,12,32
A,36,38,10,11
A,39,40, 8, 9,10,38

LGLUE,ALL

!------------------------------ MESH AND EXTRUDE --------------------------------

TYPE,1
MSHKEY,0                  !  Use free meshing (1 for mapped meshing)
MSHAPE,0,2D               !  Use quadrilaterals (1 for triangles)
ESIZE,0.010               !  Set max element edge length
AMESH,10,14
ESIZE,0.008
AMESH,1,3
ESIZE,0.004
AMESH,5,9

MSHKEY,1                  !  Use mapped meshing (0 for free meshing)
ESIZE,0.004
LSEL,S,LINE,,15,19        !  Concatenate lines for mapped meshing
LCCAT,ALL
AMESH,4
LDEL,58                   !  Delete concatenated line to allow extrusion
MSHKEY,0

EXTOPT,ON                 !  Carry over all attributes of areas to volumes

AGEN,2,1 ,14,,d1          !  Copy areas and elements to critical junctions
AGEN,2,15,28,,d2
AGEN,2,29,42,,d3
AGEN,2,43,56,,d4
AGEN,2,57,70,,d5

VOFFST,1 ,d1,0                !  Extrude volumes from areas
VOFFST,2 ,d1,0
```

```
VOFFST,3 ,d1,0
VOFFST,4 ,d1,0
VOFFST,5 ,d1,0
VOFFST,6 ,d1,0
VOFFST,7 ,d1,0
VOFFST,8 ,d1,0
VOFFST,9 ,d1,0
VOFFST,10,d1,0
VOFFST,11,d1,0
VOFFST,12,d1,0
VOFFST,13,d1,0
VOFFST,14,d1,0

VOFFST,15,d2,0
VOFFST,16,d2,0
VOFFST,17,d2,0
VOFFST,18,d2,0
VOFFST,19,d2,0
VOFFST,20,d2,0
VOFFST,21,d2,0
VOFFST,22,d2,0
VOFFST,23,d2,0
VOFFST,24,d2,0
VOFFST,25,d2,0
VOFFST,26,d2,0
VOFFST,27,d2,0
VOFFST,28,d2,0

VOFFST,29,d3,0
VOFFST,30,d3,0
VOFFST,31,d3,0
VOFFST,32,d3,0
VOFFST,33,d3,0
VOFFST,34,d3,0
VOFFST,35,d3,0
VOFFST,36,d3,0
VOFFST,37,d3,0
VOFFST,38,d3,0
VOFFST,39,d3,0
VOFFST,40,d3,0
VOFFST,41,d3,0
VOFFST,42,d3,0

VOFFST,43,d4,0
VOFFST,44,d4,0
VOFFST,45,d4,0
VOFFST,46,d4,0
VOFFST,47,d4,0
VOFFST,48,d4,0
VOFFST,49,d4,0
VOFFST,50,d4,0
VOFFST,51,d4,0
VOFFST,52,d4,0
VOFFST,53,d4,0
VOFFST,54,d4,0
VOFFST,55,d4,0
VOFFST,56,d4,0

VOFFST,57,d5,0
```

```
VOFFST,58,d5,0
VOFFST,59,d5,0
VOFFST,60,d5,0
VOFFST,61,d5,0
VOFFST,62,d5,0
VOFFST,63,d5,0
VOFFST,64,d5,0
VOFFST,65,d5,0
VOFFST,66,d5,0
VOFFST,67,d5,0
VOFFST,68,d5,0
VOFFST,69,d5,0
VOFFST,70,d5,0

V,41,49,50,44,45,52,51,48        !  Steel support plate
V,49,42,43,50,52,46,47,51

VGLUE,ALL
ALLSEL,ALL

ESIZE,,numdiv1                   !  Mesh volumes from area elements at faces
VSWEEP,3,3
VSWEEP,2,2
VSWEEP,1,1
VSWEEP,110,14
VSWEEP,76,13
VSWEEP,128,12
VSWEEP,75,11
VSWEEP,109,10
VSWEEP,108,9
VSWEEP,74,8
VSWEEP,127,7
VSWEEP,73,6
VSWEEP,107,5
VSWEEP,4,4

ESIZE,,numdiv2
VSWEEP,79,95
VSWEEP,78,90
VSWEEP,77,85
VSWEEP,114,710
VSWEEP,94,559
VSWEEP,133,799
VSWEEP,93,556
VSWEEP,112,705
VSWEEP,113,702
VSWEEP,91,553
VSWEEP,132,794
VSWEEP,92,549
VSWEEP,111,698
VSWEEP,140,100
VSWEEP,89
VSWEEP,90

ESIZE,,numdiv3
VSWEEP,82,185
VSWEEP,81,180
VSWEEP,80,175
VSWEEP,118,730
```

```
VSWEEP,98,633
VSWEEP,135,823
VSWEEP,97,628
VSWEEP,116,720
VSWEEP,117,725
VSWEEP,95,617
VSWEEP,134,817
VSWEEP,96,622
VSWEEP,115,715
VSWEEP,129,190

ESIZE,,numdiv4
VSWEEP,85,275
VSWEEP,84,270
VSWEEP,83,265
VSWEEP,122,750
VSWEEP,102,653
VSWEEP,137,834
VSWEEP,101,648
VSWEEP,120,740
VSWEEP,121,745
VSWEEP,99,637
VSWEEP,136,828
VSWEEP,100,642
VSWEEP,119,735
VSWEEP,130,280

ESIZE,,numdiv5
VSWEEP,88,365
VSWEEP,87,360
VSWEEP,86,355
VSWEEP,126,770
VSWEEP,106,673
VSWEEP,139,845
VSWEEP,105,668
VSWEEP,124,760
VSWEEP,125,765
VSWEEP,103,657
VSWEEP,138,839
VSWEEP,104,662
VSWEEP,123,755
VSWEEP,131,370

TYPE,3
E,1,3
E,1,7
E,1,6
E,1,5
E,1,4
E,2,3
E,2,7
E,2,6
E,2,5
E,2,4
R,1,10,100,100,0.1,0.1          !  Arbitrary dimensions of support beams

NUMMERG,NODE,0.0001,0.0001      !  Merge redundant nodes
NUMMERG,KP,0.001,0.001          !  Merge redundant kp's, lines, and areas
```

```
NSEL,S,LOC,Z,0.0204,0.1742       !  Assign material properties
ESLN,S,1
MPCHG,2,ALL
ALLSEL,ALL
NSEL,S,LOC,Z,-1,0
ESLN,S,1
MPCHG,3,ALL
ALLSEL,ALL

/PNUM,MAT,1                      !  Show materials distribution
/NUMBER,1                        !  Show materials distribution as colors

!-------------------- DEFINE STRUCTURAL LOADS AND SUPPORTS ----------------------

NSEL,S,LOC,Z,-1                  !  Beam support condition
D,ALL,UX
D,ALL,UY
D,ALL,UZ

ALLSEL,ALL
NSEL,S,LOC,X,1.375               !  Symmetry axis at mid-span
DSYM,SYMM,X
D,ALL,UY

ALLSEL,ALL
NSEL,S,LOC,Z,0.1946
NSEL,R,LOC,X,0.81,0.99
SF,ALL,PRES,5.610E5              !  Vertical structural load

ALLSEL,ALL

!----------------------------- ADD THERMAL EFFECTS -------------------------------

TUNIF,20                         !  Set initial temperature for all nodes

ASEL,S,AREA,,680
ASEL,A,AREA,,660
ASEL,A,AREA,,640
ASEL,A,AREA,,645
ASEL,A,AREA,,665
ASEL,A,AREA,,685

NSLA,S,1
D,ALL,TEMP,%tcoldface1%          !  Cold face temp boundary at thinner portion
ALLSEL,ALL

ASEL,S,AREA,,782
ASEL,A,AREA,,762
ASEL,A,AREA,,742
ASEL,A,AREA,,848
ASEL,A,AREA,,837
ASEL,A,AREA,,826
ASEL,A,AREA,,847
ASEL,A,AREA,,836
ASEL,A,AREA,,825
ASEL,A,AREA,,774
ASEL,A,AREA,,754
ASEL,A,AREA,,734
```

```
NSLA,S,1
D,ALL,TEMP,%tcoldface2%          !  Cold face temp boundary at thicker portion
ALLSEL,ALL

NSEL,S,LOC,Z,0.1946
SF,ALL,CONV,hfcold,bfttop        !  Convection at outer face of upper face sheet
ALLSEL,ALL

NSEL,S,LOC,Z,0
NSEL,R,LOC,X,0.175,1.375
D,ALL,TEMP,%thotface%            !  Temp boundary bottom of lower face sheet
ALLSEL,ALL

NSEL,S,LOC,Z,tc
NSEL,R,LOC,X,0.175,1.375
D,ALL,TEMP,%tmidlayer%           !  Temp boundary within lower face sheet
ALLSEL,ALL

FINISH

!-------------------- TRANSIENT THERMAL-STRUCTURAL ANALYSIS ---------------------

/SOLU

ANTYPE,TRANS
TIMINT,ON,THERM                      !  Activate transient effects
NEQIT,25                             !  Maximum number of iterations
NSUBST,numstep                       !  Number of substeps
KBC,1                                !  Stepped loading (0 for ramped)
TIME,totaltime                       !  Time at end of fire exposure
AUTOTS,ON                            !  Automatic time stepping
OUTPR,ALL,ALL
OUTRES,ALL,ALL

FINISH
END
```